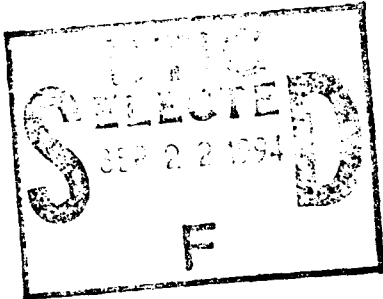


(L)

AD-A284 975



Low Frequency Ocean Noise Analysis

N00014-90-J-1683

Final Technical Report

ANALYSIS OF LOW FREQUENCY OCEAN NOISE:

- (1) FROM A LONG-TERM EXPERIMENT ACROSS THE U.S. EAST COAST, AND**
- (2) FROM THE WAKE ISLAND HYDROPHONE ARRAY DURING NORTHWEST PACIFIC TYPHOONS**

Charles S. McCreery, Frederick K. Duennebie, and Daniel A. Walker
School of Ocean and Earth Sciences and Technology
University of Hawaii at Manoa, Honolulu, HI 96822

July 22, 1994

This document has been approved
 for public release and sale; its
 distribution is unlimited.

14919 94-30412



94 9 21 042

LONG RANGE OBJECTIVES

The long-range goal of this project was a better understanding of the mechanisms of generation and propagation of ambient ocean noise at frequencies between about 0.05 and 50 Hz. Although it is generally agreed that most of the ambient noise in this band is generated by ocean gravity waves, many questions remain concerning how these waves act to produce the wide variety of characteristics observed in the ocean noise spectrum. Proposed mechanisms of noise generation include open-ocean, shoreline-enhanced, and storm-enhanced non-linear gravity wave interactions, shallow water gravity wave bottom interactions, surf, and open-ocean breaking waves or whitecaps. Propagation mechanisms include acoustic waves, non-acoustic pressure fluctuations, and Rayleigh waves. We utilized two unique long-term bottom acoustic data sets to identify specific noise mechanisms and to evaluate environmental conditions under which these mechanisms are significant contributors to the ambient noise field.

PROJECT OBJECTIVES

The East Coast experiment, called the Environmentally Controlled Ocean floor NOise Monitoring Experiment (ECONOMEX), was designed to sample ambient noise in the water column and on the ocean floor across the continental shelf and slope east of Chesapeake Bay. A vertical array of hydrophones in the water column, a horizontal array of hydrophones, and three-component seismometers were deployed for several months in the spring of 1991. The experiment was designed to coincide with the Surface Wave Dynamics Experiment (SWADE) in order to take advantage of their extensive measurements of surface winds and directional ocean wave spectra in the same region. This comprehensive and long-term data set permits the identification of specific noise generation and propagation mechanisms for the continental shelf and slope, and evaluation of their contribution to the noise field under a wide variety of ocean surface conditions.

The primary goal of studying data from the Wake Island Hydrophone Array is to quantify changes in the noise field due to the extreme ocean surface conditions produced by typhoons, and to identify mechanisms by which these storms produce noise. One such storm, Typhoon Doyle, passed directly over some of the Wake hydrophones in August, 1988, and numerous other typhoons have passed near Wake since 1982, when the regular recording of digital noise samples from the array began. A secondary objective was to identify other mechanisms that contribute significantly to the noise in deep ocean basins, utilizing this unique long-

term time series. Although the Wake study lacks the comprehensive environmental data available to ECONOMEX, it is aided by regular surface wind measurements made at Wake Island by the National Weather Service, and by ocean wave estimates from U.S. Navy wave models.

SUMMARY OF RECENT RESULTS

Wake Island Hydrophone Array. Recordings of the low frequency noise field observed on the Wake hydrophones were made between 1982 and June, 1994. It is planned that recording of this valuable time series will be restarted shortly and continue indefinitely. Analyses of these data up to 1988 were accomplished under this contract. Noise levels in the deep ocean near Wake show considerable structure in their variation. Winter months are especially characterized by recurring episodes of increased energy between 0.1 and 0.2 Hz that usually last several days. The episode shown in Figs. 35 and 36 of McCreery's dissertation, lasting from Oct. 29 to Nov. 3, 1988, is displayed for two of the Wake hydrophones - one at 850m depth (suspended) and the other at 5500m (bottom-mounted). These figures show the differences in noise levels from the mean at each frequency for the period shown. The shallower hydrophone (Fig. 36) detects the direct pressure signals from longer-period ocean gravity waves, seen between Oct. 30 and Nov. 3 centered at about 0.06 Hz. Narrow-band striations appear within this packet of energy, indicating dispersion with low frequencies arriving first. Making the assumption that this dispersion reflects the arrival time of a train of gravity waves at the hydrophone, the group velocity dispersion relationship yields a distance and origin time of waves that are consistent with generation by a strong extratropical cyclone that was moving to the northeast off the coast of Japan. This strongly implies that the propagation mechanism of this noise to the hydrophone is direct pressure variations at the hydrophone from waves passing overhead. However, increased noise between 0.1 and 0.2 Hz. arrives at the hydrophones more than a day earlier than the 0.06 Hz signal. If we assume that this noise was generated by the same storm, then the higher frequency energy must have traveled to the hydrophones by a much faster mechanism than ocean surface gravity waves, perhaps as Rayleigh waves generated at the storm, or at a shore line near the storm. Although we observe that the higher frequency noise is roughly twice the frequency of the lower frequency noise, it does not appear likely that the higher frequency energy is generated by the classical non-linear wave interaction microseism mechanism from waves passing directly over the hydrophone, as it arrives much earlier than the lower frequency noise.

An argument in favor of Rayleigh wave propagation for energy near the microseism peak is that the noise between 0.1-0.2 Hz measured on the deep hydrophones is 15 to 20 dB higher than levels observed on the shallow

<input checked="" type="checkbox"/>
<input type="checkbox"/>
<input type="checkbox"/>

per ltr

ity Codes
and/or
pecial

A-1

phones. This difference is similar to the relative levels for Rayleigh waves from earthquakes (FIGURE 1). To investigate this possibility further, a preliminary frequency-wavenumber analysis was made on this noise using the deep hydrophones to the north of Wake. Convincing evidence for the presence of Rayleigh waves was not found, although a more detailed analysis is warranted.

ECONOMEX. Spectral processing of long-term ambient noise data from the differential pressure gauges (DPGs) and geophones from ECONOMEX reveals a complex structure (Fig. 2). These figures show the difference from average noise level at each frequency as height above the page lit from the top of the page. While it is difficult to obtain absolute levels from this plot, the temporal structural changes in noise level are highlighted. Pressure variations at a depth of 95m on the shelf (top left figure) are dominated by distinctive modal bands of energy that are subtle or absent in the vertical geophone record (top right). Also apparent in the shallow DPG data is the direct pressure signal of ocean swell from a very distant source, increasing in frequency between 0.05 and 0.07 Hz over a period of about four days. The gravity wave group velocity dispersion formula yields a distance of about 14,000 km for the source of these waves, possibly originating at an Antarctic storm. Similar signals were observed in the ULF/VLF data off Oregon in 1991. In deeper water, both the DPG and geophone signals are characterized by packets of energy between 0.1 and 0.2 Hz that are similar to those seen in the Wake data. However, the numerous narrow features that sweep rapidly downward in frequency over a period of hours as they grow in strength have not been observed in the deep ocean near Wake. These narrow features are almost certainly related to increases in wind speed or changes in wind direction leading to the rapid building of seas from high to low frequencies. The fact that these features are not observed at the Wake hydrophones implies that the proximity of a shoreline is involved with the mechanism. Either the shoreline reflects the waves to produce wave-wave interactions over the sensors, or the noise is generated at the shoreline, and propagates to the sensors as Rayleigh waves. Work to correlate these distinctive features with particle motions and the SWADE environmental data, and possibly resolve this question, has not been accomplished.

SUMMARY OF RESULTS IN CHARLES MCCREERY'S DISSERTATION AND PUBLICATIONS

The HOLU Spectrum: The slope of the noise spectrum from roughly 0.4 to 6 Hz often saturates, reaching a particular level which is only surpassed under special circumstances. This saturation level has been

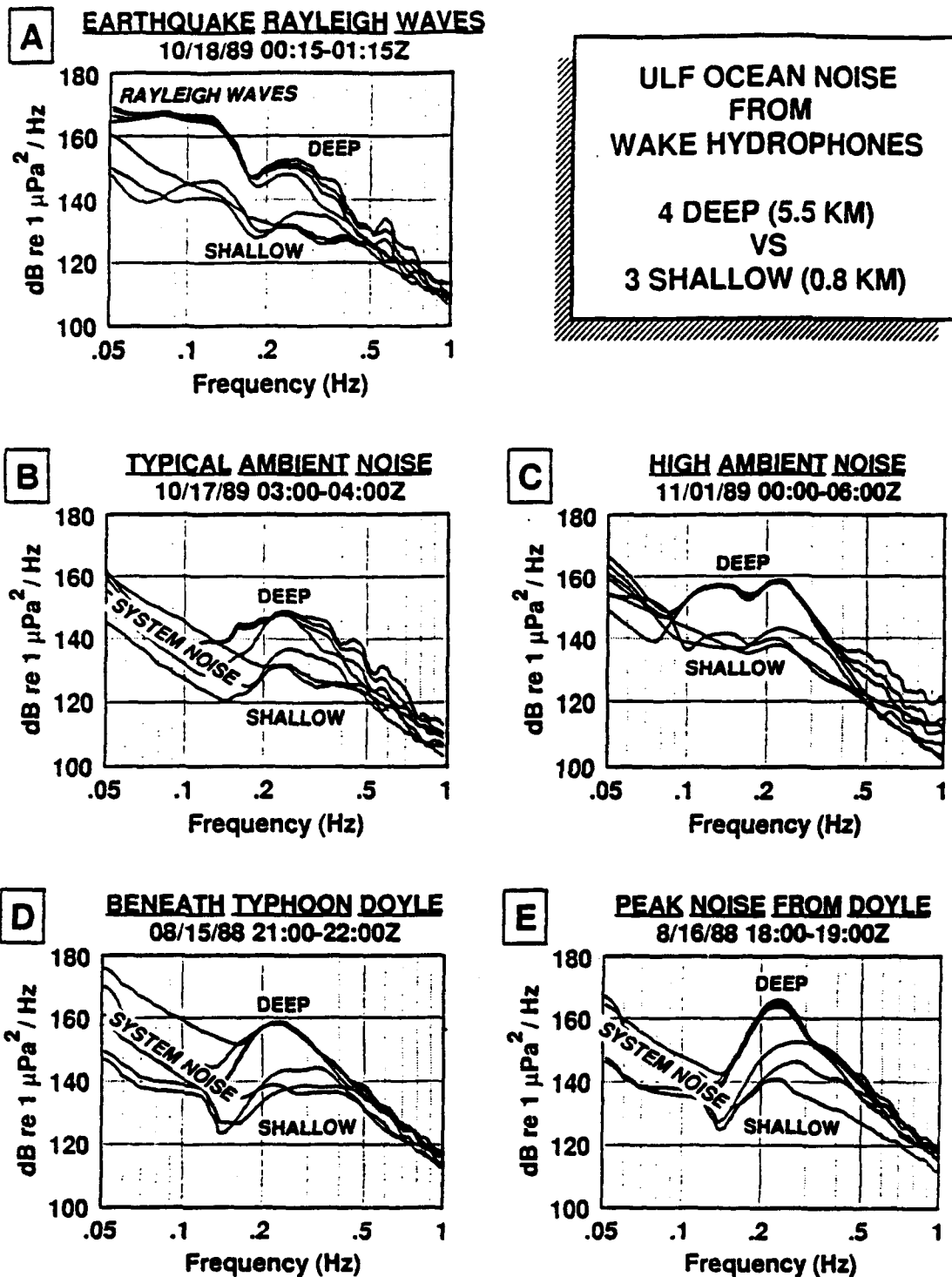


Figure 1. Wake shallow and deep hydrophone spectra showing earthquake Rayleigh waves (A), typical noise (B), high ambient noise (C), and noise at the time of typhoon Doyle (D and E).

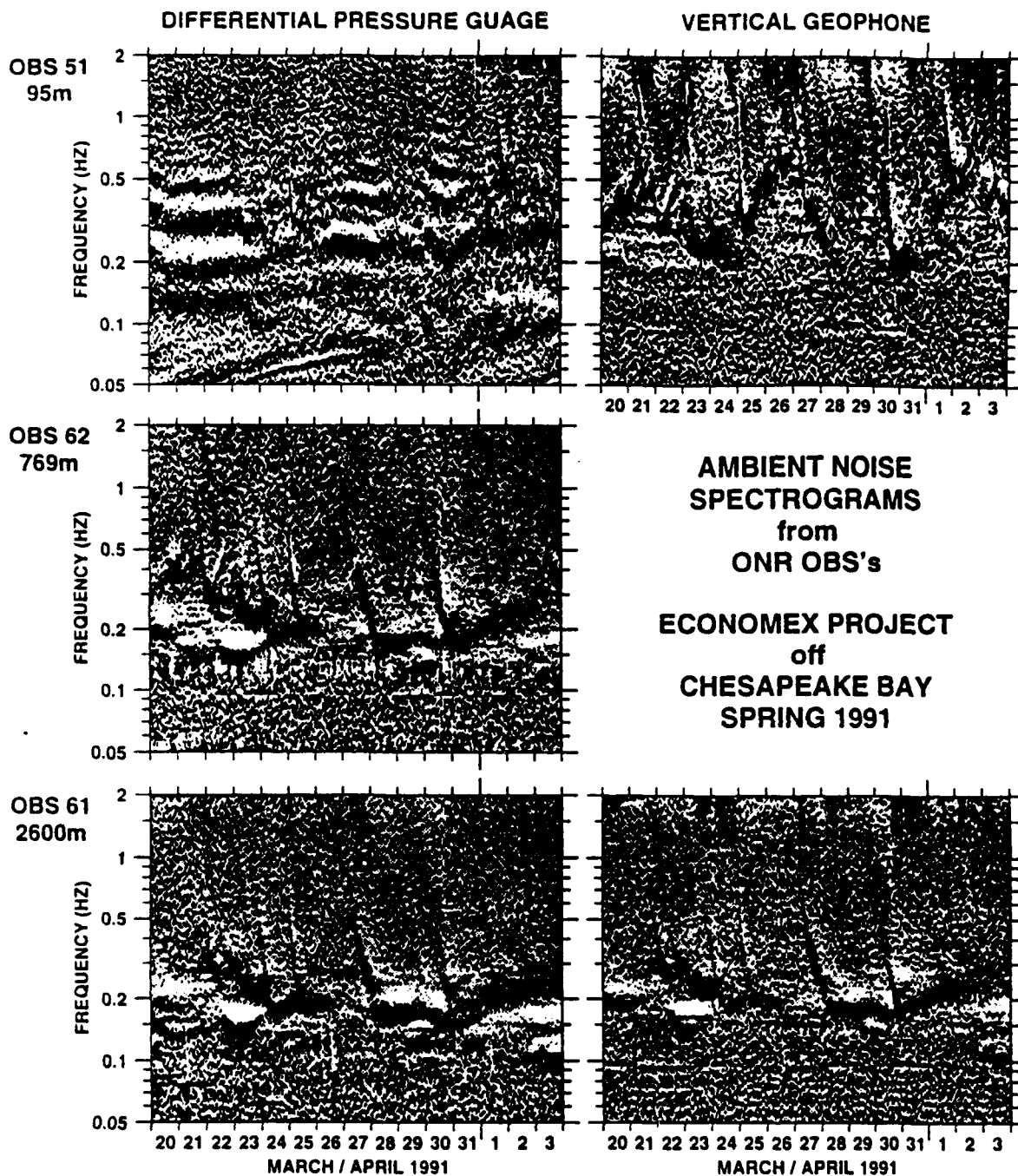


Figure 2. ECONOMEX ambient noise spectrograms. These figures show the difference from average noise level at each frequency as height above the page lit from the top of the page. While it is difficult to obtain absolute levels from this plot, the temporal structural changes in noise level are highlighted.

observed many times (OSS Experiment, ULF/VLF Experiment, and others). It appears to be related to the ocean wave spectrum directly above the hydrophone, and the noise level appears to have little or no dependence on water depth. This saturation level and the slope of the noise curve are well predicted by the non-linear wave interaction mechanism for propagation to the ocean floor of pressure fluctuations from ocean wave activity (Longuet-Higgins, 1963), coupled with the predicted ocean wave spectrum (Phillips, 1980, and Hasselmann et al, 1976), with the connection between the wave spectrum and the noise spectrum made by Webb and Cox, 1986. There appears to be no dependence on wave direction in this part of the wave spectrum. The ocean wave amplitude spectrum saturates at high frequencies, as non-linear effects transfer energy to lower and lower frequencies with increasing wind speed and fetch. This saturation level is characterized by the Phillips' constant of the ocean wave spectrum. The energy in the wave spectrum is propagated downward, by the apparently lossless mechanism described by Longuet-Higgins, as pressure variations detected by hydrophones. The Phillips' constant is observed in the ocean acoustic noise spectrum as the HOLU spectrum. This is believed to be a world-wide constant, independent of ocean depth (except in very shallow water where the direct pressure mechanism begins to dominate.) At Wake, the Holu spectrum is observed to have a value of 75 dB re $1\mu\text{Pa}/\sqrt{\text{Hz}}$ at 4 Hz, and a slope of about -23 dB/oct averaged over many years of data, but with a standard deviation of less than 4 dB at 4 Hz. This observation is slightly higher than predicted by the theory, with a slightly lower slope (68 dB at 4 Hz with a slope of -25 dB/oct.) The cause of the difference is unknown, but is probably a combination of uncertainties in calibration of the WAKE hydrophones, and lack of continuous saturation at lower frequencies in the data.

Typhoon Doyle. The crossing of Typhoon Doyle over the Wake hydrophone array in 1988, provided excellent data for study of the acoustic noise spectrum under extreme conditions. Of particular interest is the depression of the HOLU spectrum at the time when winds were strongest (Figure 32, McCreery Dissertation.) When noise levels above 5 Hz reach their maximum levels when the wind speed over the hydrophone reaches its highest levels, noise levels at 2 and 3 Hz are depressed well below expected HOLU levels. One possible explanation for this phenomenon is that the high winds and breaking waves generate foam at the ocean surface that attenuates the higher frequency waves. Note that the depression of the HOLU spectrum begins and ends at about the same time as the increase in noise level above 5 Hz (thought to be generated by acoustic noise from braking waves.)

Another important observation is the change in noise level as the eye of Typhoon Doyle passed directly over hydrophone 76 (Figure 33, McCreery Dissertation.) . A slight but significant reduction in the noise level above 2 Hz. is observed, implying that an appreciable amount of the observed noise at frequencies above 2 Hz is propagated directly to the bottom without a significant horizontal path.

Correlation of estimated ocean wave spectrum with Wake hydrophone noise spectrum. The double frequency microseism mechanism of Longuet-Higgins implies that there should be a strong correlation between wave height above the hydrophone at one frequency with acoustic noise at twice that frequency. In Figure 27 (McCreery Dissertation), a correlation is made between the ocean wave spectrum at Wake predicted by the U.S. Navy Spectral Ocean Wave Model and the noise levels observed at the same time by hydrophone 74. This figure clearly shows that the expected 2:1 correlation is not observed, except possibly at frequencies below 0.2 Hz. Furthermore, the weakest correlation is seen at frequencies between 0.2 and 0.3 Hz, where the microseismic noise is highest. Above 0.3 Hz a strong correlation between 5:1 and 10:1 is observed. It is unlikely that the SOWM model could be in error enough to explain this change from the expected 2:1 correlation at frequencies above 0.2 Hz, and we have no explanation for the observed correlation. The decrease in correlation between 0.2 and 0.3 Hz suggests that much of the energy in this band (where the microseism peak is located) is generated at considerable distance from Wake.

Two documents are included as appendices to this report, the University of Hawaii PhD Dissertation of Charles McCreery, and a reprint of a paper, Correlation of deep ocean noise (0.4-30 Hz) with wind, and the Holu Spectrum - A world-wide constant. Although this is a final report, work still progresses on these results, however slowly due to lack of funds.

1993 PUBLICATIONS SUPPORTED BY ONR

- McCreery, C.S., F.K. Duennebie, and G.H. Sutton, (1993), Correlation of deep ocean noise (0.4-30 Hz) with wind, and the Holu Spectrum - a worldwide constant, J. Acoust. Soc. Am. 93 (5), 2639-2648.
- McCreery, C.S., G.H. Sutton, and T.A. Schroeder (in prep.), Long-term 0.05-1Hz deep ocean noise from Wake hydrophones: relation to north Pacific storms and waves, J. Acoust. Soc. Am.
- McCreery, C.S., F.K. Duennebie, and T.A. Schroeder, (in prep.), Ocean noise, 0.1-30 Hz, measured under a typhoon, J. Acoust. Soc. Am.

Correlation of deep ocean noise (0.4–30 Hz) with wind, and the Holu Spectrum—A worldwide constant

Charles S. McCreery and Frederick K. Duennebieer

School of Ocean and Earth Science and Technology, University of Hawaii, 2525 Correa Road, Honolulu, Hawaii 96822

George H. Sutton

Woods Hole Oceanographic Institution, RD2, Box 167C, Stone Ridge, New York 12484

(Received 8 July 1991, revised 15 July 1992; accepted 2 December 1992)

One year of ambient ocean noise data, 0.4 to 30 Hz, from the Wake Island hydrophone array in the northwestern Pacific are compared to surface wind speeds, 0–14 m/s (0–28 kn). Between 0.4 and 6 Hz, noise levels increase with wind speed at rates of up to 2 dB per m/s until a saturation is reached having a slope of about -23 dB/octave and a level of 75 dB relative to $1 \mu\text{Pa}/\sqrt{\text{Hz}}$ at 4 Hz. This noise saturation, called the "Holu Spectrum," likely corresponds to saturation of short-wavelength ocean wind waves. It is probably a worldwide constant. Between 4 and 30 Hz, noise also increases with wind speed at rates of up to 2 dB per m/s, but no saturation level is observed and the slope increases to about 4 dB/octave. This may be acoustic noise from whitecaps. On a hydrophone less than 3 km from Wake, noise between 0.5 and 10 Hz increases with wind speed at a rate up to 2 dB per m/s, but absolute noise levels are significantly higher than levels on the other hydrophones more distant from Wake, and no saturation is apparent. Surf breaking against the shore of the island is the probable source of this noise.

PACS numbers: 43.30.Nb, 43.30.Pc

INTRODUCTION

The relationship between ambient infrasonic noise in the deep ocean and corresponding wind and wave conditions on the ocean's surface is a subject that has been studied since at least 1950, when Longuet-Higgins published his theory on the origin of microseisms,¹ the large amplitude, 3–10-s period signals commonly observed on land seismic records. That work, based on the theoretical considerations of Miche² and subsequently developed by Hasselman,³ describes how nonlinear interactions between opposing sets of ocean-surface gravity waves of the same frequency produce double-frequency pressure fluctuations in the water column that do not attenuate with depth. Those double-frequency pressure fluctuations couple into the solid earth and propagate onto land where they are observed as microseisms. There was additional research activity on this subject in the 1960s because of the rapid expansion of instrumental seismology and a corresponding increase in interest in the source and mechanisms of microseismic noise.^{4–8} Those studies utilized data collected both on land and in the deep ocean to correlate microseismic noise increases with oceanic storms and surf, and to identify Rayleigh waves as a propagation mechanism for this noise in the solid earth. Within the past 20 years there have been many additional studies that further quantify the relationships between ambient deep ocean noise and various environmental conditions including storms, ocean swell, atmospheric turbulence, wind, wind waves, and breaking wind waves.^{9–17} However, most investigators would agree that there are still too few high-quality data in the infrasonic band to produce a comprehensive picture of

the different kinds of deep-ocean noise, their sources, mechanisms of propagation, and the environmental conditions under which they are significant. This paper presents a portion of what has been learned by analyzing a unique long-term set of hydrophone and wind data from the deep ocean near Wake Island in the northwestern Pacific. The data presented here mostly pertain to frequencies above 0.4 Hz.

1. DATA

The Hawaii Institute of Geophysics (HIG) has digitally recorded signals from at least eight of the hydrophones in the 12-element Wake Island hydrophone array (WIHA) (Fig. 1) since September 1982. This array was built in the late 1950s by the U.S. Air Force, and has been used by HIG since the early 1960s. Signals from these hydrophones have been utilized for studies of guided oceanic-lithosphere seismic phases P_0 and S_0 , mantle-refracted P phases from distant earthquakes and underground nuclear explosions, seismicity within ocean basins, submarine volcanism, ocean noise, and numerous other topics that can be uniquely studied with long-term data from hydroacoustic sensors located in a mid-ocean basin.^{18–21} Six elements of WIHA are located on the ocean bottom (5.5-km depth) at the center and vertices of a 40-km pentagon. The other six elements are located in pairs at three sites, and are at a depth of about 0.85 km—the approximate depth of the SOFAR (sound fixing and ranging) or deep sound channel axis. These passive, moving-coil-type hydrophones are cabled directly to Wake Island. Although designed for signals at frequencies

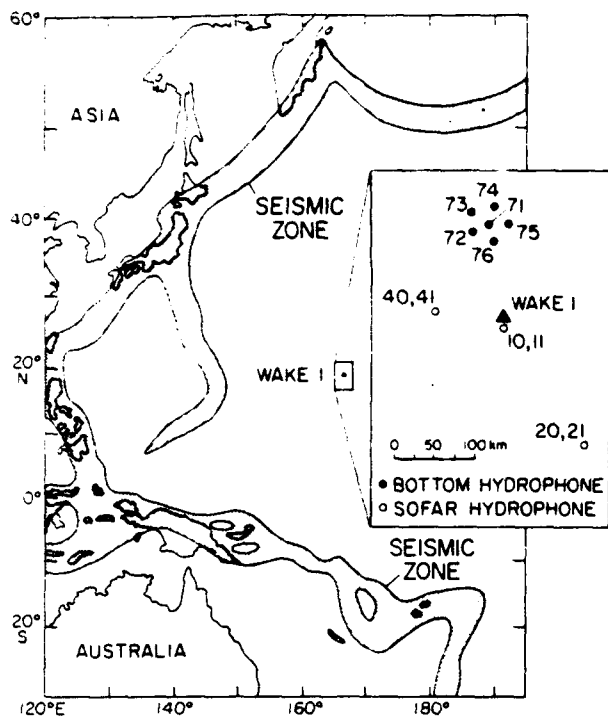


FIG. 1. The position of Wake Island in the northwestern Pacific Ocean, and the relative position of hydrophones in the Wake Island hydrophone array. The hydrophones used in this study are 74, 76, 10, and 20.

greater than 20 Hz, the hydrophones are sensitive to much lower frequencies. Signals with frequencies as low as 0.05 Hz are routinely recorded from moderate to large earthquakes.

The electrical signals generated by the passive hydrophones and transmitted through the long cables must first be amplified by very low-noise preamps. Then, after further amplification, pre-whitening, and anti-alias filtering, the signals are digitized with 16 bits of resolution, multiplexed, and recorded on tape shipped regularly to HIG for analysis. The digitization rate of the data used in this study is 80 Hz. (The digitization rate was increased to 100 Hz in September 1989.) The estimated hydrophone-cable-amplifier-filter-digitizer response curves for the four hydrophones used in this study are shown in Fig. 2. The amplifier-filter-digitizer response was modified for optimal pre-whitening and anti-aliasing during the system installation and was measured in place at Wake Island. The hydrophone response is an estimate extrapolated from data published by Thanos²² describing the Columbia-Pt. Arena Ocean Bottom Seismic Station (OBSS), an instrument with an identical hydrophone. A small hydrostatic pressure compensation hole in the hydrophone reduces its long-period response by 6 dB/octave below some corner frequency. Thanos put this corner at 3 Hz,²² although Barstow *et al.*²³ move it to 0.3 Hz based on a comparative analysis of OBSS hydrophone and seismometer data. A 0.3-Hz corner has been assumed for the WIHA hydrophones, although uncertainty about it remains, particularly since the pressure compensation hole may be partially or completely filled after more than 30 yr in the water. The

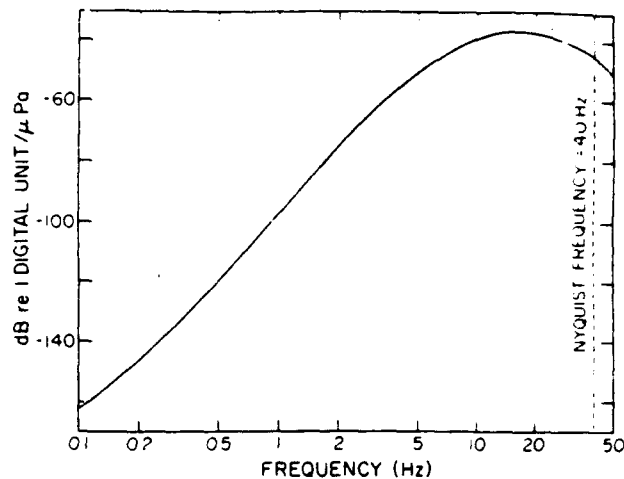


FIG. 2. Estimated response curves for hydrophones 10, 20, 74, and 76 through the recording system of the Wake Island hydrophone array. The general shape of these curves was chosen, by the design of the amplifiers, to whiten the ambient noise between about 0.5 and 20 Hz and to provide anti-aliasing. Notches at 60 Hz are to reduce 60-Hz crosstalk.

cables have an attenuating effect at frequencies greater than about 5 Hz that increases with both frequency and cable length. The depth dependence of the hydrophone response in combination with the different cable lengths lead to four separate response curves for the four hydrophones.

Ambient noise samples, 3 min in length, were extracted from the continuous data at an average rate of one noise sample per hour. The spacing between samples was randomized to minimize the possibility of contamination by electrical noise sources at Wake (such as radio transmissions) which might be on a fixed schedule. A subset of these data, consisting of noise samples from two deep hydrophones, 74 and 76, and two SOFAR hydrophones, 10 and 20, with noise samples spaced approximately every 6 h over the first year of operation is analyzed in this study. The two deep hydrophones are anchored on relatively flat, sediment-covered ocean floor; SOFAR hydrophone 10 is anchored on the submarine flank of Wake Island; and SOFAR hydrophone 20 is suspended above the side of a seamount.

Complementing the ambient noise data are weather data from the National Weather Service (NWS) station at Wake Island. Among the various measurements made by NWS at Wake are wind speed and wind direction, measured every hour with daily averages reported in monthly summaries.²⁴

II. DATA REDUCTION

A. Spectral computation

The first major step in the analysis of these data was transformation from the time domain to the frequency domain. Each 3-min time series was divided into 27 adjacent 512-point segments that were each demeaned, deskewed, Lanczos-windowed (to approximately preserve absolute amplitudes), and then transformed with a 512-point fast

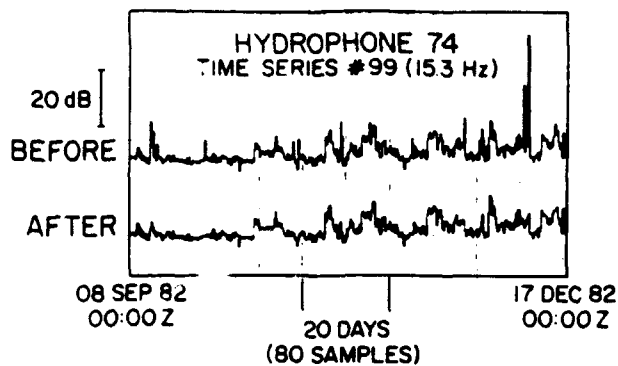


FIG. 3. A sample 100-day time series of ambient noise fluctuations before (upper) and after (lower) the removal of extraneous transient signals.

Fourier transform (FFT). Mean power spectral levels at each of the resulting 256 frequencies were computed by averaging data from the 27 transformed segments. This procedure produces spectral levels with more stability than their constituent spectral estimates, with a sacrifice in frequency resolution relative to that that would be achieved by transforming the entire 3-min time series with one FFT. The hydrophone-cable-recording system responses were then applied to the data to put them into absolute pressure units. Finally, the data were normalized to a 1-Hz bandwidth.

Four large data sets were produced, one for each hydrophone. Each data set consists of 256 time series of spectral noise levels—one for each of the 256 spectral frequencies. Each time series is 1460 samples in length (i.e., 365 days \times 4 samples/day = 1460 samples). These time series represent the ambient noise level fluctuations over a 1-yr period for a particular hydrophone at a particular frequency. Only the first 192 (0 to 30 Hz) of each hydrophone's 256 time series were analyzed further.

B. Removal of transients

Unwanted high-energy transients were present in each of the time series, and an attempt was made to remove them. Sources for these transients include earthquakes, nearby shipping, and geophysical surveys. A transient was empirically defined as any individual sample with a power level at least 3 dB greater than the level of the two adjacent samples in the time series. Transients were replaced by the mean value of those two adjacent samples. This procedure successfully removed extraneous spikes in the data, while preserving most of the original character of the time series (Fig. 3). At a maximum, only about 10% of the data points of any time series were modified by this procedure (Fig. 4). It is interesting to note that the percent number of transients in a particular time series appears to be directly proportional to the noise frequency that the time series represents, at least for frequencies between 0 and 20 Hz. This is partially a consequence of rapidly decreasing absolute noise levels between 0.2 and 10 Hz.

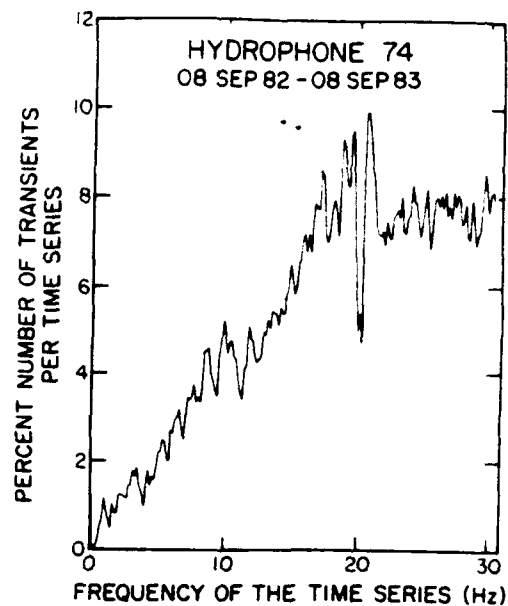


FIG. 4. The percent number of data points considered to be extraneous transients in each time series are plotted as a function of the frequency of the time series. The feature at 20 Hz is an artifact caused by an aliased 60-Hz signal.

III. ONE-YEAR MEAN NOISE LEVEL SPECTRA

The 1-yr mean noise spectra from the four hydrophones studied exhibit characteristics typical of deep ocean noise spectra (Fig. 5). Levels are highest at the lowest frequencies. The microseism peak is somewhere between 0.1 and 0.3 Hz, although the spectral resolution of this study (0.156 Hz) is too coarse to resolve that peak with any precision. Between 0.3 and 6 Hz, levels fall off rapidly with frequency, and above 10 Hz the spectral slope is flat or slightly positive. A narrow peak at 20 Hz in the spectra of hydrophones 74 and 76 is an artifact (60-Hz energy aliased to 20 Hz). A broader rise in level at about 17 Hz on all hydrophones, however, is caused by whales. Whale signals are easily identified in the time record and similar signals have been described and identified by Urick,²⁵ Watkins *et al.*,²⁶ and Northrop *et al.*²⁷ The standard deviations shown around each curve in the figure should be viewed with some caution since the actual distribution of data points about the mean at any frequency is not Gaussian, as will be demonstrated later.

Differences between the four 1-yr means are shown in Fig. 6, using hydrophone 74 as the reference at 0 dB. The two bottom hydrophones, 74 and 76, have nearly identical means as might be expected from their 40-km spacing and similar environment. Differences between these two curves at frequencies above 10 Hz may be the result of small errors in the estimates of their respective cable responses. Suspended SOFAR hydrophone 20 is quieter than 74 below about 2 Hz, and noisier above 3 Hz. Increased levels at high frequencies are due to this hydrophone's location within the SOFAR channel, a highly efficient waveguide capable of propagating noise at these frequencies over many thousands of kilometers. Levels are consistently lower below about 2 Hz, with the difference increasing to

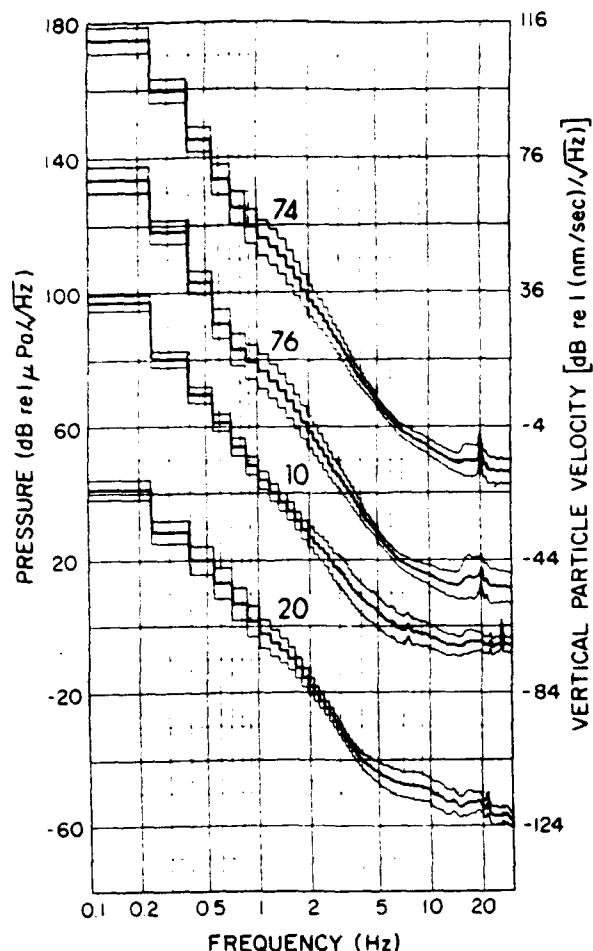


FIG. 5. One-year mean ambient noise level spectra, plus and minus one standard deviation, for hydrophones 74, 76, 10, and 20. Vertical particle velocities corresponding to acoustic pressure fluctuations are computed using the formula: pressure = water density \times sound velocity in water \times vertical particle velocity.

18 dB near 0.15 Hz. Although this difference could be nearly eliminated by using a higher frequency pressure compensation corner in the response curve of hydrophone 20, its shallower depth (780 vs 5400 m) could also be the cause of the difference. For example, if the low-frequency noise is predominantly fundamental mode Rayleigh waves, then for a given amplitude of bottom motion the pressure in the water below a certain frequency is proportional to the depth (i.e., the water simply acts as a passive load on the bottom²⁸). In this case, the difference in depth would produce a 17-dB difference in level, in good agreement with the above observation. SOFAR hydrophone 10 is generally noisier than all other hydrophones. This is most likely the result of its location only 3 km from the shores of Wake, where breaking surf is an additional energetic source of noise.

The 1-yr mean noise spectra of hydrophones 74 and 20 are compared to several other oceanic and continental ambient noise spectra in Fig. 7. The WIHA curves are most similar to the other oceanic curves, two from hydrophones in the Atlantic¹² and one from a differential pressure gauge in the Pacific.²⁹ Two continental noise spectra, corrected to

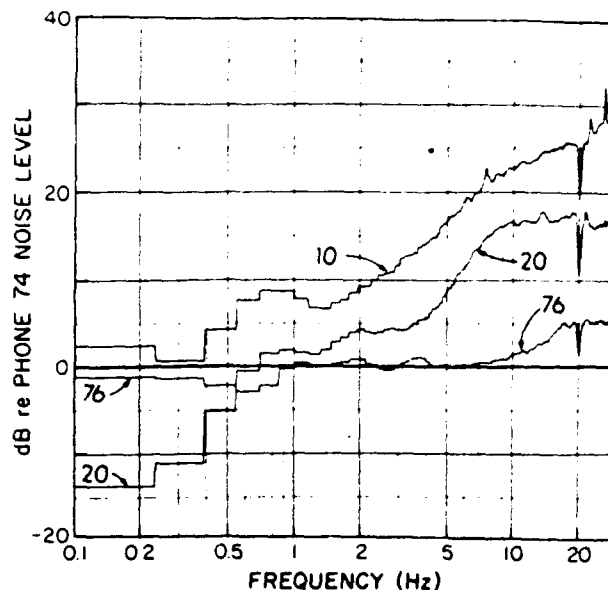


FIG. 6. The one-year noise means of hydrophones 76, 10, and 20 measured relative to the one-year noise mean of hydrophone 74 at 0 dB.

pressure, are also shown for reference. One of them represents the average ambient noise on continents,³⁰ and the other is from an extremely low noise site in Texas.³¹

IV. TEMPORAL VARIATIONS OF THE NOISE AND WIND

In order to graphically view the information contained in the 192 time series associated with each hydrophone, the data were reduced into only 15 time series for each hydrophone. These new time series represent the ambient noise level fluctuations over the 1-yr period in 15 contiguous 2-Hz bands from 0 to 30 Hz. Computation of the new time series was made as follows. Each 2-Hz band represents approximately 13 original time series (i.e., 192 original/15 new = 12.8). Each data point in an original time series represents the noise level for a particular 6-h time period in a 0.156-Hz frequency band (i.e., 30 Hz/192 = 0.156 Hz). By averaging the dB noise levels from the appropriate original time series for each 2-Hz band, 15 new time series are formed. If an original time series was just fractionally represented in a particular 2-Hz band, then it was included in the average only if that fraction was greater than one-half. Note that by averaging in log space (dB), similarities in the shapes of the original time series are emphasized—the original time series with the most power does not unduly influence the result. Similarly, note that in the 0–2 Hz band this type of averaging will de-emphasize the microseism peak data since it is represented only in the two lowest-frequency original time series.

The 15 time series from hydrophone 74 are shown in Fig. 8. The 2–4 Hz time series appears truncated across the top, and exhibits noise lows that are as much as 15 dB below the apparent noise ceiling. Similar features at these frequencies were reported by Duennebie *et al.*³² in the ambient noise data from a long-term deployment of HIG's ocean sub-bottom seismometer down a deep-sea drill hole

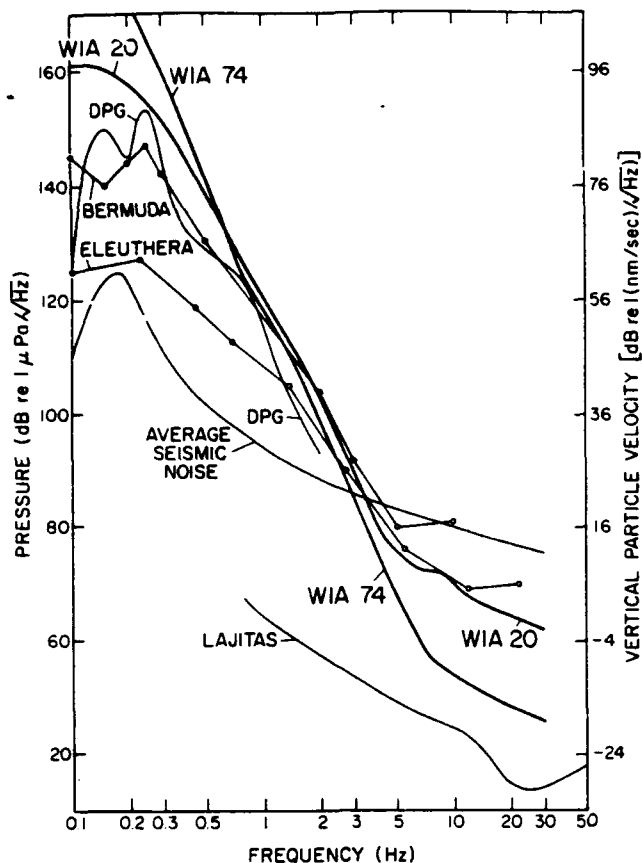


FIG. 7. The one-year mean noise spectra of WIHA hydrophones 74 and 20 compared to noise measurements made elsewhere. The Eleuthera Island measurement is a 6-week average made by Nichols¹² using a hydrophone at 1300-m depth. The Bermuda Island measurement is an average of four 10-min samples taken during 6.4-m/s average winds using a hydrophone at 4300-m depth (Talpey-Worley data reported by Nichols¹²). The differential pressure gauge data (DPG) reported by Cox *et al.*²⁹ was collected at 1600-m depth off the California coast. The "average seismic noise" reported by Brune and Oliver³⁰ is from vertical seismometer measurements made on continents. The Lajitas, Texas curve given by Herrin³¹ represents very low continental noise.

near the Kuril Islands. The time series for frequencies above 6 Hz, on the other hand, appear truncated at the bottom and exhibit noise peaks with amplitudes 20 dB or more above the apparent noise floor. The 4–6 Hz time series seems to be a transition between the 2–4 and >6 Hz bands, and is flat-middled with some lows and some peaks. Only the 0–2 Hz curve appears to be unrestricted throughout its amplitude range. Some of the large amplitude signals most prominent on the 16–18 Hz curve but also visible on adjacent curves are caused by whales.

One hundred days of ambient noise in six of the fifteen 2-Hz bands for all four hydrophones is shown in Fig. 9. Curves for the two bottom hydrophones, 74 and 76, appear similar in all bands as might be expected given that these two hydrophones are at the same depth and are only 40 km apart. Comparisons between curves for the bottom and the SOFAR hydrophones show far fewer similarities. They appear perhaps the most coherent in the 0–2 Hz range where absolute noise levels are also the most similar. Above 2 Hz, the SOFAR hydrophones are decreasingly coherent with

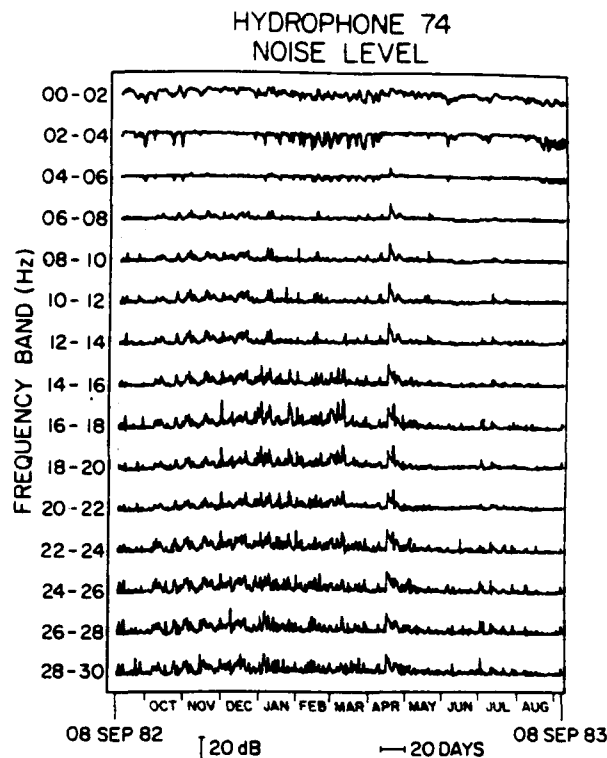


FIG. 8. A plot of the temporal variations in ambient noise over one year for all fifteen 2-Hz bands from Wake bottom hydrophone 74.

respect to the bottom hydrophones and with respect to each other.

The relationship between ambient ocean noise and wind is demonstrated in Fig. 10. It compares six of the 1-yr-long, 2-Hz-wide time series from hydrophone 76 with time series of the Wake daily mean wind speed and direction from the NWS monthly summaries. At 0–2 Hz, the two data sets are remarkably similar, with nearly all major features represented in both curves. At 2–4 Hz and 4–6 Hz, noise lows nearly always correspond with low wind, and above 6 Hz noise peaks nearly always correspond with high wind.

To quantify these similarities, correlation coefficients and lag times were computed between the wind speed curve and each noise curve. Values are given in Table I. The 0–2 Hz noise data have a fairly high correlation coefficient, 0.77, and a lag time of +6 h, indicating that the noise is delayed relative to the wind by an amount equal to one sampling interval. This time shift may be an indication of the lag between the onset of winds and the full development of waves that produce the noise. The correlation coefficient for the 2–4 Hz data is 0.54 with a lag of +6 h. That correlation can be improved to 0.71, with the same lag, by truncating the wind speed curve for values above 6.26 m/s (the mean wind speed) to give it a character more like the 2–4 Hz noise curve. The correlation coefficient for the 4–6 Hz curve is 0.49 with a lag of 0 h. This lower correlation is probably attributable to the relative lack of features in the noise curve for this frequency band. The 12–14 Hz curve has a correlation coefficient of 0.67 with a lag of 0 h. Similar correlation and lag values are

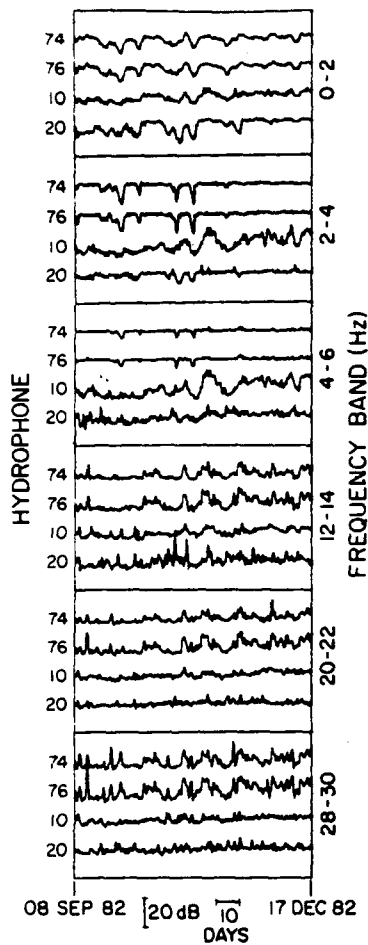


FIG. 9. Comparison in six frequency bands between temporal noise level fluctuations of the four hydrophones studied over a 100-day period.

TABLE I. Correlation coefficients and lag times for the wind speed time series compared to each ambient noise time series. Values shown are the maximum correlation coefficient followed by its corresponding lag in hours. A positive lag indicates that the noise lagged behind the wind.

Frequency band (Hz)	Hydrophone 74	Hydrophone 76	Hydrophone 10	Hydrophone 20
00-02	0.77/+06	0.80/+06	0.80/+06	0.78/+12
02-04	0.54/+06	0.56/+06	0.65/+12	0.38/+12
04-06	0.49/+00	0.57/+00	0.65/+18	0.26/+36
06-08	0.64/+00	0.73/+00	0.62/+18	0.28/+30
08-10	0.65/+00	0.72/+00	0.55/+18	0.26/+30
10-12	0.66/+00	0.73/+00	0.54/+18	0.28/+12
12-14	0.67/+00	0.73/+00	0.47/+24	0.25/+06
14-16	0.57/+00	0.60/+00	0.42/+18	0.22/+06
16-18	0.27/+00	0.31/+00	0.23/+18	0.21/+12
18-20	0.30/+00	0.33/+00	0.25/+30	0.18/-06
20-22	0.34/+00	0.37/+00	0.31/+30	0.22/-06
22-24	0.48/+00	0.48/+00	0.34/+18	0.27/-06
24-26	0.52/+00	0.52/+00	0.40/+12	0.30/+00
26-28	0.54/+00	0.54/+00	0.35/+18	0.27/-06
28-30	0.51/+00	0.51/+00	0.36/+18	0.20/+00

found for all other curves between 6 and 16 Hz. A much lower correlation, 0.34 with a lag of 0 h, was found for the 20-22 Hz data, and low values were also found for 16-18 and 18-20 Hz curves (not shown). These low correlation values are probably the result of partial contamination of the noise data by the aforementioned 20-Hz artifact and whale noises. The correlation coefficient for the 28-30 Hz curve is 0.51 with a lag of 0 h, and similar values were found for the other curves between 22 and 28 Hz. The 0-h lag found for all curves above 4 Hz indicates that noise at these frequencies responds quickly to changes in wind speed. Correlations and lags for hydrophone 76 are very

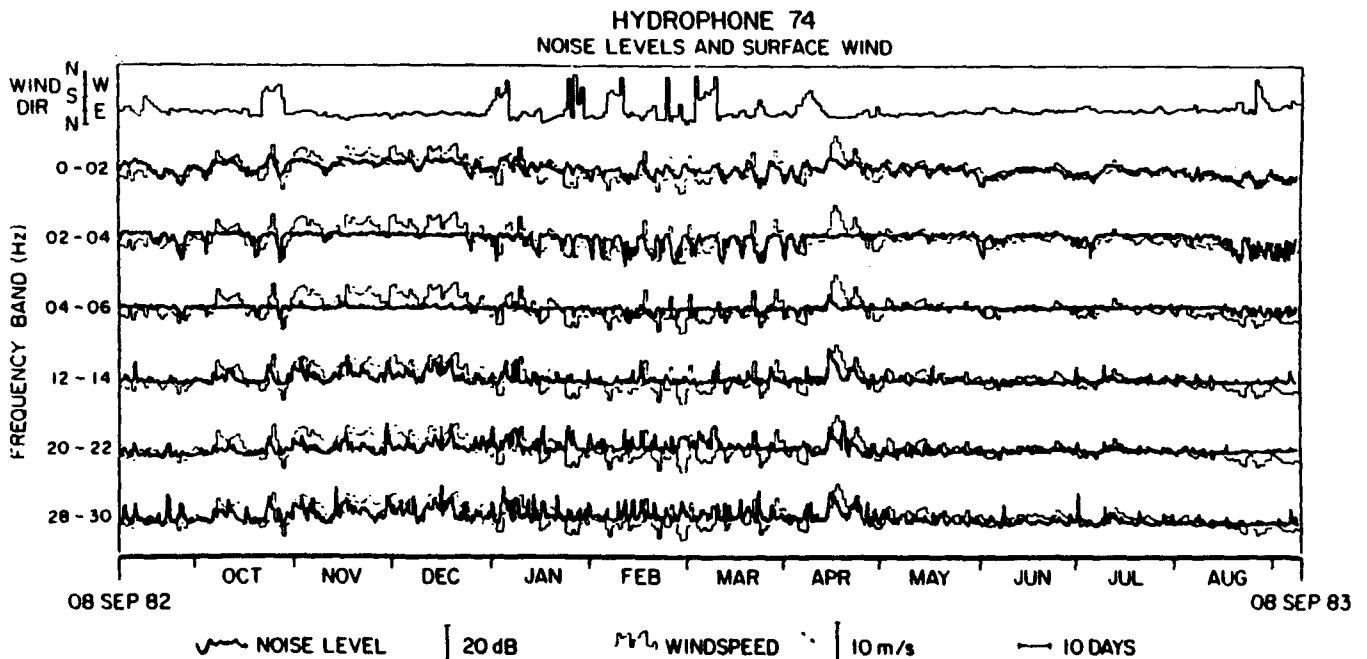


FIG. 10. Comparison between the temporal fluctuations of the ambient ocean noise on hydrophone 74 in six frequency bands (thick lines), the daily mean wind speed at Wake Island (thin lines), and the daily mean wind direction at Wake Island (top).

similar to those for hydrophone 74, as might be expected. Slightly higher correlation values for hydrophone 76 may be because this hydrophone is 40-km closer to Wake Island where the wind speeds are measured.

Hydrophone 10, located just offshore of Wake Island, has a correlation of 0.80 and a lag of +6 h for its 0–2 Hz time series compared to wind speed. The 2–4 Hz time series has a correlation coefficient of 0.65 with a lag of +12 h. These values are similar to those found for the deep bottom hydrophones, although the 2–4 Hz lag is one sample longer. Between 4 and 16 Hz the six correlation coefficients average 0.54, but there are five lags of +18 h and one lag of +24 h. These long lags are consistent with a hypothesis that this noise is from waves breaking on the shoreline of Wake. The longer wavelength ocean waves associated with surf take more time to develop in the wind. Between 16 and 22 Hz, correlations are again much lower, averaging 0.26. Above 22 Hz there is only a slight increase in the average correlation to 0.36. Lag times for these seven curves are also long, averaging more than 20 h.

The correlation coefficients for hydrophone 20 at 0–2 and 2–4 Hz are 0.78 and 0.38, respectively, with lags of +12 h. This somewhat longer lag relative to the other hydrophones could be caused by a combination of hydrophone 20's location more than 150 km to the southeast of Wake and the northwesterly approach of most frontal systems passing Wake. Above 4 Hz, correlation coefficients are uniformly low, averaging 0.25, with lags that vary from –6 h to +30 h. These low correlations are also probably due to hydrophone 20's long distance from Wake, as well as its location at the depth of the SOFAR channel axis. At this depth it is probably receiving noise generated over a broader region of the ocean's surface relative to the region heard by the deep bottom hydrophones whose noise levels above 4 Hz correlated more highly with wind speed. This contention is supported by the data in Fig. 6 showing that hydrophone 20 also has significantly higher absolute noise levels above 4 Hz relative to the bottom hydrophones.

Also shown in Fig. 10 is a time series of the daily mean wind direction at Wake. Kibblewhite and Ewans¹¹ have noted significantly increased ambient noise levels between 0.1 and 5 Hz measured by land seismometers along the west coast of New Zealand at the time of large shifts in the offshore wind direction, even in a moderate wind field. They attribute this elevated noise to increased pressure fluctuations on the ocean floor which are in turn caused by enhanced nonlinear wave interactions (Longuet-Higgins' theory¹) due to the wind shift. The Wake data, however, do not seem to exhibit the effect observed by Kibblewhite and Ewans, since there are many large changes in wind direction unaccompanied by corresponding increases in noise.

V. NOISE SPECTRA VERSUS WIND SPEED

The mean noise spectra for eight wind speed ranges from each of the four hydrophones is shown in Fig. 11. Each individual spectrum was determined by averaging all noise spectra over the 1-yr period from data recorded when the wind speed was within that particular range. The num-

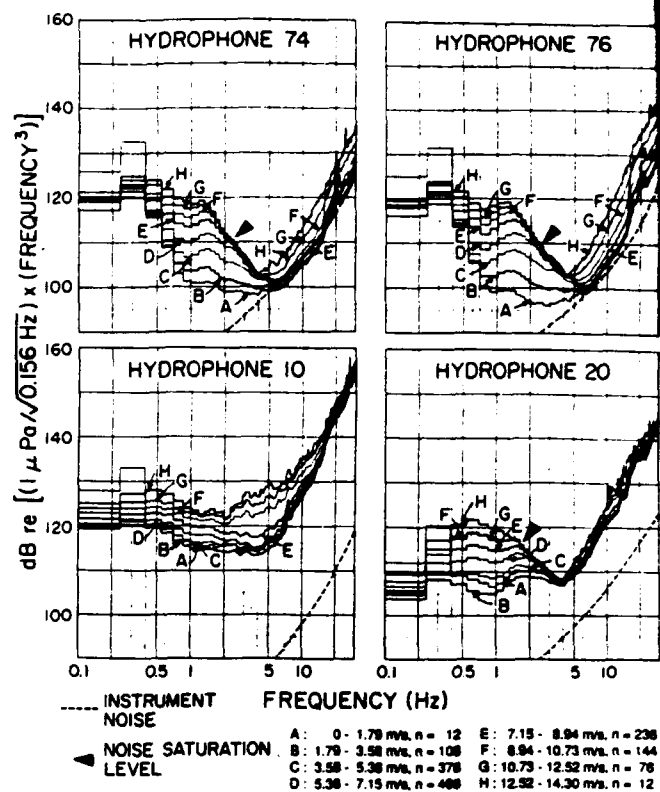


FIG. 11. Noise spectra from each hydrophone averaged in eight wind speed ranges. The number of spectra averaged together in each wind speed group, n , is indicated in the legend. Estimated instrumental noise levels are indicated by the dashed lines on each plot. The spectral data are multiplied by their frequency in Hz^2 to aid in visualization.

ber of spectra averaged in each wind speed range is different and is indicated on the plot. The spectral level of each data point, in microPascals (μPa), has been multiplied by its frequency squared before converting it to decibels (dB). This procedure has the effect of "rotating" each spectrum counterclockwise about its value at 1 Hz by 12 dB per octave. This rotation helps to visually clarify differences between individual spectra. Without it, the seven spectra in each plot would be indistinguishably bunched together because of their steep spectral slope. To convert a data point on this plot back to more conventional units of "dB relative to $1 \mu\text{Pa}/\sqrt{\text{Hz}}$ " simply add a correction term to its dB value on the plot. This correction term, $-40 \times \log_{10}(f)$, where f is the frequency of the data point in Hz, undoes the rotation. Figures 5 and 7 show similar data in these more conventional units.

The spectra in Fig. 11 from the two deep hydrophones, 74 and 76, are nearly identical. At the lowest frequencies, between 0.1 and 0.2 Hz, there is little variation that correlates with local winds. This is the band that contains the prominent worldwide spectral peak of double-frequency storm microseisms. The low correlation is not surprising since winds less than 14 m/s, the highest found in these data, are not expected to efficiently generate the 0.05 to 0.1 Hz swell required.³³ However, the observed variation in this band is large (20 to 30 dB) and is probably produced by Rayleigh waves generated near Wake by the interaction

of storm swell and its reflection from the Wake platform, or Rayleigh waves propagating from more distant sources. Sutton and Barstow¹⁵ present a clear demonstration of Rayleigh wave generation near an ocean-bottom seismometer by swell from distant storm centers. Further investigations of this frequency band, using spectra of higher resolution, are in progress.

Between 0.4 and 6 Hz, noise levels increase regularly with wind speed at rates of up to 2 dB per m/s until a saturation is reached, above which levels do not rise. This saturation is clearly apparent between about 1.5 and 5 Hz with a slope of about -23 dB/octave (-11 dB/octave on the rotated plot) and an absolute level of about 75 dB (99 dB on the rotated plot) at 4 Hz. It occurs at the highest frequencies when winds are low, but migrates to lower frequencies as winds increase. The saturation is not instrumental, since transient signals commonly exceed these levels by tens of dB. Between 0.3 and 0.8 Hz, the noise is bounded from below by minimum levels having a slope of about -30 dB/octave (-18 dB/octave on the plot). This feature does not appear related to the wind speed and it may be the high-frequency flank of the microseism peak. It is being investigated further. Between 6 and 30 Hz, low wind speed levels are close to the estimated system noise (dashed line). When the wind speed exceeds about 8 m/s, noise levels increase at rates of up to 2 dB per m/s. The spectral slope of this noise increases with frequency to about $+4$ dB/octave ($+16$ dB/octave in the figure) for frequencies > 10 Hz. Between 4 and 6 Hz this type of noise sometimes rises above the aforementioned saturated noise.

The phenomenon generating noise between 0.4 and 6 Hz is most likely local wind waves. If a 2:1 relationship between noise and wave frequencies is assumed, as predicted by nonlinear wave interaction theory, then the waves responsible for this noise have frequencies between 0.2 and 3 Hz. Phillips³⁴ has compiled data showing that ocean waves at these frequencies also exhibit a saturation or equilibrium above which they do not grow. Ocean waves with frequencies above 1.5 Hz have wavelengths less than 0.7 m and phase velocities less than 1 m/s. Such waves should reach equilibrium often in the winds common to Wake, and as a consequence, the ocean noise above 3 Hz near Wake should also be frequently saturated. From the figure it appears such saturation occurs about half the time. It is likely that deep ocean noise worldwide is also commonly saturated in this band. McCreery and Duennebie have named this saturated ocean noise the "Holu Spectrum," from the Hawaiian word for deep ocean.³⁵ Not only is the slope of the Holu Spectrum constant, its absolute level appears to have little if any variation with depth in the water column (note that levels on SOFAR hydrophone 20 are similar to those on the deep hydrophones), implying that it can be used as a constant for *in situ* calibration of ocean seismoacoustic instrumentation. In addition, noise levels in this band may yield a direct estimate of the ocean wave spectrum at short wavelengths.

At frequencies above 4 Hz, deep ocean noise may be acoustic signals from whitecaps or open-ocean breaking waves. This mechanism was proposed by Duennebie

*et al.*³⁶ based on data from a deep sea borehole seismometer. Like the WIHA deep hydrophones, the borehole seismometer exhibited noise levels that only began to rise when winds exceeded a certain speed. This characteristic is suggestive of whitecaps, since they too begin to form only when winds are above a certain speed. The Beaufort scale puts the whitecap wind speed threshold at 4 m/s, although Wake noise levels do not begin to increase until wind speeds exceed about 8 m/s. Measurements of this type of noise on WIHA hydrophones in the extreme winds of a typhoon show that it grows without bounds. These typhoon noise data will be presented in a later report.

The spectral view of the noise (Fig. 11) complements the time series view (Figs. 8, 9, and 10) discussed earlier. The flat top of the 2–4 Hz time series is the spectral saturation level; the flat middle of the 4–6 Hz time series is also the saturation level, sometimes overridden at high wind speeds by the higher frequency noise mechanism; and the flat bottoms of the time series above 6 Hz reflect the spectral noise minimum in this frequency band. Only the 0–2 Hz time series has a relatively unrestricted range, as do most of the spectral data in that band. In this band the noise is seldom saturated, thus reflecting a continuous variation with wind speed.

The noise spectra of suspended SOFAR hydrophone 20, also shown in Fig. 11, are very similar to those of the bottom hydrophones. Levels regularly increase with wind speed between 0.4 and 4 Hz at rates of up to 2 dB per m/s. Saturation of the noise is clearly visible between 1.5 and 4 Hz with a slope of about -20 dB/octave (-8 dB/octave on the plot), only slightly less steep than that observed on the deep hydrophones. This slight difference could be due to calibration errors. Absolute levels of the Holu Spectrum on this SOFAR hydrophone are very close to those found on the deep bottom. Above 4 Hz there is again a sharp difference in spectral slope to $+3$ dB/octave ($+15$ dB/octave on the plot) at frequencies > 10 Hz; however, noise levels increase with wind speed at rates less than 0.4 dB per m/s (this relation is not easily seen in the figure due to the closeness of the curves). The reduced rate of these increases with wind speed and the higher absolute amplitudes relative to those observed on the deep bottom hydrophones may be caused by this hydrophone's location at the depth of the SOFAR channel axis, and thus its susceptibility to high-frequency noise from more distant sources. Instrumental noise is not a factor in these spectra.

The spectra from SOFAR hydrophone 10 are also clearly wind related, although they have a much different character than those of the other three hydrophones. Over the entire band shown in the figure, 0.1 to 30 Hz, noise levels grow with increasing wind speed. The highest rates of growth, up to 2 dB per m/s, are found between about 2 and 6 Hz. There is no saturation level apparent in these spectra, nor is there an abrupt change in spectral slope at around 4 Hz, but only a more gradual change between 1 and 10 Hz. In addition, as noted previously, absolute noise levels are generally higher than those observed on the other three hydrophones. These differences are probably the result of hydrophone 10's close proximity to Wake Island,

HYDROPHONE 74

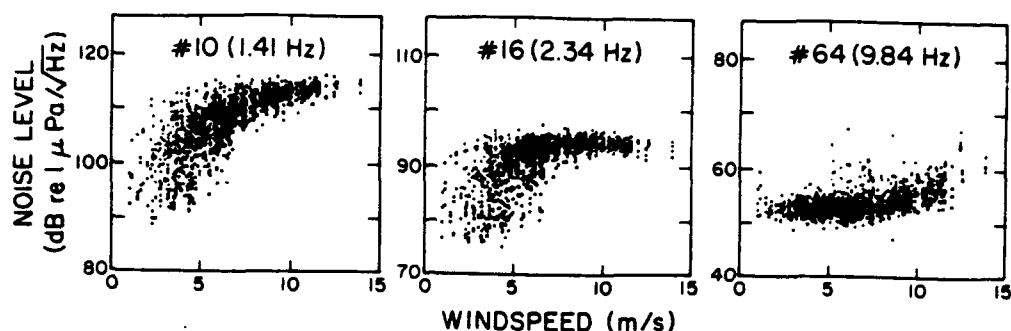


FIG. 12. Each of the 1460 noise level measurements from hydrophone 74 made over a 1-yr period at three discrete frequencies, plotted as a function of wind speed to show the level of scatter in the data. The spectral estimate number and its corresponding frequency are noted for each plot.

where additional noise is generated by the breaking of wind waves and swell on the shore of the island.

VI. NOISE LEVEL VERSUS WIND SPEED SCATTER

The distribution of the 1460 individual noise level measurements from hydrophone 74, were examined at three discrete frequencies out of the possible 192 as a function of wind speed (Fig. 12). The largest range of noise levels is at 1.41 Hz, although the saturation level is clearly visible. Scatter at this frequency varies from about 20 dB at the lower wind speeds to less than 5 dB at the higher wind speeds where the noise is saturated. At 2.34 Hz the saturation level is dominant over a wider interval of wind speeds, as can also be seen in the spectra of Fig. 11. Interestingly, the saturation level appears to be slightly lower at the highest wind speeds. This phenomenon may be caused by the high speed winds blowing the tops off of short-wavelength waves and beating them down with spray. Scatter at 2.34 Hz is similar to that observed at 1.41 Hz. At 9.84 Hz, the noise level is fairly constant at the lower wind speeds (the noise floor), and scatter is generally less than 10 dB throughout the plot.

At least three factors may contribute to scatter in these data. The first is simply the error in the measurement due to the randomness of the stochastic processes producing the noise. The chi-squared statistics underlying these spectral measurements lead to a range of scatter of about 3 dB for 90% of the data. This may be all that is needed to explain the scatter in the saturated noise. The second factor is that wind speed is measured at Wake Island, and not directly over the hydrophones. Hydrophone 74, for example, is more than 100 km away from Wake. Thus, there may be a lead time or a lag time or even no correspondence at all between wind speeds at Wake Island and wind speeds directly over the hydrophones. The third factor is that wind wave heights are a function of the duration of the wind and the fetch over which it blows, as well as the wind speed. For example, in the case of a fresh wind blowing over a calm sea, it is well known that long-period wind waves take more time to reach saturation than short-period wind waves. There is supportive evidence for this phenomenon in the correlation lags between the noise and wind

speed time series previously discussed. A delay between the onset of wind and the corresponding onset of noise has also been observed and described by Duennebier *et al.*³⁶ Thus, scatter is introduced into these plots by the nature of the mechanism that converts wind energy into wave energy, since it seems likely that the noise is caused by the wind waves rather than by the wind.

Note from these plots that the distribution of the 1460 noise levels at each frequency is not Gaussian. Referring back to Fig. 5, the standard deviations shown should be viewed appropriately.

Also note that from the Fig. 12 plots for 1.41 and 2.34 Hz, it might be misconstrued that the saturation level is merely an artifact of plotting noise levels using a logarithmic scale (dB). If noise levels in non-logarithmic units ($\mu\text{Pa}/\sqrt{\text{Hz}}$) are linearly related to wind speed, and the scatter is uniform at all wind speeds, then plots of these data in dB might look similar to the plots in the figure. The data would bend to the right, and the scatter would appear reduced at higher noise levels. However, the WIHA data were tested for this possibility by making such non-logarithmic plots, and the saturation level remained a clear feature of the data.

VII. CONCLUSIONS

Ambient infrasonic ocean noise levels observed over a period of 1 yr on four hydrophones in the northwestern Pacific near Wake Island vary with wind speed at the ocean's surface at rates of up to 2 dB per m/s. This wind-related noise is categorized into three types. The first type, observed between 0.4 and 6 Hz on two deep-bottom hydrophones and one suspended SOFAR hydrophone, is characterized by levels that rise with wind speed to a clearly defined saturation level—the Holu Spectrum. The data suggest that this noise is directly related to the spectrum of wind waves on the ocean's surface, with a correspondence between saturation of the wind waves and saturation of the noise. The Holu Spectrum has a slope of about -23 dB/octave and a level of about 75 dB relative to $1 \mu\text{Pa}/\sqrt{\text{Hz}}$ at 4 Hz, and it appears to vary little if at all with depth in the water column. It is probably a worldwide constant. Between 0.3 and 0.8 Hz, the noise has minimum

levels that define a slope of about -30 dB/octave. This slope may be the high-frequency flank of microseism-peak-type noise. The second type of wind-related noise, observed between 4 and 30 Hz on all four hydrophones studied, is characterized by spectral slopes markedly less steep than those observed for the first type of noise, and also by the absence of a saturation level. At higher wind speeds this noise overrides the saturation level of the first type of noise. Wind waves breaking on the sea surface may be the source of this noise. The third type of wind-related noise is observed between about 0.5 and 10 Hz on the SOFAR hydrophone anchored near Wake Island. It is characterized by much higher absolute levels relative to those observed on the other three hydrophones. These higher levels and the close proximity of this hydrophone to Wake Island suggest that this noise is probably generated by wind waves breaking on the shore of the island.

ACKNOWLEDGMENTS

Appreciation is expressed to Daniel Walker, Eduard Berg, Robert Cessaro, William Prothero, and Thomas Schroeder for their valuable comments and discussions. Firmin Oliveira patiently programmed and ran many of the data collection and processing routines. Kentron Corporation and the U.S. Air Force, Det. 4, 15th ABW provided diligent day-to-day support of the data collection system at Wake Island. Editorial comments and corrections were made by Barbara Jones. Support for this research came from the Office of Naval Research, Code 1125GG, the Air Force Office of Scientific Research (Contract No. F49620-86-C-0003 and Grant No. 86-0039), and the U.S. Arms Control and Disarmament Agency. This work was performed in partial fulfillment of the requirements for the degree of Doctor of Philosophy in geology and geophysics. School of Ocean and Earth Science and Technology 3159.

- ¹ M. S. Longuet-Higgins, "A Theory of the Origin of Microseisms," *Philos. Trans. R. Soc. London Ser. A* **243**, 1-35 (1950).
- ² M. Miche, "Mouvements Ondulatoires de la Mer en Profondeur Constante on Decroissante," *Ann. Ponts Chaussees* **114**, 25-87 (1944).
- ³ K. Hasselmann, "A Statistical Analysis of the Generation of Microseisms," *Rev. Geophys.* **1**, 177-210 (1963).
- ⁴ R. A. Haubrich, W. H. Munk, and F. E. Snodgrass, "Comparative spectra of microseisms and swell," *Bull. Seismol. Soc. Am.* **53**, 27-37 (1963).
- ⁵ G. Latham, R. Anderson, and M. Ewing, "Pressure Variations Produced at the Ocean Bottom by Hurricanes," *J. Geophys. Res.* **72**, 5693-5704 (1967).
- ⁶ G. Latham and A. Nowroozi, "Waves, Weather, and Ocean Bottom Microseisms," *J. Geophys. Res.* **73**, 3945-3956 (1968).
- ⁷ J. Oliver and M. Ewing, "Microseisms in the 11- to 18-second Period Range," *Bull. Seismol. Soc. Am.* **47**, 111-127 (1962).
- ⁸ G. M. Wenz, "Acoustic Ambient Noise in the Ocean: Spectra and Sources," *J. Acoust. Soc. Am.* **34**, 1936-1956 (1962).
- ⁹ N. Barstow, G. H. Sutton, and J. A. Carter, "Particle Motion and Pressure Relationships of Ocean Bottom Noise at 3900 m depth: 0.003 to 5 Hz," *Geophys. Res. Lett.* **16**, 1185-1188 (1989).
- ¹⁰ B. R. Kerman, "Underwater Sound Generation by Breaking Wind Waves," *J. Acoust. Soc. Am.* **75**, 149-165 (1984).
- ¹¹ A. C. Kibblewhite and K. C. Ewans "Wave-wave Interactions, Microseisms, and Infrasonic Ambient Noise in the Ocean," *J. Acoust. Soc. Am.* **78**, 981-994 (1985).
- ¹² R. H. Nichols, "Infrasonic Ambient Ocean Noise Measurements: Eleuthera," *J. Acoust. Soc. Am.* **69**, 974-981 (1981).
- ¹³ R. H. Nichols, "Infrasonic Ocean Noise Sources: Wind Versus Waves," *J. Acoust. Soc. Am.* **82**, 1395-1402 (1987).
- ¹⁴ A. J. Perrone, "Infrasonic and Low-Frequency Ambient Noise Measurements on the Grand Banks," *J. Acoust. Soc. Am.* **55**, 754-758 (1974).
- ¹⁵ G. H. Sutton and N. Barstow, "Ocean-Bottom Ultralow-Frequency (ULF) Seismo-Acoustic Ambient Noise: 0.002 to 0.4 Hz," *J. Acoust. Soc. Am.* **87**, 2005-2012 (1990).
- ¹⁶ S. C. Webb and C. S. Cox, "Observations and Modeling of Seafloor Microseisms," *J. Geophys. Res.* **91**, 7343-7358 (1986).
- ¹⁷ J. H. Wilson, "Very Low Frequency (VLF) Wind-Generated Noise Produced by Turbulent Pressure Fluctuations in the Atmosphere near the Ocean Surface," *J. Acoust. Soc. Am.* **66**, 1499-1507 (1979).
- ¹⁸ C. S. McCreery, "Yield Estimation from Spectral Amplitudes of Direct P and P Coda Recorded by the Wake Island Deep Ocean Hydrophone Array," *Bull. Seismol. Soc. Am.* **77**, 1748-1766 (1987).
- ¹⁹ C. S. McCreery, D. A. Walker, and G. H. Sutton, "Spectra of Nuclear Explosions, Earthquakes, and Noise from Wake Island Bottom Hydrophones," *Geophys. Res. Lett.* **10**, 59-62 (1983).
- ²⁰ D. A. Walker, "Deep Ocean Seismology," *Eos* **65**, 2-3 (1984).
- ²¹ D. A. Walker and C. S. McCreery, "Deep Ocean Seismology: Seismicity of the Northwestern Pacific Basin Interior," *Eos* **69**, 742-743 (1988).
- ²² S. N. Thanos, *OBS Calibration Manual* (Lamont Geological Observatory, Columbia Univ., New York, 1966), p. 23.
- ²³ N. Barstow, G. H. Sutton, and J. A. Carter, "Particle Motion and Pressure Relationships of Ocean Bottom Noise: 3900 m Depth; 0.003 to 5 Hz," *Geophys. Res. Lett.* **16**, 1185-1188 (1989).
- ²⁴ "Local Climatological Data, Monthly Summaries for Wake Island, PC," National Climatic Data Center, Asheville, NC.
- ²⁵ R. J. Urick, *Principles of Underwater Sound* (McGraw-Hill, New York, 1983), p. 423.
- ²⁶ W. A. Watkins, P. Tyack, K. Moore, and J. E. Bird, "The 20-Hz signals of finback whales (*Balaenoptera physalus*)," *J. Acoust. Soc. Am.* **82**, 1901-1912 (1987).
- ²⁷ J. Northrop, W. C. Cummings, and M. F. Morrison, "Underwater 20-Hz Signals Recorded Near Midway Island," *J. Acoust. Soc. Am.* **49**, 1909-1910 (1971).
- ²⁸ H. Bradner, "Probing the sea-bottom sediments with microseismic noise," *J. Geophys. Res.* **68**, 1788-1791 (1963).
- ²⁹ C. Cox, T. Deaton, and S. Webb, "A Deep-sea Differential Pressure Gauge," *J. Atmos. Ocean Technol.* **1**, 237-246 (1984).
- ³⁰ J. Brune and J. Oliver, "The seismic noise of the earth's surface," *Bull. Seismol. Soc. Am.* **49**, 349-353 (1959).
- ³¹ E. Herrin, "The resolution of seismic instruments used in treaty verification research," *Bull. Seismol. Soc. Am.* **72**, S61-S67 (1982).
- ³² F. K. Duennebie, R. K. Cessaro, and P. Anderson, "Geo-acoustic noise levels in a deep ocean borehole," in *Ocean Seismo-Acoustics*, edited by T. Akal and J. M. Berkson (Plenum, New York, 1986), pp. 743-751.
- ³³ A. C. Kibblewhite and C. Y. Wu, "The theoretical description of wave-wave interaction as a noise source in the ocean," *J. Acoust. Soc. Am.* **89**, 2241-2252 (1991).
- ³⁴ O. M. Phillips, *The Dynamics of the Upper Ocean* (Cambridge U.P., Cambridge, England, 1977), p. 113.
- ³⁵ C. S. McCreery and F. K. Duennebie, "The Holu Spectrum: A Worldwide Deep-Ocean Constant, and Indicator of the Ocean Wave Spectrum," *Eos* **69**, 1245 (1988).
- ³⁶ F. K. Duennebie, C. S. McCreery, D. Harris, R. K. Cessaro, C. Fisher, and P. Anderson, "OSS IV: noise levels, signal-to-noise ratios, and noise sources," *Init. Rep. DSDP* **88**, 89-103 (1987).

LONG-TERM AMBIENT OCEAN NOISE, 0.05-30 HZ,
FROM THE WAKE ISLAND HYDROPHONE ARRAY

A DISSERTATION SUBMITTED TO THE GRADUATE DIVISION OF THE
UNIVERSITY OF HAWAI'I IN PARTIAL FULFILLMENT OF THE
REQUIREMENTS FOR THE DEGREE OF

DOCTOR OF PHILOSOPHY

IN

GEOLOGY AND GEOPHYSICS

MAY 1992

BY

Charles Stoddard McCreery

Dissertation Committee:

Daniel A. Walker, Chairperson
Frederick K. Duennebier
George H. Sutton
Gerard J. Fryer
Thomas A. Schroeder

We certify that we have read this dissertation and that, in our opinion, it is satisfactory in scope and quality as a dissertation for the degree of Doctor of Philosophy in Geology and Geophysics.

DISSERTATION COMMITTEE

Daniel A. Walker

Chairperson

John D. ...

Joseph W. ...

Grand J. ...

Thomas A. ...

ACKNOWLEDGMENTS

I first wish to thank my committee chairman, Daniel A. Walker, for his unwavering support, inspiration, and advice throughout the long course of this project. I am also very indebted to the other members of my committee, Frederick K. Duennebier, George H. Sutton, Gerard J. Fryer, and Thomas A. Schroeder, for their numerous and useful discussions and suggestions. Further appreciation is expressed to Patricia Cooper and L. Neil Frazer who served as committee member proxies at the dissertation defense and offered helpful comments. The Office of Naval Research (ONR) - Code 1125GG, provided funding for most of the research, and I am grateful to Randy Jacobson and Joseph Kravitz of that agency for their encouragement and insights. Mike Purdy and George Frisk of the Woods Hole Oceanographic Institute also deserve mention for the role they played in helping to secure ONR support for this work. Additional funding was received from the Air Force Office of Scientific Research and the U.S. Arms Control and Disarmament Agency. The U.S. Air Force, Detachment 4, 15th Air Base Wing, along with Kentron Corporation and Intelcom Corporation provided outstanding logistical support for the hydrophone data collection system at Wake Island. Firmin Oliveira wrote the real-time data collection software, and a substantial portion of the initial data processing software. Mike Simpson, Bob Cunningham, Pat Townsend, and Julie Jirikowic are largely responsible for the excellent computing facilities used to perform the analysis. And many other friends and colleagues within the School of Ocean and Earth Science and Technology have contributed in helpful ways to this research. Finally, on the personal side, I wish to express the deepest gratitude to my parents, to all the members of my family, and to my wife for their long-term support and sacrifices that have enabled me to do this work.

ABSTRACT

Samples of ambient ocean noise, 0.05-30 Hz, from the Wake Island Hydrophone Array are compared to measured local winds and estimated local ocean waves. In addition, continuous noise data during the passage of a typhoon directly over the array, and during a 41-day period are spectrally analyzed in fine detail. The noise is divided into six frequency bands, based upon properties it is found to exhibit. From 0.05 to 0.1 Hz, a region of the ocean noise spectrum known to have extremely low levels, the Wake data are limited by system noise. However, Rayleigh waves from moderately sized earthquakes are frequently observed in this band, and the primary pressure signal from local ocean swell is also observed on a hydrophone at 850m depth. Between 0.1 and 0.2 Hz, the noise appears to be caused by double-frequency pressure fluctuations from local ocean swell, as predicted by nonlinear wave interaction theory. During periods of large swell, levels of this noise are the maximum in the spectrum. More commonly, however, peak spectral levels are found between 0.2 and 0.3 Hz. Noise in this band correlates less strongly with estimated local ocean waves, and it may have a more distant origin with conversion to Rayleigh wave-type propagation. From 0.3 to 1.5 Hz, the noise correlates strongly with both wind and waves, indicating its source is the local wind waves. The frequency correspondence between this noise and the estimated ocean waves, however, is between 5:1 and 10:1, a puzzling result. Between 1.5 and 6 Hz, noise levels increase with wind speed to a clearly defined saturation level that almost certainly corresponds to the known saturation of short wavelength ocean wind waves. Between 2 and 5 Hz, noise levels are saturated more than 80% of the time. This saturated noise is probably a constant in all the world's oceans, and is called the holu spectrum from the Hawaiian word for deep ocean. From 4 to 30 Hz, noise levels remain constant until wind speeds exceed about 8 m/s, suggesting this noise may be from whitecaps. Levels in this band grow unbounded, and during the typhoon they increased by more than 30 dB.

TABLE OF CONTENTS

ACKNOWLEDGMENTS	iii
ABSTRACT	iv
LIST OF TABLES	viii
LIST OF FIGURES	ix
LIST OF ABBREVIATIONS	xii
CHAPTER 1. INTRODUCTION	1
CHAPTER 2. DATA	7
Noise Data from the Wake Island Hydrophone Array	7
• History of the Array	7
• Description of the Array	9
• Recording Systems and Data Formats	12
<i>September, 1982 - March, 1988</i>	12
<i>April, 1988 - January, 1989</i>	14
<i>September, 1989 - March, 1990</i>	14
• Calibration of the Hydrophone Data	16
<i>Hydrophones</i>	17
<i>Cables</i>	19
<i>Amplifiers</i>	19
<i>Analog-to-Digital Convertor</i>	21
<i>Complete System</i>	21
• System Noise	24
Surface Wind Measurements	24

Ocean Gravity Wave Estimates	25
• Spectral Ocean Wave Model.....	26
• Global Spectral Ocean Wave Model.....	26
Typhoon Data	26
CHAPTER 3. METHODOLOGY	28
Spectral Analysis	28
• Discrete Fourier Transform - Derivation and Meaning	28
• Implementation of the FFT	32
• Spectral Units	34
<i>Normalization</i>	34
<i>Resolution</i>	35
<i>Decibels</i>	35
<i>Calibration</i>	36
• Statistical Properties of the Spectral Estimates.....	36
• Summary	37
Computer Programs	38
• FPLOT - Time Series Plots.....	38
• TFORM - Time to Frequency Domain Transformation	39
• SPCGRM - Spectrogram Plots.....	39
• SPCPLT - Spectrum Plots.....	40
CHAPTER 4. 0.5-30 HZ NOISE AND WIND	41
Data Set	41
Data Reduction	41
• Spectral Computation.....	41

• Removal of Transients	42
One-Year Mean Spectra	45
Temporal Variations	51
Spectral Variations	60
Distribution of the Data	66
CHAPTER 5. 0.1-5 HZ NOISE AND OCEAN WAVES	72
Data Set	72
Long-Term Noise Characteristic	73
Noise and Waves	84
CHAPTER 6. TYPHOONS	90
Typhoon Owen	90
Typhoon Doyle	93
Other Typhoons	100
CHAPTER 7. 0.05-0.5 HZ FINE SCALE NOISE CHARACTERISTICS	102
CHAPTER 8. CONCLUSIONS	109
0.05-0.1 Hz	109
0.1-0.2 Hz	110
0.2-0.3 Hz	111
0.3-1.5 Hz	112
1.5-6 Hz	113
4-30 Hz	113
REFERENCES	115

LIST OF TABLES

<u>Table</u>	<u>Page</u>
1. Noise and Wind Speed: Correlations and Lags	58
2. Earthquakes Producing Rayleigh waves observed on the WIHA hydrophones: October 21 - November 3, 1989	106

LIST OF FIGURES

<u>Figure</u>	<u>Page</u>
1. Generic ambient ocean noise power spectral density curve	4
2. Some possible mechanisms for the generation of 0.05-30 Hz seismoacoustic noise in deep ocean basins by ocean waves.....	6
3. Location of Wake Island in the northwestern Pacific Ocean.....	10
4. Layout of the Wake Island Hydrophone Array.....	11
5. Response curves for the WIHA hydrophones.....	18
6. Response curves for the WIHA sea cables	20
7. Response curves for the WIHA amplifiers	22
8. Response curves for some of the WIHA hydrophone-amplifier configurations	23
9. An example of the effect of removing transients from a time series of noise level variations.....	43
10. Percent number of transients in the noise data of hydrophone 74 as a function of frequency	44
11. One-year mean ambient noise level spectra, plus and minus one standard deviation, for hydrophones 74, 76, 10, and 20.....	46
12. The one-year noise means of hydrophones 76, 10, and 20 measured relative to the one-year mean of hydrophone 74 (at zero dB)	50
13. One-year mean noise spectra of hydrophones 74 and 20 compared to ambient noise measurements made elsewhere.....	52
14. Temporal variations in the ambient noise over a one-year period for all fifteen 2-Hz bands from WIHA bottom hydrophone 74.....	54

<u>Figure</u>	<u>Page</u>
15. Temporal noise level fluctuations over a 100-day period in six frequency bands for WIHA hydrophones 74, 76, 10, and 20	55
16. Hydrophone 74 temporal noise level fluctuations in six frequency bands compared to the wind speed and wind direction measured at Wake Island	56
17. Noise spectra from WIHA hydrophones 74, 76, 10, and 20 for seven wind speed ranges	61
18. Scatter in the noise level measurements as a function of wind speed	68
19. A forty-day comparison of ocean noise, estimated ocean waves, and daily mean wind speeds typical of summertime	75
20. A forty-day comparison of ocean noise, estimated ocean waves, and daily mean wind speeds typical of wintertime.....	76
21. Cross correlations between the hydrophone 74 noise level fluctuations at different frequencies	78
22. Distribution of noise levels from hydrophone 74 over a 46-month period.....	79
23. Distribution of noise levels from hydrophone 74 over a 46-month period, with only the summer months of April through September represented	80
24. Distribution of noise levels from hydrophone 74 over a 46-month period, with only the winter months of October through March represented.....	81
25. Amplitudes and frequencies of the microseism peak on hydrophone 74 from measurements made every six hours over a 46 month period	83
26. Cross correlations between the noise and the waves for a ± 6 month range of lags.....	86

<u>Figure</u>	<u>Page</u>
27. Cross correlations at zero lag comparing each wave frequency with each noise frequency	88
28. The track of Typhoon Owen, October 13-28, 1982, taken from the JTWC Annual Tropical Cyclone Report	91
29. Spectra from WIHA hydrophone 74 during the passage of Typhoon Owen.....	92
30. The track of Typhoon Doyle, August 13-24, 1988, taken from the JTWC Annual Tropical Cyclone Report	94
31. The track of Typhoon Doyle across the WIHA hydrophones	95
32. Spectrogram showing the hydrophone 76 noise level fluctuations due to Typhoon Doyle over a four day period.....	96
33. Spectrogram showing the noise from typhoon Doyle just as it passed directly over hydrophone 76	98
34. Spectra from Typhoon Doyle.....	99
35. Spectrograms of ocean noise over a two week period from deep hydrophone 74	104
36. Spectrograms of ocean noise over a two week period from SOFAR-depth hydrophone 20	105

LIST OF ABBREVIATIONS

<u>Abbreviation</u>	<u>Meaning</u>
OBSS	Columbia - Point Arena Ocean Bottom Seismic Station
WIHA	Wake Island Hydrophone Array
SOFAR	SOund Fixing And Ranging - the deep sound channel
SOWM	Spectral Ocean Wave Model
GSOWM	Global Spectral Ocean Wave Model
UCT	Universal Coordinated Time
HIG	Hawaii Institute of Geophysics
NCDC	National Climatic Data Center
JTWC	Joint Typhoon Warning Center
FFT	Fast Fourier Transform
DFT	Discrete Fourier Transform
NWS	National Weather Service

CHAPTER 1. INTRODUCTION

The study of low-frequency ocean noise began with the study of low-frequency seismic noise observed on continents. Peak levels of this continental noise usually occur at frequencies between about 0.1 and 0.3 Hz, and are called microseisms - a misnomer since they are not related to small earthquakes. They are a dominant and persistent feature on long-period seismographs, with vertical particle amplitudes as high as 10^{-3} cm. As far back as the latter half of the 19th century, it was recognized that increased levels of microseismic noise were associated with oceanic storms (Bertelli, 1872). Using an array of seismometers located near St. Louis, Missouri, Ramirez (1940a and 1940b) found microseisms coming from the direction of atmospheric pressure lows off the U.S. East Coast, and his method was later used to track hurricanes in the Caribbean (Gilmore, 1946). Some investigators believed that the microseismic energy was generated by oscillatory atmospheric pressure fluctuations at the sea surface (Gherzi, 1924; Scholte, 1943) or by waves hitting steep coastlines (Tams, 1933). It was generally not believed, however, that the microseisms could be due to pressure fluctuations from ocean surface gravity waves. It was known that travelling ocean waves have pressure fluctuations that decay exponentially with depth to the point where they are insignificant at the ocean bottom if the water depth is much greater than a few wavelengths. Ocean waves with the same frequencies as the microseisms have wavelengths less than 200 m, and most of the ocean is much deeper than that. From some theoretical work first presented by Miche (1944), Longuet-Higgins (1950) showed that microseisms might be caused, however, by pressure fluctuations on the ocean floor from a field of standing waves on the sea surface. According to his theory, nonlinear interactions between these waves generate second-order pressure fluctuations that do not attenuate with depth and can thus reach the deep ocean bottom. The amplitude of these pressure fluctuations is proportional to the product of the interacting wave heights, and the frequency of the pressure fluctuations is double the frequency of the waves. These

pressure fluctuations in the water column might then excite Rayleigh waves in the solid earth that could propagate onto continents and be observed as microseisms. This phenomenon should also be detectable in the oceans, as a feature of the ocean noise, using hydrophones or ocean bottom seismometers as sensors. Thus, the study of microseismic noise observed on land became intertwined with the study of low-frequency noise in the ocean. Hasselman (1963) advanced the nonlinear wave interaction theory by considering contributions to the deep ocean pressure fluctuations from a statistical distribution of directional wave components on the sea surface, and tested his theory with some success against simultaneous measurements of ocean waves and seismic noise made near San Diego by Haubrich et al. (1963). He also considered the enhanced interactions that might occur when ocean waves are reflected by a coastline. Most recently, the theory has been advanced by Cato (1991a and 1991b). He considered the non-vertical dipole components of noise due to the interaction of sea surface waves other than standing waves, and found their contribution to the noise field to be of the same order of magnitude as the vertical dipole components of the standing waves considered by Longuet-Higgins and Hasselman. Cato's result implies a depth and frequency dependence that has been tested successfully to some extent by Lindstrom (1991) against wave and noise data recently collected off Chesapeake Bay.

High quality, long-term measurements of ocean noise at frequencies below 20 Hz are few. Some of the best measurements were made more than two decades ago with the Columbia - Point Arena Ocean Bottom Seismic Station (OBSS) deployed at 4-km depth off San Francisco from May, 1966 to September, 1972 (Sutton et al., 1965). This instrument contained 3-component long and short-period seismometers, a crystal hydrophone, and a coil hydrophone. Studies of these data confirm the presence of a strong microseism peak with a greater amplitude but the same frequency as the peak simultaneously observed on nearby land seismometers (Latham and Nowroozi, 1968).

These data also exhibit particle motions at microseism frequencies consistent with those of fundamental mode Rayleigh waves, but increased microseism levels were only sometimes coincident with increased ocean wave heights (*ibid.*). Analysis of these unique noise data have continued to the present day with further studies of particle motions and coherency between the OBSS components using digital data analysis techniques (Barstow et al., 1989; Sutton and Barstow, 1990). These studies confirm fundamental mode Rayleigh wave propagation for single and double frequency microseism noise, and suggest that the observed Rayleigh waves were excited somewhere near the OBSS, rather than at a shoreline or near the center of ocean storms. Also, an exact 1:2 frequency relationship was not observed between the single and double frequency microseisms as it was for the land-based data of Haubrich (1963). A variety of other ocean noise measurements from hydrophones and ocean bottom seismometers (Latham et al., 1967; Nichols, 1981; McCreery et al., 1983; Webb and Cox, 1986; Duennebier et al., 1987; Schreiner and Dorman, 1990) confirm the shape and character of the low-frequency ocean noise spectrum, including its general dependency on weather and waves, but fail to lead to an unambiguous mechanism for the generation and propagation of the observed noise. It is likely that there is no single mechanism, but rather a variety of mechanisms that are more or less important depending upon the local environment of the sensor, and the atmospheric and wave conditions.

It is generally agreed, though, that most of the ambient ocean noise in the five-decade frequency band spanning 0.001 to 100 Hz is due to ocean gravity waves (Fig. 1). At frequencies below about 0.02 Hz, the noise is caused by the primary pressure fluctuations from infragravity waves. These waves have wavelengths longer than the water depth, and are formed near coastlines by a nonlinear transfer of energy from shorter period gravity waves (Webb et al., 1991). Between about 0.02 and 0.05 Hz is an extreme low in the spectrum, often referred to as the 20-second noise hole. The source of the noise at the

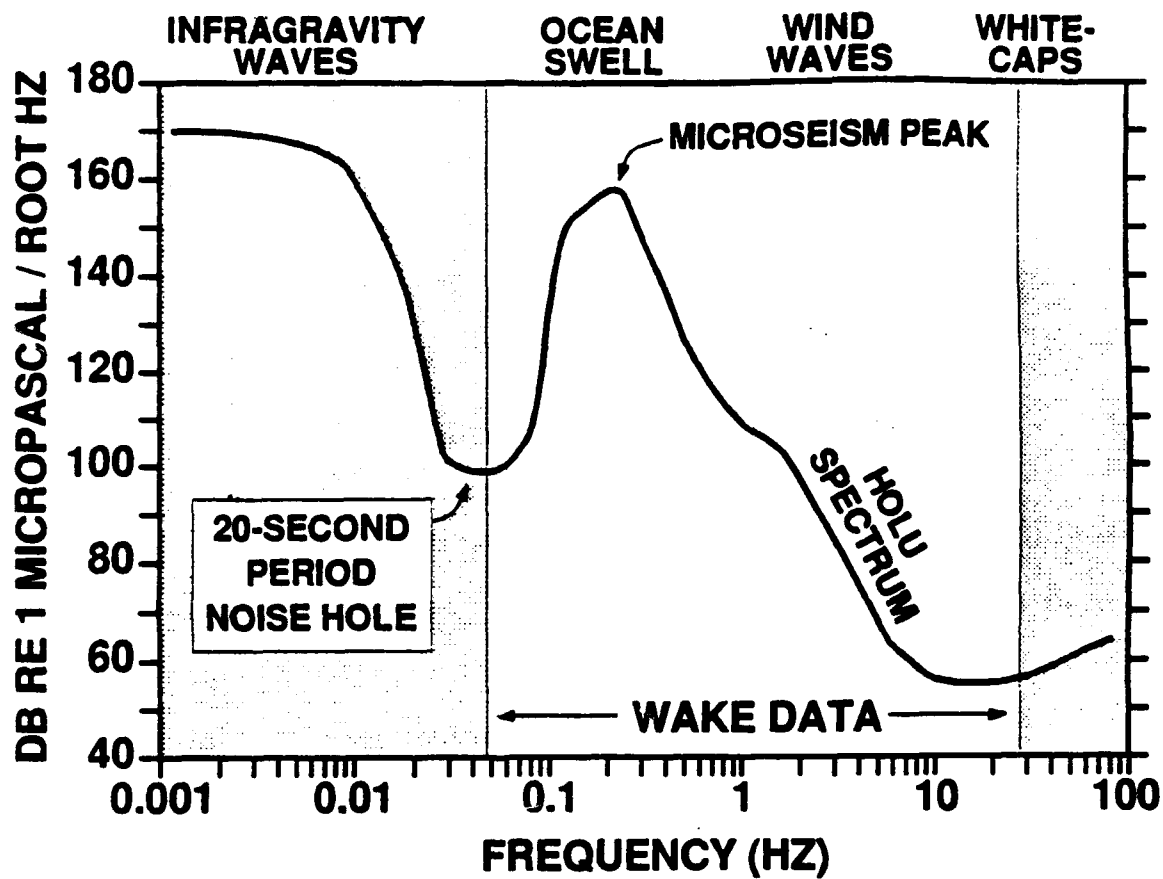
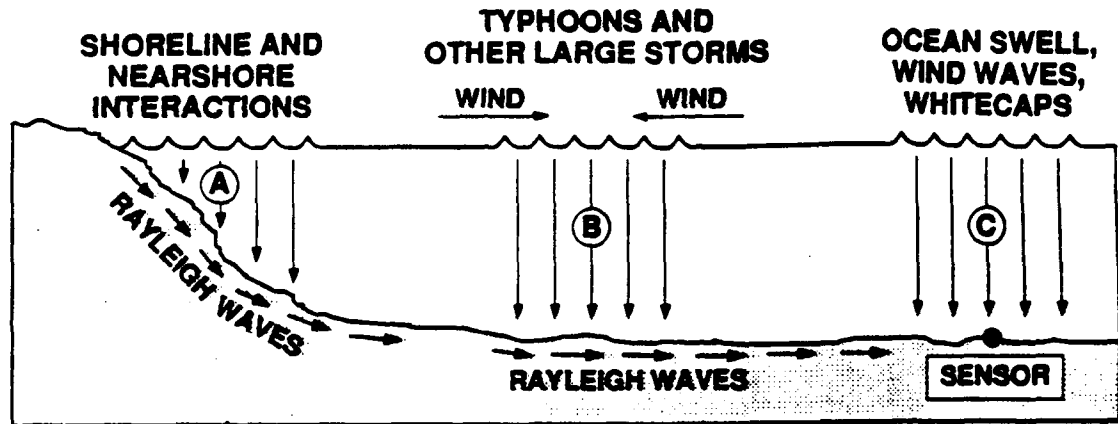


Fig. 1. Generic ambient ocean noise power spectral density curve. Probable sources for this noise are noted across the top at appropriate frequencies. Prominent and ubiquitous features of the spectrum are also noted. Ocean noise data from the Wake Island Hydrophone Array span frequencies from about 0.05 to 30 Hz.

bottom of this hole is unknown. Between 0.05 and 0.5 Hz is the microseism peak. As previously noted, the noise in this band is thought to be due to the single and double frequency pressure fluctuations from ocean swell. From 0.5 to about 5 Hz, the noise may also be double frequency pressure fluctuations from the shorter period wind waves. And above 5 Hz, the noise could be acoustic noise from breaking waves (Duennebier et al., 1986). The question of interest that has occupied investigators for several decades now is exactly how, where, and when do ocean waves produce the wide variety of noise that is observed across this spectrum.

Most investigators would agree that there are still too few high-quality data to produce a comprehensive picture of the different kinds of deep-ocean noise in the infrasonic band, their sources, their mechanisms of propagation, and the environmental conditions under which they are significant. For instance, it is not known how much of the noise on the deep ocean floor is generated by waves directly over the sensor, by waves under a distant storm, or by waves interacting with a distant shoreline (Fig. 2). And, the widely accepted theory of non-linear wave interactions used to explain the mechanism by which wave energy on the surface is converted into pressure fluctuations that propagate down to the deep ocean floor has been inadequately tested in the deep ocean, away from extended shorelines. This study addresses these topics for the subset of frequencies from 0.05 to 30 Hz using the unique long-term data set from the Wake Island Hydrophone Array in combination with a variety of environmental data including wind speeds, estimated directional ocean wave spectra, and typhoon locations and intensities.



- (A) — OCEAN SWELL FEELS BOTTOM IN SHALLOW WATER
 WAVES BREAK AGAINST THE SHORE
 SHORE REFLECTED WAVES GENERATE NONLINEAR WAVE INTERACTIONS
- (B) — OPPOSING WAVE FIELDS GENERATE NONLINEAR WAVE INTERACTIONS
- (C) — NONLINEAR WAVE INTERACTIONS
 ACOUSTIC NOISE FROM BREAKING WAVES OR WHITECAPS

Fig. 2. Some possible mechanisms for the generation of 0.05-30 Hz seismoacoustic noise in deep ocean basins by ocean waves. Wave energy at the surface is converted to pressure fluctuations by nonlinear wave interactions. These pressure fluctuations may be felt directly by the sensor (C). Enhanced interacting waves under a large storm (B), or near a steep shoreline because of reflections (A), may produce pressure fluctuations strong enough to excite Rayleigh waves in the solid earth which propagate to the sensor. Or, dissipation of the wave energy at a more gradually shoaling shoreline by feeling bottom and breaking (A) may also excite Rayleigh waves that propagate to the sensor. At the highest frequencies, noise may be generated locally by whitecaps that produce acoustic energy in the water column (C).

CHAPTER 2. DATA

This study of ocean noise has utilized four different kinds of data: (1) ambient ocean noise data from an array of hydrophones near Wake Island in the northwestern Pacific -- unique because of their long-term nature and their location in a deep ocean basin far from any extended coastlines, (2) wind speeds and directions from observations made at Wake by the National Weather Service, (3) estimated directional ocean wave spectra from U.S. Navy models, and (4) typhoon positions, sizes, and intensities from the Joint Typhoon Warning Center located at Guam.

Noise Data from the Wake Island Hydrophone Array

All of the ambient ocean noise data used in this study have come from the Wake Island Hydrophone Array (WIHA). This array was built over thirty years ago for a U.S. Air Force project, but it has been operated exclusively by the University of Hawaii since 1976. Several recording systems have been used since then to collect the WIHA data for a variety of scientific endeavors. Thus, the WIHA data exist in several different formats and only for certain time intervals. Calibration of the data has been hampered by uncertainties in the hydrophone and cable responses, but these uncertainties have been greatly reduced over time.

• History of the Array

The Wake hydrophones were installed along with hydrophones at Midway, Enewetak, and Oahu in the late 1950s as part of the U.S. Air Force's Pacific Missile Range - Missile Impact Location System. As the name implies, these hydrophones were used to locate the impact of missiles splashing down in the western Pacific after being launched from California as part of the then incipient intercontinental ballistic missile program. The U.S. Air Force and Navy continuously recorded signals from the hydrophones throughout the

sixties and the early seventies, after which these arrays were literally abandoned. Much of these early data, in the form of analog magnetic tapes and seismograms, were shipped to the University of Hawaii for secondary use by the T-phase project -- a project to investigate properties of sound propagation in the ocean and to locate natural and artificial sources of transient undersea signals (e.g., Johnson, 1966; Duennebier and Johnson, 1967). Although most of these seismograms were saved, the taped data were unfortunately discarded.

In 1976, a University of Hawaii research vessel was scheduled to do some seismic refraction work in the vicinity of Wake, so it was decided to attempt a reactivation of the hydrophones for the purpose of recording the refraction signals. The building housing the cable terminations was found gutted and open to the elements, but 12 of the 16 original hydrophones were found to still be in good working order. The refraction data were not collected owing to some excess noise in the recording system preamps, but after that problem was corrected two months of continuous data from five of the hydrophones were successfully recorded on analog FM tape. Based on enthusiasm generated by the discovery in these data of frequencies greater than 20 Hz in oceanic seismic phases Po and So, formerly called high-frequency Pn and Sn (Walker et al., 1978), a permanent three-channel analog cassette tape recording system was installed at Wake in July, 1979. This system ran until March, 1981, when Typhoon Freda hit the island and waves washed through the building destroying the recorder. In July, 1981 the building was cleared of sand and coral boulders from the storm, and another cassette recording system was installed. The armored hydrophone cables, formerly buried from the building down to the shoreline, were now strewn in giant loops along the beach, but were found to still be working properly. The cassette data demonstrated the ability of the Wake hydrophones to detect signals from underground nuclear test explosions (Sutton et al., 1980; McCreery et al., 1983), so in September, 1982, a 9-track tape, digital recording system was installed at Wake to permit further study of these explosion signals. This system ran almost continuously through

January, 1989, when tape drive problems forced us to shut it down. After some delays for a modification, the system was reinstalled in September, 1989 to record in a digital format on 8-mm video cassettes, reducing tape volume by a factor of about 500. This system ran for only a few months though, through March, 1990, before a leak in the roof shorted one of the recording system cables. The leak proved to be irreparable due to the deteriorated state of the old building, forcing a move to a smaller but more sound building adjacent to the original one. Preparation of that building is now complete, and data collection is scheduled to resume in March, 1992.

- Description of the Array

The Wake Island Hydrophone Array consists of twelve working hydrophones, out of an original sixteen, located near Wake Island in the northwestern Pacific Ocean (Figs. 3 and 4). Six of the hydrophones, 71-76, are at 5.5-km depth on the ocean bottom to the north of Wake and are laid out to form the center and vertices of a pentagon, approximately 20 km on a side. The other six hydrophones, 10, 11, 20, 21, 40, and 41, are located in pairs to the south and west of Wake at about 850-m depth, the depth of the deep sound channel axis also known as the SOFAR (SOund Fixing And Ranging) axis. The entire array spans an area measuring about 100 by 300 km.

The passive, moving-coil hydrophones are connected to Wake via long cables, each hydrophone requiring a pair of conductors. The hydrophones and their cables can be tested by measuring the loop resistance across the two conductors, and by measuring the resistance between each conductor and ground. The loop resistance indicates the electrical continuity down one conductor, through the hydrophone coil, and back up the other conductor. The proper loop resistance values for each hydrophone and cable are known and can be used to verify current measured values. A resistance to ground other than infinite indicates there is a leak to seawater somewhere along the cable, and the value of

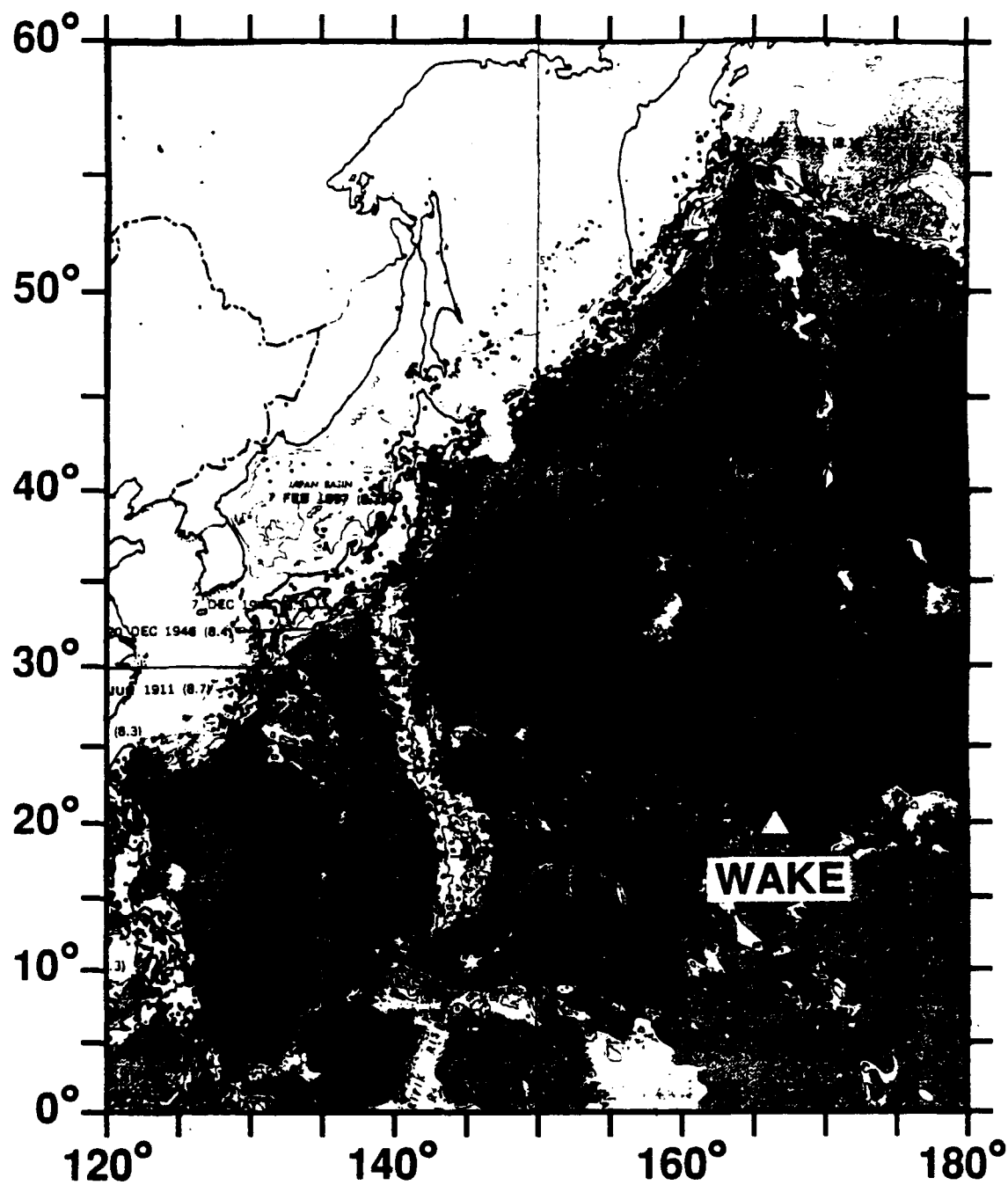


Fig. 3. Location of Wake Island in the northwestern Pacific Ocean. The base map is from the U.S. Geological Survey's World Seismicity Map (Tarr, 1974). The small red, green, and blue dots are earthquake epicenters. Signals from earthquakes in the northwestern Pacific are commonly observed on the Wake hydrophones.

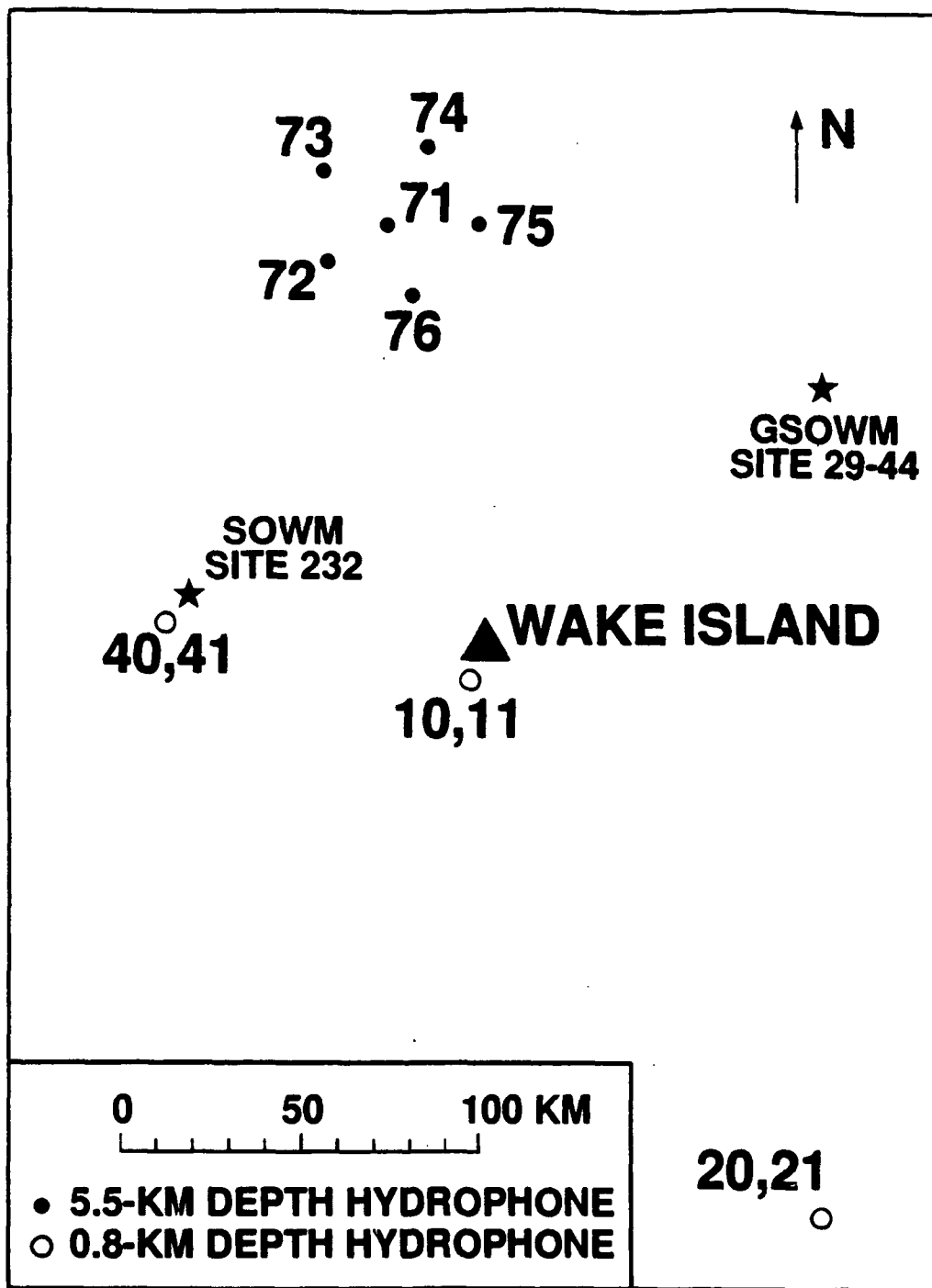


Fig. 4. Layout of the Wake Island Hydrophone Array. Six hydrophones are to the north of Wake, and another six are in three pairs to the south and west of Wake. Also shown are the sites nearest to Wake for which regular estimates of the directional ocean wave spectrum were made by the U.S. Navy using either the Spectral Ocean Wave Model (SOWM) or Global Spectral Ocean Wave Model (GSOWM).

the resistance indicates the severity of the leak. Since 1976, these measurements have remained essentially the same for the Wake hydrophones. Four hydrophones have improper loop resistances, are completely shorted to ground, and are unusable. The other twelve hydrophones have the correct loop resistances, but have varying degrees of leakage to ground. The hydrophones with the least leakage to ground are 71, 74, 76, 10, 11, 20, and 21. These hydrophones also appear to have the best signal-to-noise ratios, and are the ones that have been used for most studies. The other five hydrophones, 72, 73, 75, 40, and 41, have equivalent signal levels but are susceptible to having small amounts of excess noise.

- Recording Systems and Data Formats

Two of the Wake recording systems and three of the data formats were used for the studies of noise presented here. The recording systems and data formats are described below according to the time intervals that they span.

- *September, 1982 - March, 1988*

In September, 1982, the first digital recording system was installed at Wake. It consisted of an LSI-11/2 computer, a 16-channel, 16-bit, analog-to-digital convertor, a satellite clock, four 1600-bpi, 9-track tape drives, and a bank of low-noise amplifiers. The amplifiers were designed to prewhiten the noise and provide anti-aliasing. Amplifier gains were set so that ocean background noise would be at a level of around ± 50 digital units. This strategy ensured that the noise would be adequately recorded while still leaving plenty of dynamic range for large amplitude signals to be sampled without clipping. The satellite clock, accurate to a millisecond, provided absolute Universal Coordinated Time (UCT) as well as a synchronization signal for the analog-to-digital convertor. The LSI-11/2 computer, chosen for its real-time architecture and proven reliability, was programmed to manage the data collection. It controlled the analog-to-digital convertor, read the satellite

clock, assembled the data records, controlled the tape drives, accepted commands from an operator, and produced a hard copy log of events. It would also restart itself automatically after a power failure -- a useful feature on a remote island. The recording system was designed to record 11 hydrophones continuously at 80 samples per second per hydrophone, producing four tapes per day. Because there were four tape drives, an operator at Wake would only need to service the recording system once a day. In reality, however, one of the tape drives was almost always out of service, so the software was modified to record only 8 hydrophones in order to generate only three tapes per day. The eight hydrophones recorded were: 71, 73, 74, 75, 76, 10, 20, and 40.

The data were written on the tape in 6600-byte records once every five-seconds. The first 100 2-byte words of each record are a header consisting of the date and time, satellite clock status, and information about the recording system configuration. The remaining 3200 2-byte words are a multiplexed data stream from the 8 hydrophones (8 hydrophones \times 80 samples/second \times 5 seconds = 3200 samples).

Each week, 21 data tapes were sent back to the Hawaii Institute of Geophysics (HIG). It was too expensive and too space consuming to save all these data, so a scheme was devised to only save intervals with signals of interest and regular noise samples. The signals of interest were mostly seismic phases from earthquakes and nuclear tests, but included signals from undersea volcanic eruptions and whales, and signals of unknown origin seen on monitor records. The noise samples consisted of three-minute-long intervals of data extracted at the rate of about one per hour. The actual spacing between noise samples was made random to avoid contamination by any artificial noise sources at Wake that might also be on an hourly schedule. Each original data tape was read on a mainframe computer at HIG, and the intervals and noise samples were stripped off, written to other tapes, and cataloged. The original tapes were then sent back to Wake for recycling. The five-and-a-half years of data processed in this manor produced 271 tapes

containing over 4700 signal intervals and 275 tapes containing over 40,000 noise samples.

From the noise samples collected during this time period, two studies were done. The first was a one-year comparison between the ambient noise, 0.5-30 Hz, and the wind, and the second was a three-year comparison between the ambient noise, 0.1-5 Hz, and the ocean waves. More detailed information about this recording system can be obtained from the author upon request.

April, 1988 - January, 1989

Data from this time interval are the continuous, unreduced data collected by the recording system described above. These data were not processed in the usual way at HIG, since an upgrade to an 8-mm video tape recording format for Wake was already being built, leaving no reason to conserve the remaining supply of 9-track tapes. In addition, it was felt that continuous data might be more useful in the future in some unanticipated way. This proved to be true, since continuous data were very useful for studying the noise produced by typhoon Doyle as it passed over the array in August, 1988. There are about 600 tapes containing these ten months of data. Unfortunately, as previously mentioned, there were tape drive problems at Wake during this time period, so there are gaps in these data as well as many tapes that are hard to read.

September, 1989 - March, 1990

The recording system installed in September, 1989 was essentially the same as the one used the previous seven years, with a few important modifications. Firstly, the hydrophone amplifiers were altered to boost the gain by about a factor of 2 for frequencies below 5 Hz, and to improve the anti-aliasing. These small changes were made to better record the lowest frequencies and further lessen the chances of contamination of the digital data by aliased high-frequency signals. Secondly, two new amplifiers were installed, each with a

long-period and a short-period output. The long-period output was intended to optimize the detection of signals at frequencies in the noise hole below the microseism peak. The short-period output was intended to match the output of the other amplifiers. These two amplifiers were connected to deep hydrophones 74 and 76. Thirdly, the 9-track tape recorders were replaced with two Exabyte 8-mm video cassette digital recorders. This one modification had a huge impact on our data collection operation at Wake. Because the tapes have a 2.2-gigabyte storage capacity, all twelve of the Wake hydrophones could be recorded for more than a week on a single tape. With two tape drives, this meant that someone at Wake would absolutely need to service the system only once every two weeks, although a weekly schedule was actually implemented to more frequently check the system status. In addition, because the tapes are so small (about the size of an audio cassette) and so inexpensive (less than \$8 each), there would be no reason to regularly process the data at HIG. All of it could be archived, and a year's worth of data would easily fit into one desk drawer (they are actually kept in a fireproof safe). Perhaps the biggest advantage to this recording media change was the monetary savings in terms of paying the operators at Wake, paying for people and computer charges at HIG, paying for tapes, and paying for shipping tapes back and forth. These substantial savings meant that it would be much easier to find funding to keep this important station running in future years. Finally, some changes to the operating system software were made. The most substantial modifications from a programming standpoint were those required to switch to different tape drives, since a fairly smart driver had to be written to operate the Exabyte machine. The changes that had the most impact on the data, however, were an increase in the number of recorded short-period channels from 8 to 13, an increase in the short-period sampling rate from 80 Hz to 100 Hz, and the addition of 4 long-period channels sampled at 10 Hz.

The data were written onto the 8-mm tapes in 4096-byte records. Each record contains 1.5 seconds of data. The first 38 2-byte words are a record header containing the date and

time from the satellite clock, the satellite clock status, and information about the system configuration. The next 60 2-byte words are the multiplexed data stream from the 4 long-period channels, the first two of which are hydrophones 74 and 76 with the remaining two channels unused. The last 1950 2-byte words are the multiplexed data stream from the 13 short-period channels. The first twelve of those channels are hydrophones 71, 72, 73, 74, 75, 76, 10, 11, 20, 21, 40, and 41. The remaining channel is the long-period amplifier output for hydrophone 74, highly oversampled. Filemarks are written onto the tape every six hours to facilitate quicker positioning of the tapes during playback. A complete description of the 8-mm tape format can be obtained from the author upon request.

• Calibration of the Hydrophone Data

In order to make the best use of the WIHA data, recorded as a time series of numbers or digital units, they need to be interpreted in terms of an appropriate physical unit such as pressure. Pressure in this context does not mean absolute pressure, which is on the order of 10^{12} μ Pascals (1μ Pascal = 10 dynes / cm^2) for the deep hydrophones, but instead refers to pressure variations, which range from about 10^3 to 10^8 μ Pascals per root Hz. To make the conversion to pressure units, a frequency-dependent response curve is applied to the data after they have been transformed into the frequency domain. Normally this response contains both amplitude and phase information, but since the phase response of the cables is unknown, and since absolute phase information is not needed for this study of noise, only the amplitude response is computed. The amplitude response of the total system, in decibels (dB) relative to 1 digital unit per μ Pascal, is composed of response curves for the individual components: (1) hydrophones, (2) cables, (3) amplifiers, and (4) the analog-to-digital convertor. The sum of the individual responses gives the total response of the system. Component responses are given below, along with a discussion of the measurements and assumptions used to arrive at them. A thorough discussion of the

transformation of the data to the frequency domain, and of the logarithmic decibel units is given in Chapter 3.

Hydrophones

Detailed information about the hydrophones is not available, owing to their age and formerly classified status. Most of what is known has come from information about the Columbia - Point Arena Ocean Bottom Seismic Station (OBSS) that was in operation between 1966 and 1972 at 3903-m depth on the ocean bottom off San Francisco (Barstow et al., 1989). The OBSS hydrophone is identical to the WIHA hydrophones.

The mechanism of the WIHA hydrophones is a diaphragm-actuated moving coil in the field of a permanent magnet. As pressure fluctuations in the ocean move the diaphragm, the coil moves through the magnetic field causing an emf to be induced in the coil proportional to its velocity. It is this voltage, after transmission through the cable, that is amplified and recorded at Wake. The natural frequency of the OBSS hydrophone is 200 Hz (Thanos, 1966). For frequencies well below the natural frequency, such as those encountered in this study, the response of the hydrophone (Fig. 5) is proportional to the frequency of the pressure signal (i.e., a 6 dB/octave slope). But this response is modified by another feature of the hydrophone design -- a small pressure compensation hole that permits the great absolute pressure to be equalized on both sides of the diaphragm as the hydrophone is raised or lowered in the water. This small hole reduces the long-period response below a corner frequency, making it proportional to the frequency squared of the pressure signal (i.e., a 12 dB/octave slope). Thanos (ibid.) put this corner frequency at 3 Hz. However, in a recent study Barstow et al. (1989) compared OBSS coil-hydrophone data with OBSS crystal hydrophone and seismometer data and concluded that the 3 Hz corner was in error and should be shifted to 0.3 Hz. This shift is in general agreement with a previous study showing that observed WIHA amplitudes of 0.05 Hz earthquake Rayleigh

HYDROPHONE RESPONSE CURVES

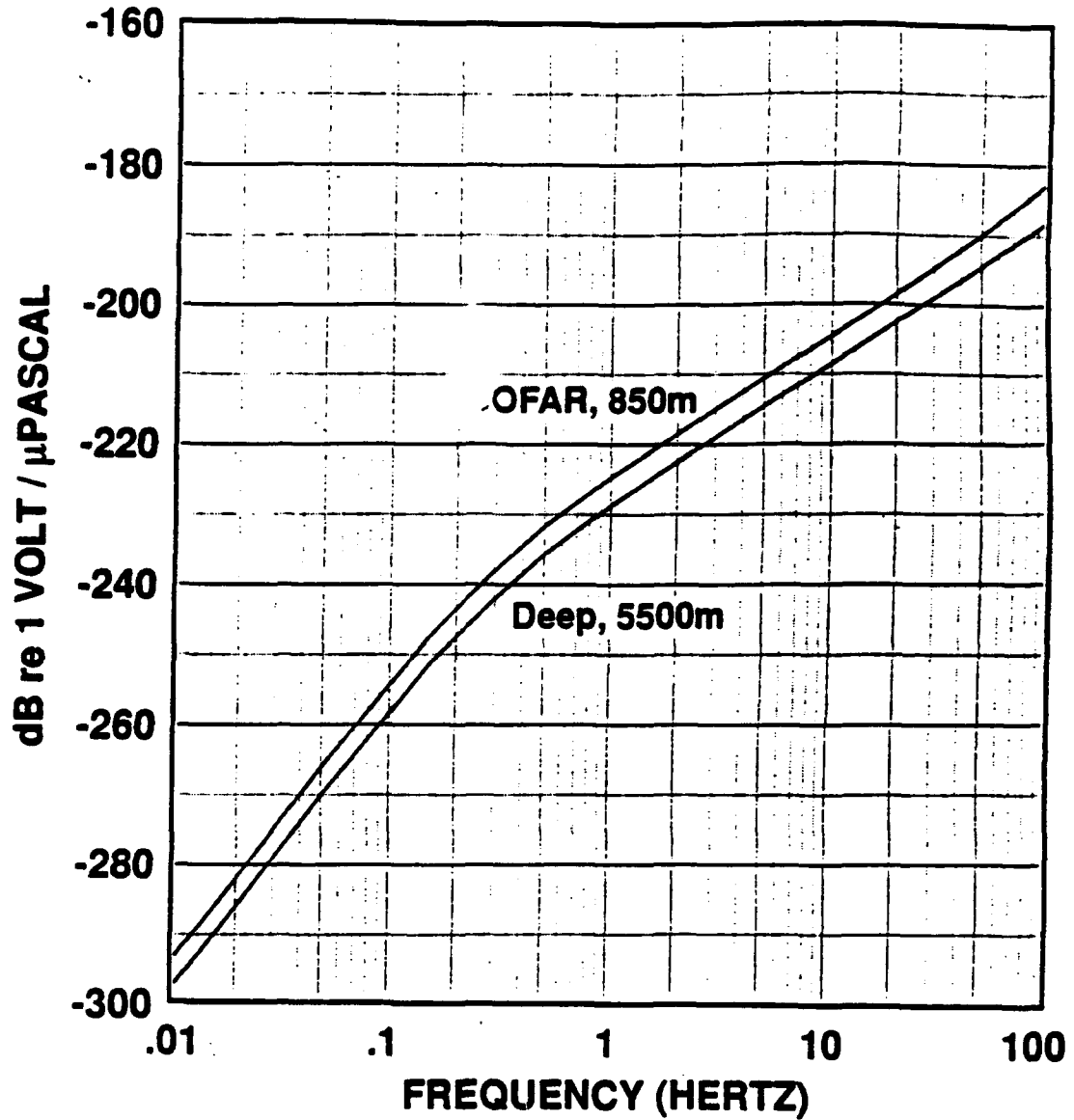


Fig. 5. Response curves for the WIHA hydrophones. The two hydrophones are identical, but their different depths have an effect on their responses.

waves are too large if the 3 Hz corner is used (McCreery and Walker, 1987). In addition, microseism peak levels measured at Wake are found to be much larger than levels measured on hydrophones at other deep ocean sites (e.g., Nichols, 1981; Webb and Cox, 1986) when the 3 Hz corner is used. In light of this combination of evidence, the corner frequency applied to the data analyzed in this study is the one at 0.3 Hz. However, it would not be surprising if, after more than 30 years in the sea, the pressure compensation holes in the WIHA hydrophones are plugged by growth or corrosion, in which case the corner should be eliminated altogether. Finally, a correction for the ambient pressure was applied, giving the shallower SOFAR hydrophones a slightly greater response at all frequencies relative to the deep hydrophones.

Cables

The WIHA hydrophones are connected to Wake Island by cables of different lengths, and each of these cables has a different response, attenuating frequencies above 1 Hz in greater amounts as the length of the cable increases. Some original estimates of the cable responses have been found, although these estimates are often in slight disagreement with each other. By comparing the relative amplitudes of T-phase signals from large earthquakes, McCreery and Walker (1987) estimated differences between the cable responses for five of the six bottom hydrophones. More recently, some comparisons of simultaneous ambient noise levels on the bottom hydrophones were made to further estimate differences in the cable responses. Combining this information, best estimates of the cable responses have been made (Fig. 6).

Amplifiers

Four different types of amplifiers have been used in the the digital recording systems employed at Wake from 1982 to present. Each of these amplifiers was designed and built

CABLE RESPONSE CURVES

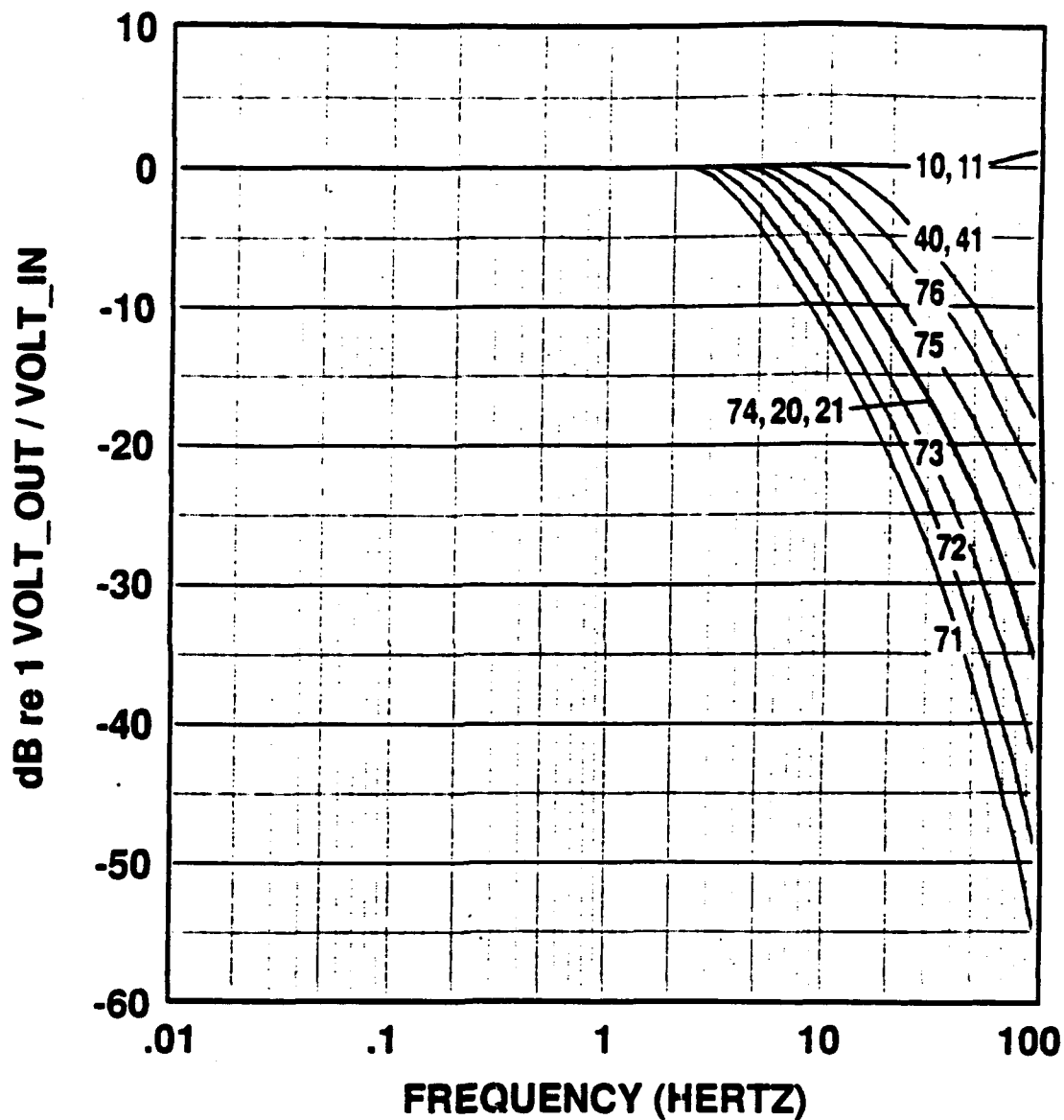


Fig. 6. Response curves for the WIHA sea cables. These cables connect the WIHA hydrophones to Wake Island and each curve is identified by the number of the corresponding hydrophone.

at HIG with final modifications made during installation at Wake. The responses were shaped to pre-whiten the noise and provide anti-aliasing, and were measured at Wake using a spectrum analyzer (Fig. 7). The first amplifier, W82SP in the figure, was used on all hydrophones from September, 1982 through January, 1988, the time period during which recordings were made on 9-track tapes. The second amplifier, W82SP*, is a modification of the first with an increase in gain and improved anti-aliasing. It was used on all hydrophones except 74 and 76 between September, 1989 and March, 1990, when the 8-mm video cassette recording system was in operation. The other two amplifiers, W89SP and W89LP, are the short- and long-period stages of amplifiers that were connected to hydrophones 74 and 76 during that same six-month interval. The short-period stage is intended to be similar to the other short-period amplifiers, while the long-period stage is designed for frequencies below 0.5 Hz.

Analog-to-Digital Convertor

The analog-to-digital convertor digitizes and multiplexes the voltage outputs of up to 16 amplifiers. The input range is ± 10 Volts. The output range is -32768 to 32767 digital units, corresponding to the range of a 16-bit twos-complement integer. The frequency-independent response is therefore 3276.8 digital units / Volt, or 70.3 dB relative to 1 digital unit / Volt.

Complete System

By adding the response curves of the appropriate individual components, a complete system response curve in dB relative to 1 digital unit / μ Pascal can be generated. Some of the various system response curves used in this study are shown in Fig. 8. When WIHA data are transformed into a spectrum, measured in dB relative to 1 digital unit per root Hz, the appropriate response curve is subtracted from that spectrum to change the units to dB

AMPLIFIER RESPONSE CURVES

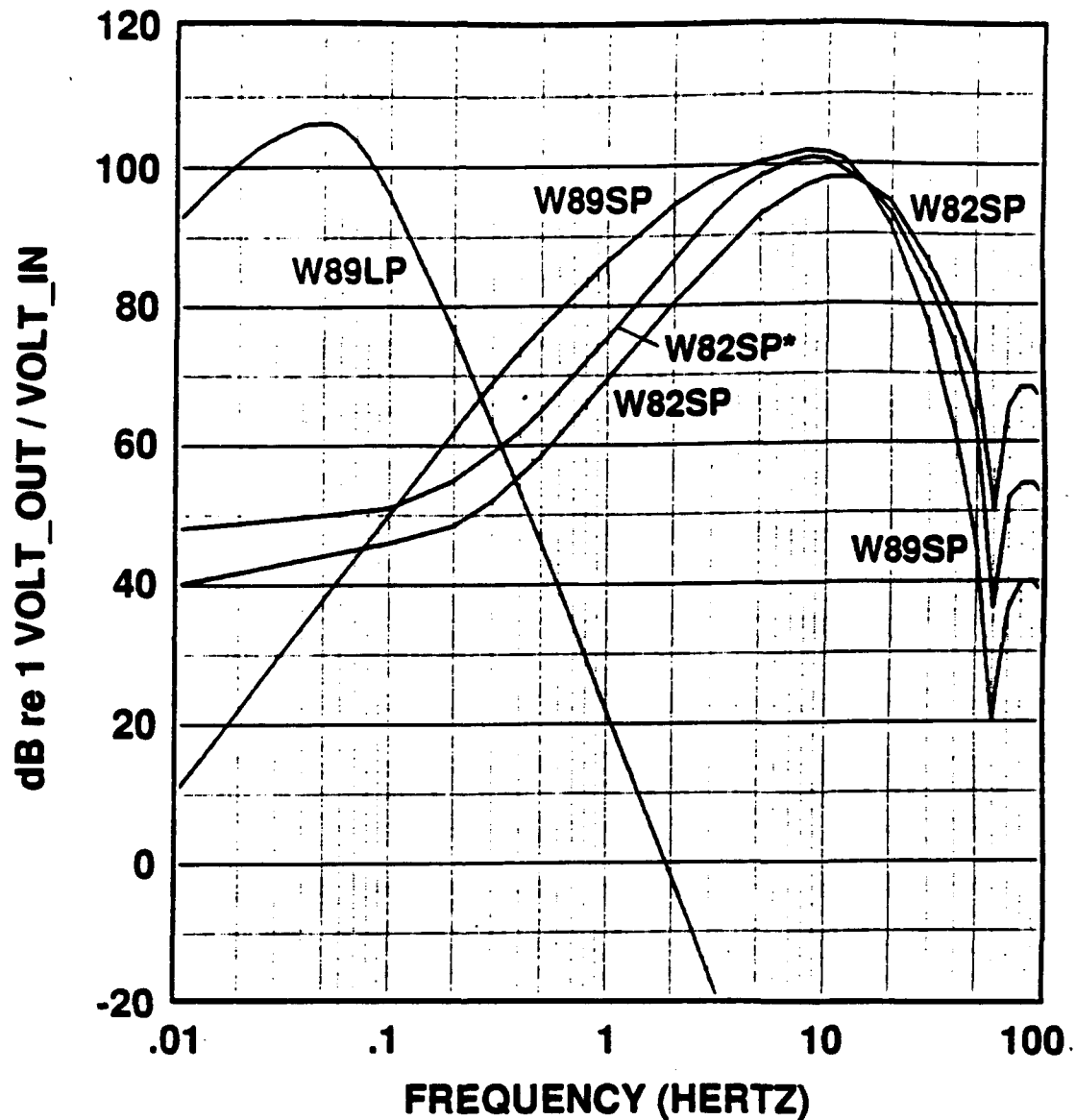


Fig. 7. Response curves for the WIHA amplifiers. A discussion of each amplifier and its usage is given in the text. Notches in these curves at 60 Hz are a design feature for reducing 60 Hz crosstalk from the line power.

SYSTEM RESPONSE CURVES

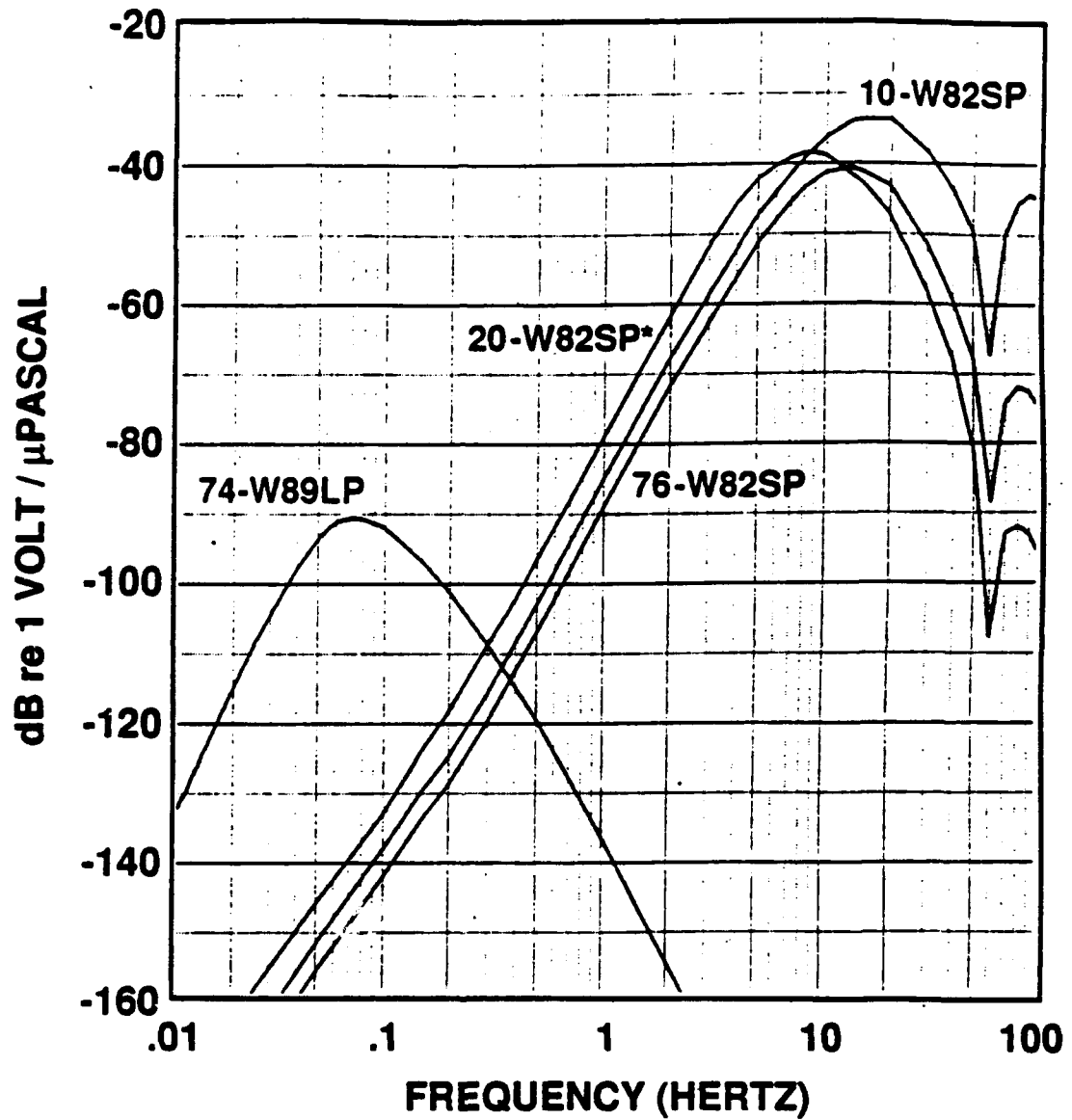


Fig. 8. Response curves for some of the WIHA hydrophone-amplifier configurations. These curves, and other similar curves, are used to convert the WIHA digital data into pressure units.

relative to 1 μ Pascal per root Hz. Data measured in these units have the most meaning, and can be easily compared to empirical and theoretical data presented by other investigators.

- System Noise

For each combination of hydrophone and amplifier, an estimate of system noise has been made. A resistor, equivalent in value to the loop resistance of the particular cable and hydrophone, was connected at the input of the amplifier. The resulting noise at the output of the amplifier was then measured either with a spectrum analyzer, or by digitizing these data through the rest of the recording system and doing the spectral analyses at a later time. All of the amplifiers were designed to have very low self noise and are not believed to be the source of the system noise measured. It is most likely due to the thermal and 1/f noise of the cables and hydrophones. There are two frequency bands where system noise is a problem in the WIHA data. At frequencies below about 0.1 Hz, the region of the noise hole, system noise levels are clearly higher than ambient ocean noise levels most of the time. The only apparent exception is when there is high amplitude noise due to Rayleigh waves from earthquakes. At frequencies above about 5 Hz, another band where the deep ocean noise is generally very low, system noise levels are very close to the ambient ocean noise levels, on the deep hydrophones. However, since the recorded noise in this band is observed to vary considerably, and these variations are correlated with the wind speed as will be discussed later, the system noise above 5 Hz is probably not masking the ocean noise most of the time. System noise levels have been noted on some of the figures where appropriate.

Surface Wind Measurements

Surface wind measurements directly over the WIHA hydrophones do not exist, but wind measurements at Wake Island are made hourly by the National Weather Service.

These measurements, wind speed and wind direction, are reported as 3-hour and daily averages in monthly summaries. The times listed in these summaries are local Wake time that can be converted to UCT by adding 12 hours.

Ocean Gravity Wave Estimates

The most important environmental measurement that could be made for the investigation of ocean noise, other than the noise itself, is the measurement of the directional ocean wave spectrum. Since most of the ambient ocean noise in the frequency band of the WIHA data is due in some way to these waves, their measurement would be of great use for studying mechanisms by which this noise is generated and propagated. Unfortunately, no such measurements exist in the vicinity of Wake, and it would be both difficult and expensive to make such measurements on a long term basis owing to the remoteness of the area, and the complexity of mooring and servicing a wave buoy in 5.5-km of water.

A substitute for direct measurements, however, are estimates of the waves made regularly by the U.S. Navy for distribution to the fleet. These estimates have been computed at regular time intervals for discrete locations on a worldwide grid using one of two theoretical models, the Spectral Ocean Wave Model (SOWM) and the Global Spectral Ocean Wave Model (GSOWM). Inputs to these models are estimates of the surface winds, and the ocean wave field from the previous model run, and output is the directional wave spectra. Comparison of estimated significant wave heights, an integration of the spectrum, predicted by these models with significant wave height measurements from buoys in the Atlantic and Pacific gives root-mean-square errors on the order of 1 m (Clancy et al., 1986). The SOWM and GSOWM data are archived at the National Climatic Data Center (NCDC) in Asheville, North Carolina, and are available for a nominal fee.

- Spectral Ocean Wave Model

The SOWM data cover the time period from January, 1956 to June, 1985, with output produced at 6-hour intervals. This output consists of directional ocean wave spectra for gridpoints spaced approximately 300 km apart in the northern hemisphere's oceans. The closest gridpoint to Wake is shown in Fig. 4. The SOWM ocean wave spectra are divided into 15 frequency bins with center frequencies ranging from 0.039 to 0.308 Hz, and 12 30°-wide directional bins. These data were used extensively in comparison with the WIHA data for the time period September, 1982 to June, 1985.

- Global Spectral Ocean Wave Model

The GSOWM data cover the time period from July, 1985 through the present, with output produced at 12-hour intervals. This output consists of directional ocean wave spectra for gridpoints at every 2.5 degrees of latitude and longitude for all the world's oceans. The closest gridpoint to Wake is shown in Fig. 4. The GSOWM data are divided into the same 15 frequency bins as the SOWM data, but the directional resolution is doubled to 24 15°-wide bins. In addition, the GSOWM wave propagation algorithm is an improvement over the SOWM algorithm, and the GSOWM is forced by better estimates of the surface winds. A comparative study by Clancy et al. (1986), showed GSOWM to be consistently superior to the SOWM for predicting significant wave heights. GSOWM data have been used in this study for comparison with a 41-day interval of continuous noise data in 1989.

Typhoon Data

Tropical storms and typhoons are a common occurrence in the northwestern Pacific, with an average of about 27 per year occurring primarily between May and November. The wind from these storms can extend hundreds of kilometers from their centers and can

produce high seas and a large swell. They are potentially a source of significant noise in the ocean. Data about these storms is available from the U.S. Navy and Air Force's Joint Tsunami Warning Center (JTWC) in Guam in the form of annual reports. These reports give each storm's track from the time that it forms as a tropical disturbance until the time that it dissipates, with maximum sustained wind speeds noted at 6-hour intervals along the track. These typhoon data were compared to WIHA noise data for the interval September, 1982 to July, 1986. The annual reports were also used, along with real-time warnings issued by the JTWC that give estimates of a storm's size, to investigate Typhoon Owen that passed near Wake in October, 1982, and Typhoon Doyle that passed directly over some of the Wake hydrophones in August, 1988.

CHAPTER 3. METHODOLOGY

The primary technique used for the study of these data has been the computation of power spectral estimates using the fast Fourier transform (FFT), a computerized implementation of the discrete Fourier transform (DFT) that is optimized for speed. This technique was used because the levels and behavior of the noise are frequency dependent and a division of the data into different frequency bands was needed. From the power spectral estimates, spectrograms, spectra, and time series plots were generated to permit a visualization of the data in a variety of forms, in order to gain new insights into the processes of noise generation and propagation. A brief discussion of this method, and the computer programs used to implement it follow.

Spectral Analysis

Although many books have been written about techniques for spectral analysis, including the techniques employed in this study, the subject can be confusing to even the learned reader because of inconsistencies in the way Fourier transforms are defined, and seeming inconsistencies in the units of the power spectral estimates presented in the literature. The following section is an attempt to clarify the techniques used in this study.

• Discrete Fourier Transform - Derivation and Meaning

The Fourier transform, $F(s)$, of a continuous time series, $f(t)$, can be defined:

$$F(s) = \int_{-\infty}^{+\infty} f(t) e^{-i2\pi st} dt, \quad (3.1)$$

where s is the frequency in Hz, t is the time in seconds, $e = 2.71828\dots$, and $i = \sqrt{-1}$. The energy density spectrum is $|F(s)|^2$, and the energy in any particular frequency band can be found by integrating this spectrum over that band. Parseval's theorem gives a relationship between the time series values and the transform values:

$$\int_{-\infty}^{+\infty} |F(s)|^2 ds = \int_{-\infty}^{+\infty} |f(t)|^2 dt , \quad (3.2)$$

which simply means that the total energy over all frequencies is equal to the integral over all time of the squared magnitude of the time series. Note that the units of energy are the squared units of the time series multiplied by time. This is not necessarily energy in the physical sense, but is a property of the time series that behaves in many ways like energy. In order for the total energy to be non-infinite, the time series must be restricted in some way. One way is for the time series to have a finite duration -- for instance if the time series is only non-zero over the interval $0 \leq t \leq T$. In this case, (3.1) and (3.2) can be modified with new limits:

$$F(s) = \int_0^T f(t) e^{-i2\pi st} dt , \quad (3.3)$$

$$\text{and } \int_{-\infty}^{+\infty} |F(s)|^2 ds = \int_0^T |f(t)|^2 dt . \quad (3.4)$$

For the case of a finite-length discrete time series, x_k , $k = \{0, 1, 2, \dots, N-2, N-1\}$, with a sampling interval Δ , equivalents to (3.3) and (3.4) are:

$$X_j = \Delta \sum_{k=0}^{N-1} x_k e^{-i2\pi jk/N} , \quad j \in \{-(N/2-1), \dots, -2, -1, 0, 1, 2, \dots, N/2\} \quad (3.5)$$

$$\text{and } \frac{1}{N\Delta} \sum_{j=-(N/2-1)}^{N/2} |X_j|^2 = \Delta \sum_{k=0}^{N-1} |x_k|^2 , \quad (3.6)$$

found directly by making the following substitutions:

$$dt = \Delta ,$$

$$t = k\Delta ,$$

$$ds = \frac{1}{N\Delta} ,$$

$$\text{and } s = \frac{j}{N\Delta}$$

Equation (3.5) is one form of the discrete Fourier transform. X_j corresponds to $F(s)$, and x_k corresponds to $f(t)$. The reason that j is limited, when s was not, is due to the fact that a discrete time series sampled at rate Δ does not contain frequencies outside of the band: $-1/2\Delta \leq s \leq 1/2\Delta$. Signals in the continuous time series outside of that frequency band are folded into that band by the sampling, and are said to be aliased. This is usually not a desirable situation, since it can destroy information about the signals that actually do reside within that band. The value $1/2\Delta$ is called the Nyquist frequency. Much care has been taken with the WIHA signals to avoid aliasing by low-pass filtering them below the Nyquist frequency before sampling, as previously mentioned.

One characteristic of a DFT is that it conserves information. For N independent complex time series values going into the transform, N independent complex frequency amplitudes come out of the transform. When the time series is real valued, as is the case for the WIHA data, the X_j are still generally complex valued, but conservation of information is maintained because $X_j = X_{N-j}^*$, $X_0 \in \mathbb{R}$, and $X_{N/2} \in \mathbb{R}$. Thus, in this case, there are N independent numbers going into and coming out of the DFT.

Because the X_j are redundant for negative values of j when the x_k are real, and because the time series spectrally analyzed in this study are real, the DFT and Parseval's Theorem can be redefined with new limits as:

$$X_j = \Delta \sum_{k=0}^{N-1} x_k e^{-i2\pi jk/N}, \quad j \in \{0, 1, 2, \dots, N/2\} \quad (3.7)$$

$$\text{and } \frac{1}{N\Delta} \left[X_0^2 + X_{N/2}^2 + 2 \sum_{j=1}^{N/2-1} |X_j|^2 \right] = \Delta \sum_{k=0}^{N-1} x_k^2. \quad (3.8)$$

The DFTs defined by (3.5) and (3.7) give exactly the same output as the original Fourier transform defined by (3.1), given the same input. The $|F(s)|^2$ and the $|X_j|^2$ are

both energy density spectra. To compute the energy in a given frequency band, integration over that band is required. But, the X_j are only computed at discrete frequencies representing frequency bands of width $1/N\Delta$ Hz. Thus, it is sometimes considered more direct to let each $|X_j|^2$ represent the total energy in the j^{th} frequency band rather than the energy density function at the j^{th} frequency. This can be accomplished by multiplying the right-hand side of the DFT by the square root of the bandwidth and adjusting Parseval's Theorem accordingly:

$$X_j = \Delta (1/N\Delta)^{1/2} \sum_{k=0}^{N-1} x_k e^{-i2\pi jk/N}, \quad j \in \{0,1,2,\dots,N/2\} \quad (3.9)$$

$$\text{and } X_0^2 + X_{N/2}^2 + 2 \sum_{j=1}^{N/2-1} |X_j|^2 = \Delta \sum_{k=0}^{N-1} x_k^2. \quad (3.10)$$

Note that now the units of the $|X_j|^2$ are the squared units of the time series multiplied by time, the same energy units mentioned earlier.

Finally, because this is a study of noise that is stationary or steady state (at least in general over time scales of less than about an hour), the most useful measurement is power. The noise power in any particular frequency band should tend to be invariant, regardless of the time length of the DFT used to measure it, since it should simply represent the size of the fluctuations in that band which are assumed to be steady state. Like its physical counterpart, spectral power is found by dividing the spectral energy by the total time, in this case the time length of the DFT, $N\Delta$. Thus, the DFT is redefined one last time so that the $|X_j|^2$ are power, and Parseval's Theorem is again modified accordingly:

$$X_j = \frac{1}{N} \sum_{k=0}^{N-1} x_k e^{-i2\pi jk/N}, \quad j \in \{0,1,2,\dots,N/2\} \quad (3.11)$$

$$\text{and } X_0^2 + X_{N/2}^2 + 2 \sum_{j=1}^{N/2-1} |X_j|^2 = \frac{1}{N} \sum_{k=0}^{N-1} x_k^2. \quad (3.12)$$

Equation (3.11) is the form of the DFT that has been used throughout this analysis. This

definition is preferred over others because its form is relatively simple, it gives power spectral estimates that have an understandable meaning, and it leads to an intuitively pleasing form of Parseval's Theorem. The units of $|X_j|^2$ are the squared units of the time series, and each $|X_j|^2$ is the power spectral estimate in the j^{th} frequency band, spanning from $(j-1/2)/N\Delta$ to $(j+1/2)/N\Delta$ Hz. Care should be taken to note that the power spectral estimates themselves are not invariant with a change in $N\Delta$, because changing $N\Delta$ changes the bandwidth of the estimate accordingly.

Parseval's Theorem has been carried along in this discussion to give some further intuitive meaning to the definitions of the X_j . The right-hand side of (3.12) is simply the mean squared value of the time series. Thus, from the left-hand side it can be deduced that each $|X_j|^2$ is one-half of the mean squared value of the time series component in the j^{th} frequency band ($j \neq 0$ or $N/2$). Although these time series components are not known explicitly, they are essentially what would result by bandpass filtering the original time series between $(j-1/2)/N\Delta$ and $(j+1/2)/N\Delta$ Hz for each j .

- Implementation of the FFT

The fast Fourier transform is a way of computing a DFT on a computer that is especially fast. It takes advantage of the fact that a DFT of length N can be formed from two DFTs of length $N/2$ which in turn can be formed from four DFTs of length $N/4$, etc. The length of time it takes to compute a DFT in a direct way is proportional to N^2 , but using an FFT it is proportional to $N \log_2 N$, a considerable savings in computer time when computing DFTs of even modest length. FFTs are only computed for time series with lengths of 2^n , $n \in \{\text{positive integers}\}$, but this is really only a minor inconvenience as will be shown. Several different FFT codes have been used in the analysis of the WIHA data. The code currently being used is one for a real-to-complex transform code from *Numerical Recipes* by Press et. al. (1990).

In practice, the FFT is applied to the data in the following manner. First, an FFT length, N is chosen which gives an adequate frequency resolution, $1/N\Delta$, and a section of time series of that length is culled from the longer time series. Or, if the time series is limited in length, as are the three-minute-long noise samples, the minimum possible FFT length is chosen that is greater than the length of the time series. The term N_D will be used for the data length to distinguish it from the FFT length N , in case they are different. Next, the mean value of the time series is computed and subtracted from each data point, demeaning the data. Also, the slope of the time series is determined using a standard least-squares fit technique, and this slope is removed, deskewing the data. Demeaning and deskewing help to ensure that the spectral data are not contaminated by spectral leakage from high amplitude signals at the lowest frequencies that would result from a large non-zero mean or slope.

The last step before the FFT is to multiply the time series by a window function. The window function determines the spectral shape of the bins in the frequency domain. If no window is used, a boxcar window with a height of unity and length of $N_D\Delta$ is implied, and the resulting bin shape is a sinc function. This sinc function is usually not considered practical for a bin shape because it has large sidelobes that result in unacceptable leakage of power to adjacent spectral bands. Some commonly used windows are the Hamming, Hanning, Parzen, and Lanczos windows. These windows are all smoothly tapered to zero at both ends in the time domain, producing much lower sidelobes in the frequency domain. The window used in this study was the Lanczos window, which also has the unique property of preserving the total power of the unwindowed time series. The Lanczos window is defined as:

$$L_k = 1.73 \operatorname{sinc}^2(y_k), \quad k \in \{0, 1, \dots, N_D - 2, N_D - 1\}$$

for $y_k = [2k/(N_D - 1)] - 1$,

and $\operatorname{sinc}(y_k) = \operatorname{sine}(\pi y_k) / \pi y_k$.

The time series values are multiplied by the corresponding values of the Lanczos window, and if $N_D < N$, the remaining $N - N_D$ data points are set to zero. These N time series values are the input to the FFT, with $N/2 + 1$ spectral estimates resulting as shown in (3.11).

• Spectral Units

Units on spectral plots are often of the form: "decibels relative to (some unit)² per Hz." In this study, the "some unit" is μ Pascals. The following section will explain the derivation of these units, and concurrently, their meaning.

Normalization

As previously stated, the units of the power spectral estimates, $|X_j|^2$, are equal to the squared units of the time series. So for the WIHA data the units are (digital units)² or d.u.². A spectral plot of $C_j |X_j|^2$ ($C_j=1$ for $j = 0$ or $N/2$ and $C_j=2$ for $1 \leq j \leq N/2-1$) versus j could be labelled "Index" on the abscissa and "d.u.²" on the ordinate. The C_j term is introduced here, so that the integration of the curve over all indices is equal to the mean squared value of the time series as shown in (3.12). Integrating this curve over a range of indices, then, gives the total power for that range of indices, corresponding to the total power for a range of frequencies. A more useful approach might be to plot the $C_j |X_j|^2$ versus frequency, $j/N\Delta$. The abscissa would be labelled "Hz", and the ordinate would have to be labelled "d.u.² per $1/N\Delta$ Hz" so that integration over the same range of frequency would produce the same result. This type of plot is somewhat awkward, however, since to compare two plots having different bandwidths (determined by their respective $1/N\Delta$ values), the $|X_j|^2$ data on one of the plots must be normalized to the bandwidth of the $|X_j|^2$ data on the other plot by multiplying it by the ratio of the bandwidths. The way to correct this shortcoming is to normalize all power spectral data to a bandwidth of 1 Hz by multiplying them by $N\Delta$ before plotting. The ordinate is then labelled "d.u.² per Hz", or, if the square root of the data are

plotted, "d.u. per root Hz". Plots made in this form can be directly compared.

Resolution

One possible problem with doing this, however, is that the spectral resolution of the plot, $1/\Delta$, is lost. For spectra that contain sharp features, knowing the resolution can be important, since a resolution wider than the spectral feature of interest will distort it. Smoothing of the spectrum by averaging adjacent estimates is also a broadening of the resolution which should be indicated. There is no standard for indicating spectral resolution on plots, so in this dissertation it is simply noted in figure captions when necessary.

Decibels

Spectral data such as these are often displayed on log-log plots, since the physical processes they represent are usually more naturally described on those scales, and since the range of the data is often not easily shown on a linear scale. For example, the WIHA data contain pressure levels ranging from 10^6 to 10^{16} $\mu\text{Pascals}^2$ per Hz. The decibel (dB) is a logarithmic unit commonly used for spectral measurements like these. It has two equivalent definitions, one for amplitude and one for energy or power:

$$A \text{ (in dB relative to } 1 \text{ U)} = 20 \log_{10} [A \text{ (in U)}/1 \text{ U}] , \quad \textit{amplitude definition}$$

$$\text{and } A \text{ (in dB relative to } 1 \text{ U}^2) = 10 \log_{10} [A \text{ (in U}^2)/1 \text{ U}^2] , \quad \textit{power definition}$$

where A is the quantity being measured (e.g., ambient ocean noise), U is the amplitude unit of that quantity (e.g., d.u. per root Hz), and U^2 is the power unit of that quantity (e.g., d.u.² per Hz). Note that the dB values are the same, regardless of whether they were calculated from the amplitude of the signal or from the power of the signal, since the squaring is accounted for by the change in the definition. Thus, sometimes confusingly,

$$A \text{ (in dB relative to 1 U)} = A \text{ (in dB relative to 1 U}^2\text{)} .$$

This takes care of the inconsistency of having different units on the ordinate if the data are plotted as amplitude versus if they are plotted as power.

Calibration

Having data in the logarithmic decibel units also make them easier to manipulate manually, since multiplications and divisions become merely additions and subtractions. This is usually the case for converting the data to physical units. It can be accomplished by subtracting the response curve, in dB relative to 1 d.u. per μPascal (or relative to 1 d.u.² per μPascal^2), from the uncalibrated data, in dB relative to 1 d.u. per root Hz (or relative to 1 d.u.² per Hz), to produce calibrated data in units of dB relative to 1 μPascal per root Hz (or relative to 1 μPascal^2 per Hz).

• Statistical Properties of the Spectral Estimates

For a time series of white noise - normally distributed, zero-mean, independent random numbers with a variance of σ^2 - it can be shown that the expected value of the power spectral estimate defined by (3.11), $E(|X_j|^2)$, is the same for every j and is equal to the value σ^2/N . It can also be shown that the random variable $\nu |X_j|^2/E(|X_j|^2)$ has a chi-squared distribution with ν degrees of freedom. The degrees of freedom are two for $1 \leq j \leq N/2 - 1$, from the normally distributed real and imaginary parts of X_j , and one for $j=0$ or $N/2$ since there is only a real part. From properties of the chi-squared distribution, namely that the mean is ν and the variance is 2ν , it is found that for all of the power spectral estimates with $\nu=2$, the standard deviation is coincidentally equal to σ^2/N , the expected value.

Although the WIHA data are not a time series of white noise, the random processes that produce it make it possible to extend some of these statistical properties to those data. In

particular, $\nu |X_j|^2 / E(|X_j|^2)$ has a chi-squared distribution with ν degrees of freedom (1 or 2 as noted above), and the standard deviation of each $|X_j|^2$, except those with $\nu=1$, is equal to the expected value. However, for the WIHA data the expected values of $|X_j|^2$ are not equal to σ^2/N , but may vary from one frequency to the next. The distribution is highly asymmetrical. In dB units, 45% of the spectral estimates with $\nu=2$ will have values between -13 dB and 0 dB relative to the expected value, and 45% will have values between 0 dB and +5 dB relative to the expected value.

It is important to note that the ratio between the standard deviation and the expected value of each power spectral estimate is a constant, 1, and it does not decrease with increasing values of N . This is a consequence of the fact that for larger N , the number of spectral estimates increases accordingly, thus no additional information is added to each X_j . To get a better estimate of the expected values of the spectral estimates, this ratio needs to be reduced. Such a reduction can be accomplished by averaging together adjacent spectral estimates, with a corresponding loss of frequency resolution, or by computing additional spectra from adjacent sections of time series and then averaging together corresponding spectral estimates. Both methods have been used on the WIHA data. If m power spectral estimates are averaged together, then the ratio is reduced by a factor of $m^{-1/2}$, as a direct consequence of the fact that the number of degrees of freedom have been increased accordingly.

• Summary

In summary then, the values plotted as the power spectral density, P_j , of the ambient ocean noise are described by the following formula:

$$P_j = 10 \log_{10} \left[C_j (N\Delta) \left| \frac{1}{N} \sum_{k=0}^{N-1} L_k x_k' e^{-i2\pi jk/N} \right|^2 \right] - R_j, \quad j \in \{0, 1, 2, \dots, N/2\}, \quad (3.13)$$

where x_k' is the demeaned and deskewed (and possibly padded with zeroes) time series of

length N in digital units, L_k is the unitless Lanczos windowing function (with a length equal to the length of the non-zero data), Δ is the sampling interval in seconds, C_j equals 1 or 2 as described above, and R_j is the response curve in "dB relative to 1 digital unit per μ Pascal." The units of P_j are "dB relative to 1 μ Pascal per root Hz," and the total power in any frequency band can be interpreted as the mean squared value of the pressure variations in that band. The P_j , which are only estimates of the power spectral density, have a distribution that is based on the chi-squared distribution of the underlying raw power spectral estimates from which they are formed. Their exact distribution is complicated by Lanczos windowing function and by the conversion to logarithmic dB units.

Computer Programs

Many computer programs were written to process the WIHA data for this study. Some of them were needed just to assemble the data from the archive. These programs read the archive tapes, demultiplexed the hydrophones of interest, checked for continuity, eliminated bad and duplicate data, rearranged data that were out of order, created new data files for further processing, and made logs of their activity. One set of programs low-pass filtered the archived data and then resampled it at a much lower rate. A total of over 20 Gbytes of archived data were read and processed using these programs. Once the archived data were assembled into data sets of manageable size, they were processed by the programs described below.

- **FPLOT - Time Series Plots**

Program FPLOT is used to make hardcopy plots of time series data. Up to 256 multiplexed channels of data can be displayed side-by-side with any time scale. They can also be high, low, or bandpass filtered. The amplitude of each channel can be individually controlled, either manually or automatically. The output is a raster file that is spooled

directly to a Versatec plotter. The main advantage of this program over other time series plotting programs is its ability to handle a time series of any size, and to make long plots analogous to those made by a multipen chart recorder. It was not used extensively to view the noise data in their time series form, except to view some of the transient signals from whales and earthquakes. However, it was used to display the time series of noise level variations at particular frequencies that are discussed in Chapter 4.

- TFORM - Time to Frequency Domain Transformation

Program TFORM transforms time series data to power spectral estimates with an FFT that corresponds to a DFT of the form:

$$X_j = \frac{1}{N} \sum_{k=0}^{N-1} L_k x_k' e^{-i2\pi jk/N}, \quad j \in \{0,1,2,\dots,N/2\},$$

where N is the length of the FFT, x_k' is the demeaned and deskewed time series, and L_k is the Lanczos window function. TFORM can demultiplex a particular channel, and then divide this input time series into segments of any length for transformation. The segments can have any amount of overlap, and are typically overlapped by 50% to counteract the effect that the Lanczos window has on the ends of each segment. Output from the program are the $|X_j|$ for each segment in a form suitable for input to the SPCGRM and SPCPLT programs. This program was used on every data set analyzed in this study.

- SPCGRM - Spectrogram Plots

Program SPCGRM generates spectrograms on a Versatec plotter from the power spectral estimates output by program TFORM. The spectrograms have time in the X-direction (the long axis of the paper), frequency in the Y-direction (the short axis of the paper), and dB power level in the Z-direction represented by either shades of gray or colors plotted in $(0.2\text{-cm})^2$ boxes. The time scale is fixed, with one 0.2-cm increment in the

X-direction equal to the time between the segments of time series transformed by TFORM. The frequency scale is flexible. It can be linear or logarithmic, and represent any range of frequencies. Spectral estimates from TFORM are averaged together appropriately to compute levels on the plot for each 0.2-cm increment in the Y-direction. Power level ranges are represented by discrete shades of gray, or by colors. The power levels displayed can be the absolute levels output by TFORM, or the absolute levels minus a mean level at each frequency. This second type of display is often more useful than the first for studying noise, since it emphasizes the changes in noise level with time. Such spectrograms were produced extensively to view the noise in this study. No provision is made to plot the calibrated power levels in the spectrogram by applying a response curve, since calibrated data are more easily viewed in a spectrum.

- SPCPLT - Spectrum Plots

Program SPCPLT makes spectra from the data output by program TFORM. These are the power spectral density curves plotted with frequency along the X-axis, and power spectral density along the Y-axis. The frequency scale can be linear or logarithmic, with any range of frequencies. The power spectral density scale is in logarithmic dB units. Usually, the spectral data are first plotted in spectrogram form using program SPCGRM. Then, an interval of time on the spectrogram is chosen, and these data are plotted as a spectrum using SPCPLT. The power spectral estimates from TFORM are averaged together if more than one FFT is represented in the time interval. Response curves can also be input, so that the resulting spectra are corrected to pressure units. In addition, the data can be normalized to a bandwidth of 1 Hz. When these two options are chosen, the output are of the form given by equation (3.13). Several spectra may be plotted on a single plot for comparison. SPCPLT was also used extensively in this study.

CHAPTER 4. 0.5-30 HZ NOISE AND WIND

This study compares the local wind, and by implication the local wind waves, to the ambient noise at frequencies between about 0.5 and 30 Hz. Chronologically, this was the first study made of the WIHA noise. It developed from a test to see if the ocean noise above 5 Hz was being masked by amplifier noise or the thermal noise of the hydrophone and cable. When temporal variations in the noise appeared strikingly similar to the temporal variations in the wind speed, the focus of the study shifted appropriately.

Data Set

The data used for this study span the one-year time interval from September 8, 1982 through September 7, 1983. This is a time interval for which three-minute-long noise samples were extracted from the continuous WIHA data at a rate of about one per hour. From these data, a subset was extracted consisting of one three-minute-long noise sample every six hours for two deep hydrophones, 74 and 76, and two SOFAR hydrophones, 10 and 20. These hydrophones were chosen for the variety of ocean environments they represent. The two deep-bottom hydrophones are anchored on flat, sediment-covered ocean floor; SOFAR hydrophone 10 is anchored on the slope descending from Wake Island; and SOFAR hydrophone 20 is suspended above the side of a seamount. Noise data from these hydrophones are compared to wind data from the National Weather Service (NWS) station at Wake Island.

Data Reduction

• Spectral Computation

The first step in the analysis was transformation of the data from the time domain to the frequency domain. Each 3-minute-long time series of 80 sample per second data was divided into 27 adjacent 512-point segments, and each of these segments was transformed

with a 512-point FFT. This length FFT gives a spectral bin width of 0.156 Hz, adequate for resolving details in the noise spectrum above 0.5 Hz, but not for lower frequencies. Mean power spectral levels at each of the 256 frequencies were computed by averaging data from the 27 transformed segments. These mean values have a chi-squared distribution with 54 degrees of freedom, and a standard deviation equal to 19% of their value (< 1 dB). Four large data sets were produced, one for each hydrophone. Each data set consists of 256 time series, one for each of the 256 spectral frequencies; and each time series is 1460 samples in length (i.e., 365 days \times 4 samples / day = 1460 samples). These time series represent the ambient noise level fluctuations over a 1-yr period for a particular hydrophone at a particular frequency. Only the first 192 (0 to 30 Hz) of each hydrophone's 256 time series were analyzed further, in order to avoid data too near the 40-Hz Nyquist frequency.

- Removal of Transients

An attempt was made to remove unwanted transients present in each of the time series. Sources for these transients are primarily earthquake phases, ships passing nearby, and signals from various artificial underwater sound sources such as those used for ocean seismic surveys. A transient was empirically defined as any individual sample with a power level at least 3 dB greater than both of the adjacent samples in the time series. Transients were replaced by the mean value of the two adjacent samples. This procedure successfully removed extraneous spikes in the data, while preserving most of the original character of the time series (Fig. 9). At a maximum, only about 10% of the data points of any time series were modified by this procedure (Fig. 10). It is interesting to note that the percent number of transients in a particular time series appears to be directly proportional to the noise frequency that the time series represents, at least between 0 and 20 Hz. This is at least partially a consequence of the fact that, in general, the absolute levels of ambient

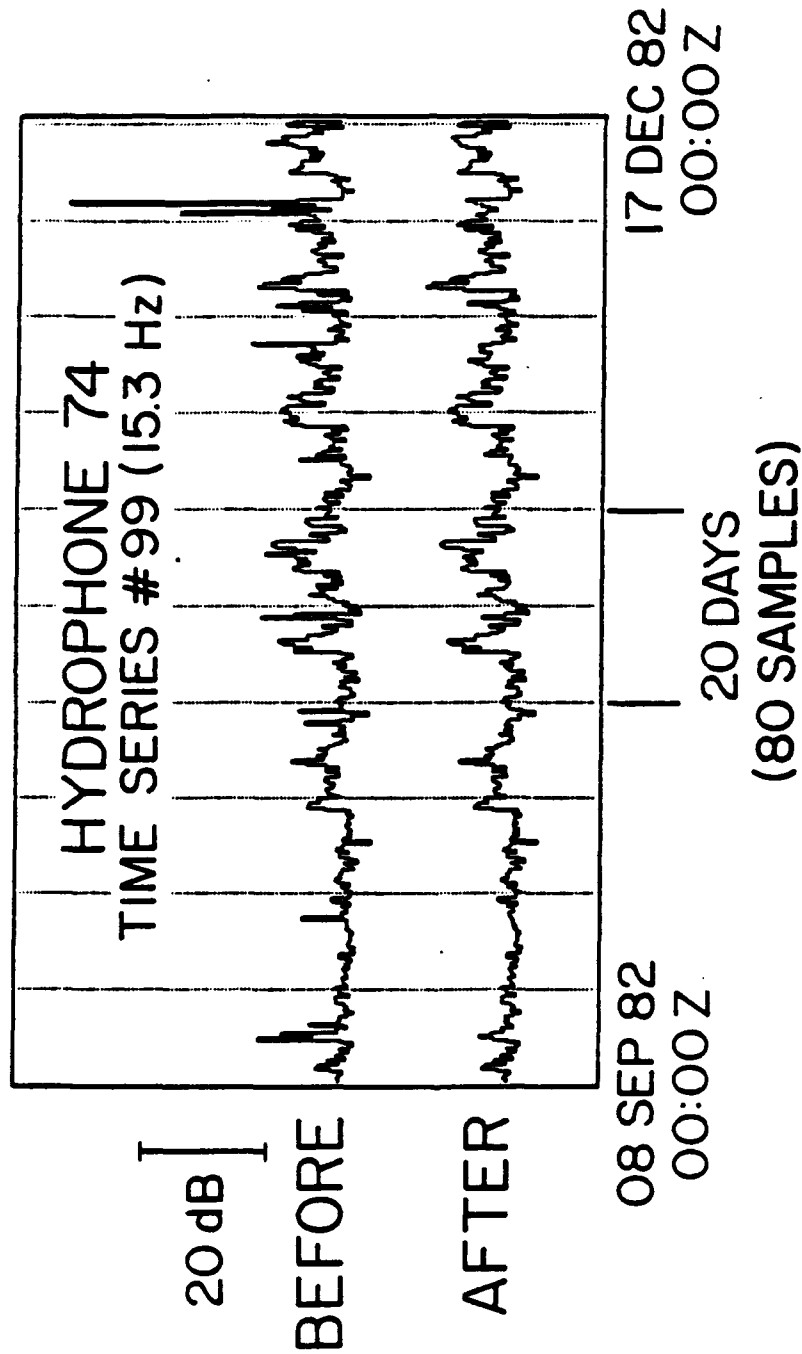


Fig. 9. An example of the effect of removing transients from a time series of noise level variations. Most of the character of the original time series is retained.

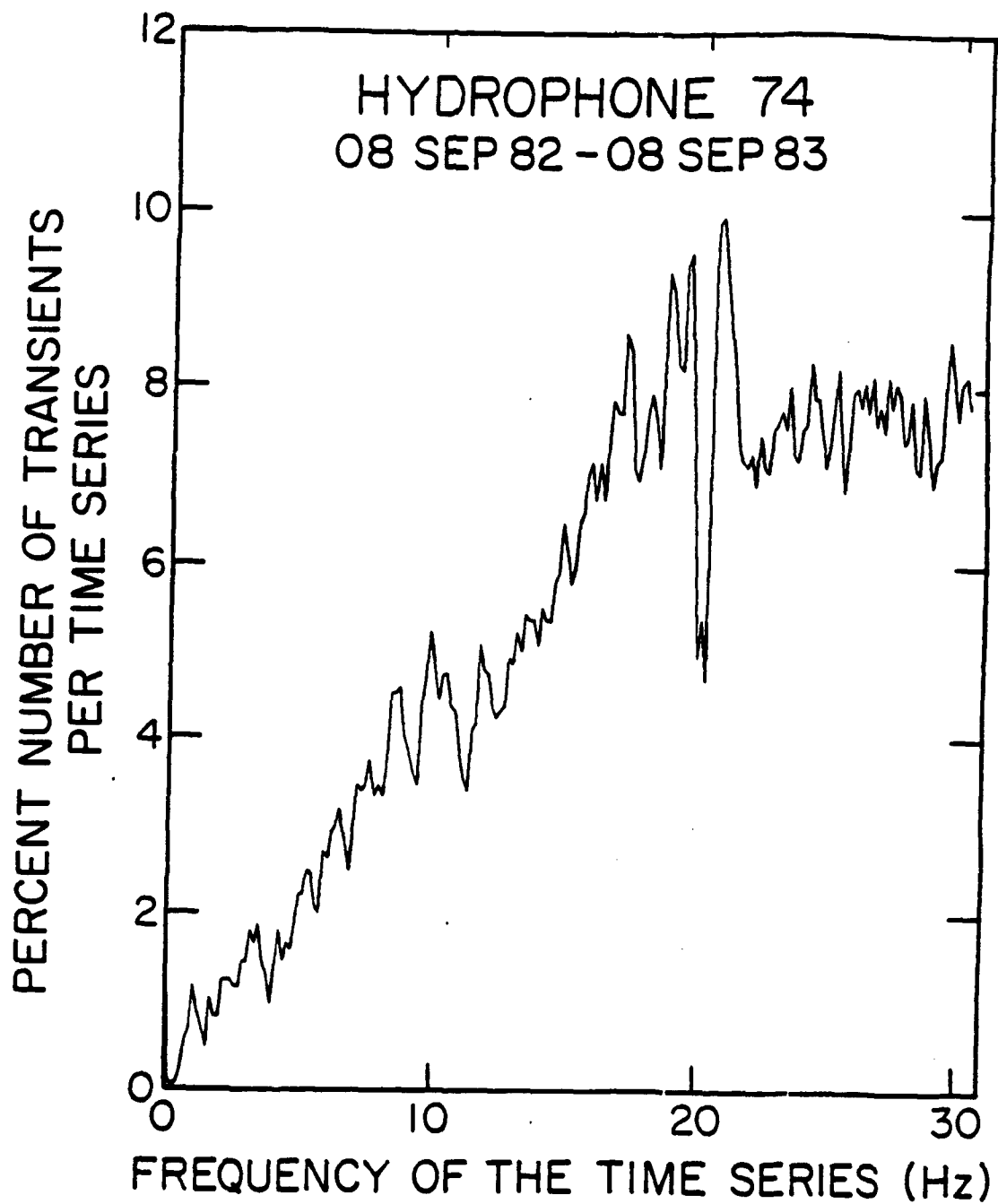


Fig. 10. Percent number of transients in the noise data of hydrophone 74 as a function of frequency. The feature at 20 Hz is an artifact due to aliased 60 Hz signals.

noise decrease rapidly with frequency over this same band.

One-Year Mean Spectra

The one-year mean noise spectra of all the hydrophones studied exhibit characteristics typical of deep ocean noise spectra (Fig. 11). Levels are highest near the microseism peak between 0.1 and 0.3 Hz, although the spectral resolution of this study, 0.156 Hz, is too coarse to resolve that peak with any precision. Between 0.3 and 6 Hz, levels fall off rapidly with frequency, and above 6 Hz the spectral slope is much less steep or even flat. A narrow peak at 20 Hz in the spectra of hydrophones 74 and 76 is an artifact due to a large 60-Hz signal that is aliased to 20 Hz. A broader rise in level at about 17 Hz on all hydrophones, however, is caused by whales. Whale signals are easily identified in the time record and similar signals have been described and identified by Northrop et al. (1971) and also by Urick (1983). The standard deviations shown around each curve in the figure should be viewed with some caution since the actual distribution of noise levels is not Gaussian, as will be demonstrated later.

Differences between the four one-year means are shown in Fig. 12, using hydrophone 74 as the reference at zero dB. The two bottom hydrophones, 74 and 76, have nearly identical means as might be expected due to their 40-km spacing and similar environment.

Differences between these two curves at frequencies above 10 Hz are probably due to small remaining errors in the estimates of their respective cable responses. Suspended SOFAR hydrophone 20 is quieter than 74 below 2 Hz, and noisier above 3 Hz. Increased noise levels at the high frequencies are due to this hydrophone's location within the SOFAR channel, a highly efficient waveguide capable of propagating noise at these frequencies over many thousands of kilometers. Increasingly low levels at frequencies below 2 Hz are not entirely understood. They might be indicative of a depth dependency related to the propagation of this noise. Or, they might be due to an error in the

**HYDROPHONE 74 (5.5-KM)
ONE-YEAR-MEAN NOISE SPECTRUM**

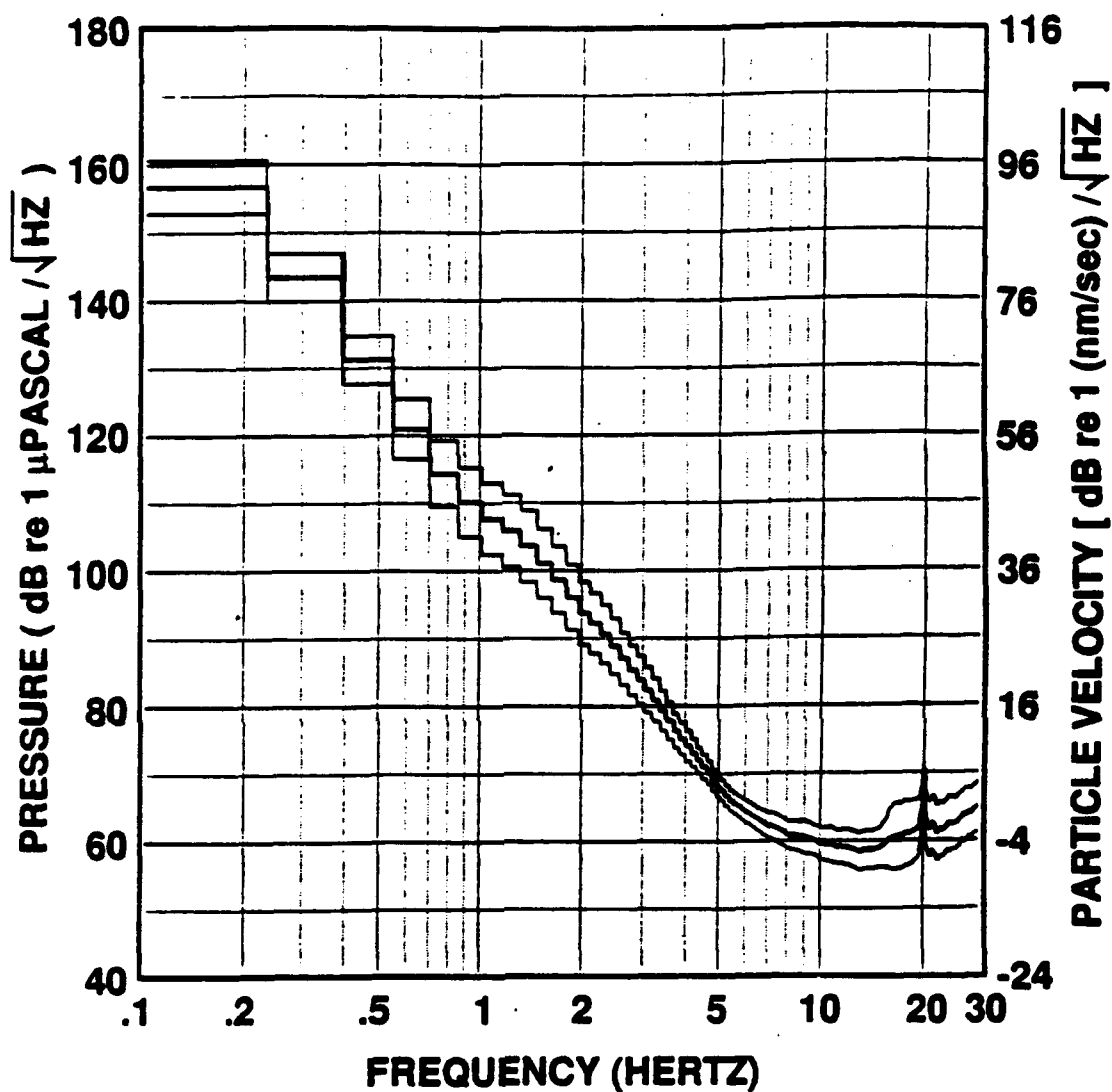


Fig. 11. One-year mean ambient noise level spectra, plus and minus one standard deviation, for hydrophones 74, 76, 10, and 20. Vertical particle velocities corresponding to acoustic pressure fluctuations are computed by the formula: pressure = seawater density \times sound velocity in seawater \times vertical particle velocity. The frequency resolution is 0.156 Hz. The figure continues on the following three pages with the particular hydrophone noted at the top.

**HYDROPHONE 76 (5.5-KM)
ONE-YEAR-MEAN NOISE SPECTRUM**

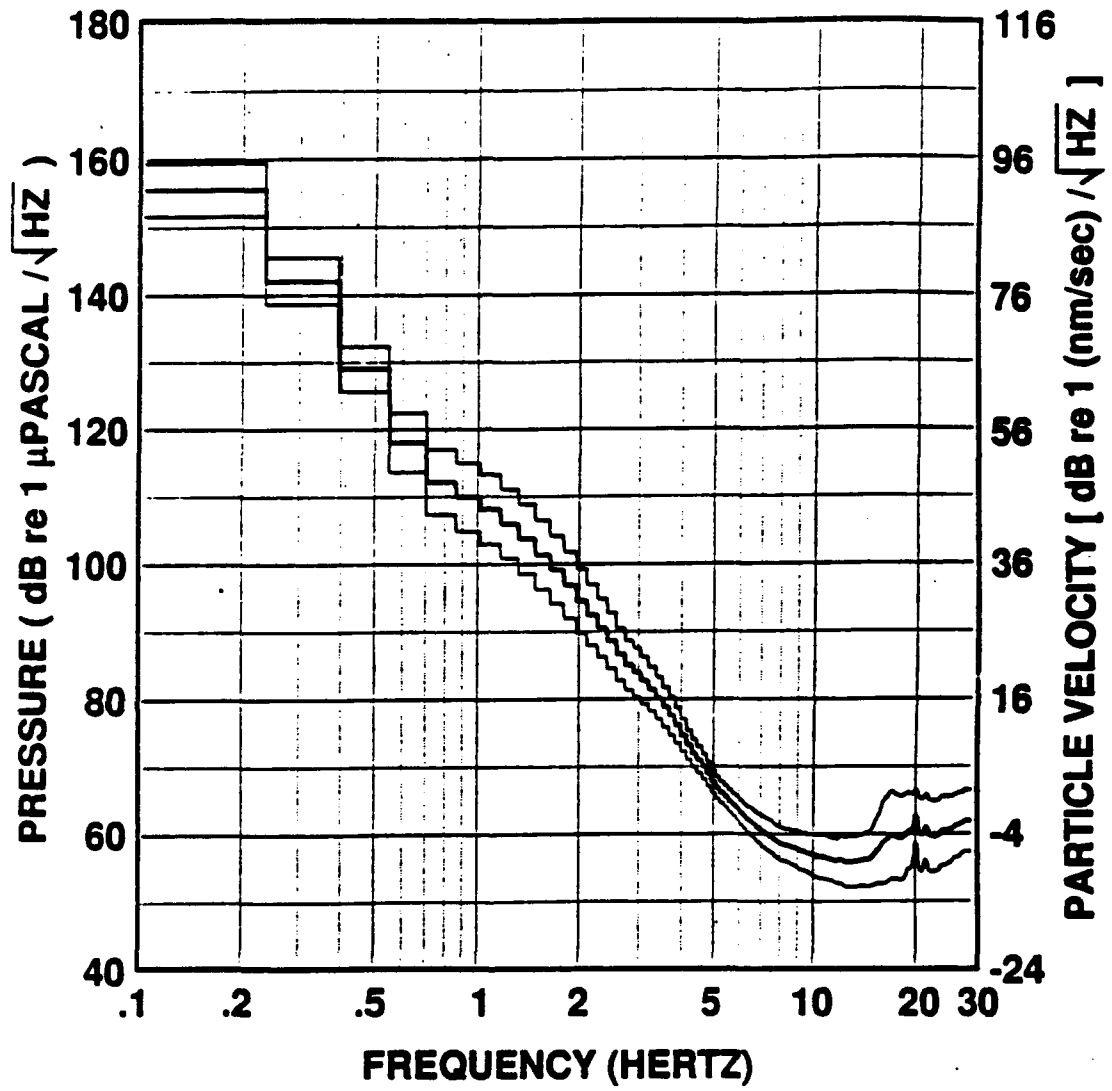


Fig. 11 (continued).

HYDROPHONE 10 (0.8-KM) ONE-YEAR-MEAN NOISE SPECTRUM

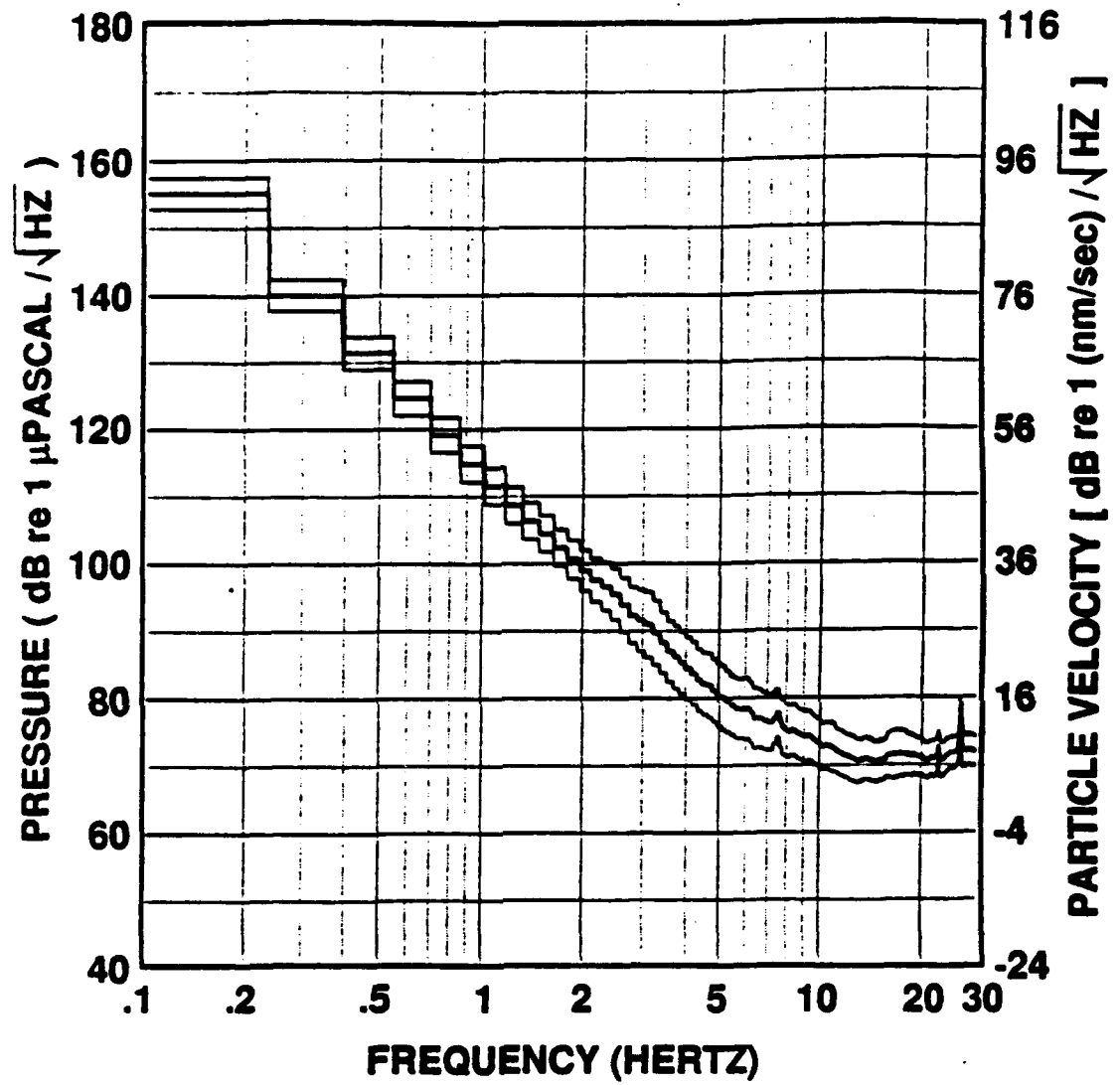


Fig. 11 (continued).

HYDROPHONE 20 (0.8-KM)
ONE-YEAR-MEAN NOISE SPECTRUM

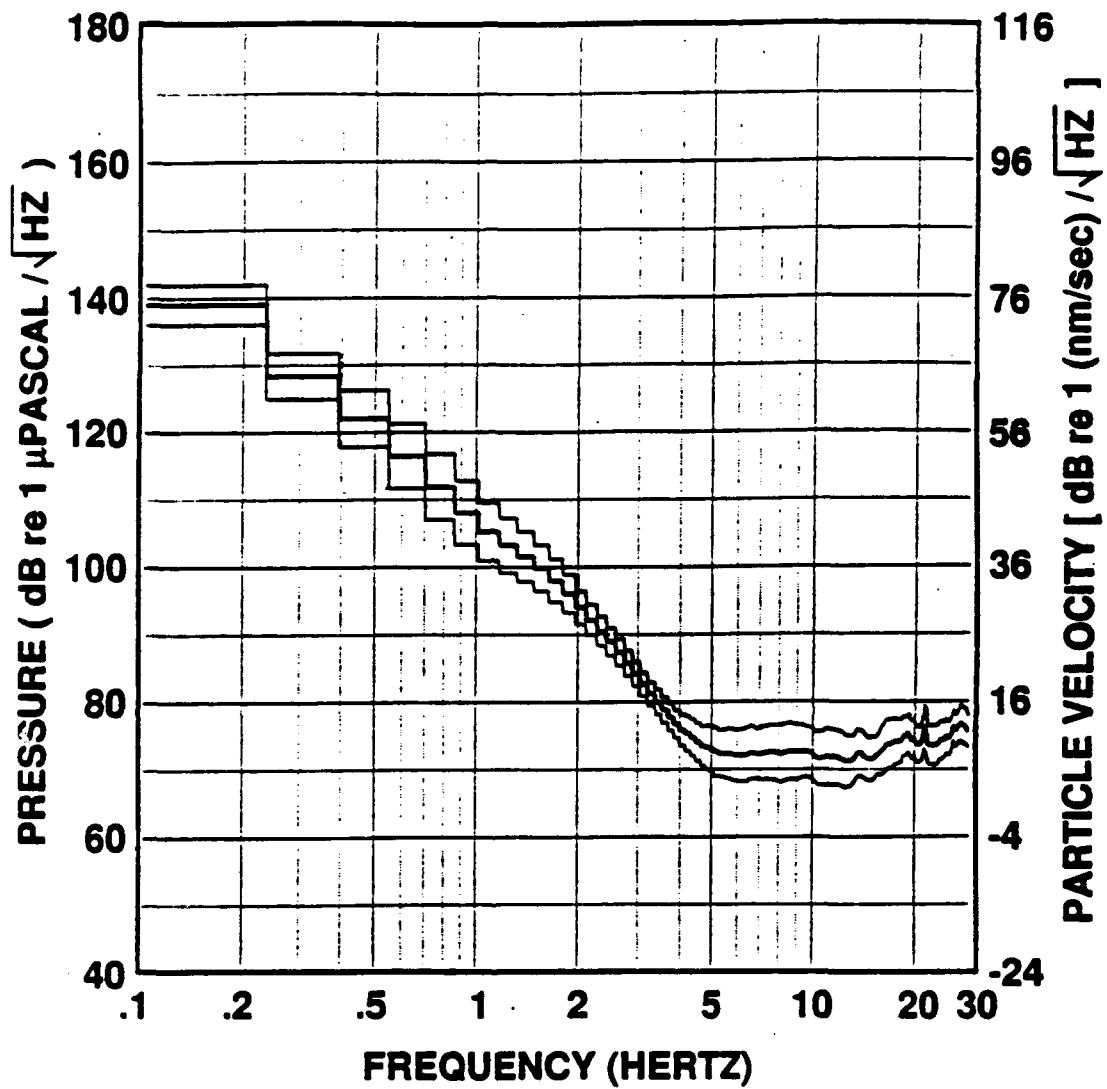


Fig. 11 (continued).

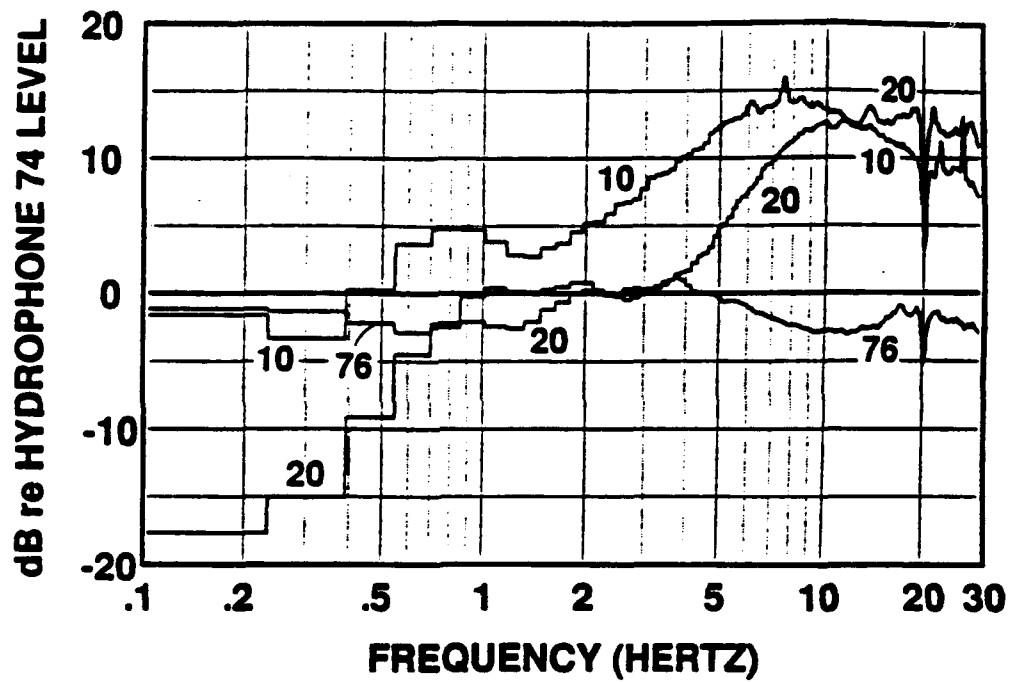


Fig. 12. The one-year noise means of hydrophones 76, 10, and 20 measured relative to the one-year noise mean of hydrophone 74 (at zero dB).

assumptions about the hydrophone response at low frequencies and the aforementioned static pressure compensation hole. SOFAR hydrophone 10, on the submarine flank of Wake Island, is noisier than all other hydrophones at all frequencies above 0.4 Hz. This is most likely the result of its location only 3 km from the shores of Wake Island, where breaking surf is an additional energetic source of noise.

The one-year-mean noise spectra of hydrophones 74 and 20 are compared to several other oceanic and continental ambient noise spectra in Fig. 13. The WIHA curves are most similar to the other oceanic curves, two from hydrophones in the Atlantic (Nichols, 1981) and one from a differential pressure gauge in the Pacific (Cox et al., 1984). Two continental noise spectra, corrected to pressure, are also shown for reference. One of them represents the average ambient noise on continents (Brune and Oliver, 1959), and the other is from perhaps the world's quietest continental site in Texas (Herrin, 1982).

Temporal Variations

In order to more easily view the information contained in the 192 time series associated with each hydrophone, these data were combined into only 15 time series for each hydrophone. The new time series represent the ambient noise level fluctuations over the one-year period in 15 contiguous 2-Hz bands from 0 to 30 Hz. Computation of the new time series was made as follows. Each 2-Hz band represents approximately 13 original time series (i.e., $192 \text{ original} / 15 \text{ new} = 12.8$). Each data point in an original time series represents the noise level for a particular 6-hour time period in a 0.156 Hz frequency band. By averaging together the dB noise levels from the appropriate original time series for each 2-Hz band, 15 new time series are formed. If an original time series was just fractionally represented in a particular 2-Hz band, then it was included in the average only if that fraction was greater than one-half. Note that by averaging in log space (dB), similarities in the shapes of the original time series are emphasized--the original time series with the most

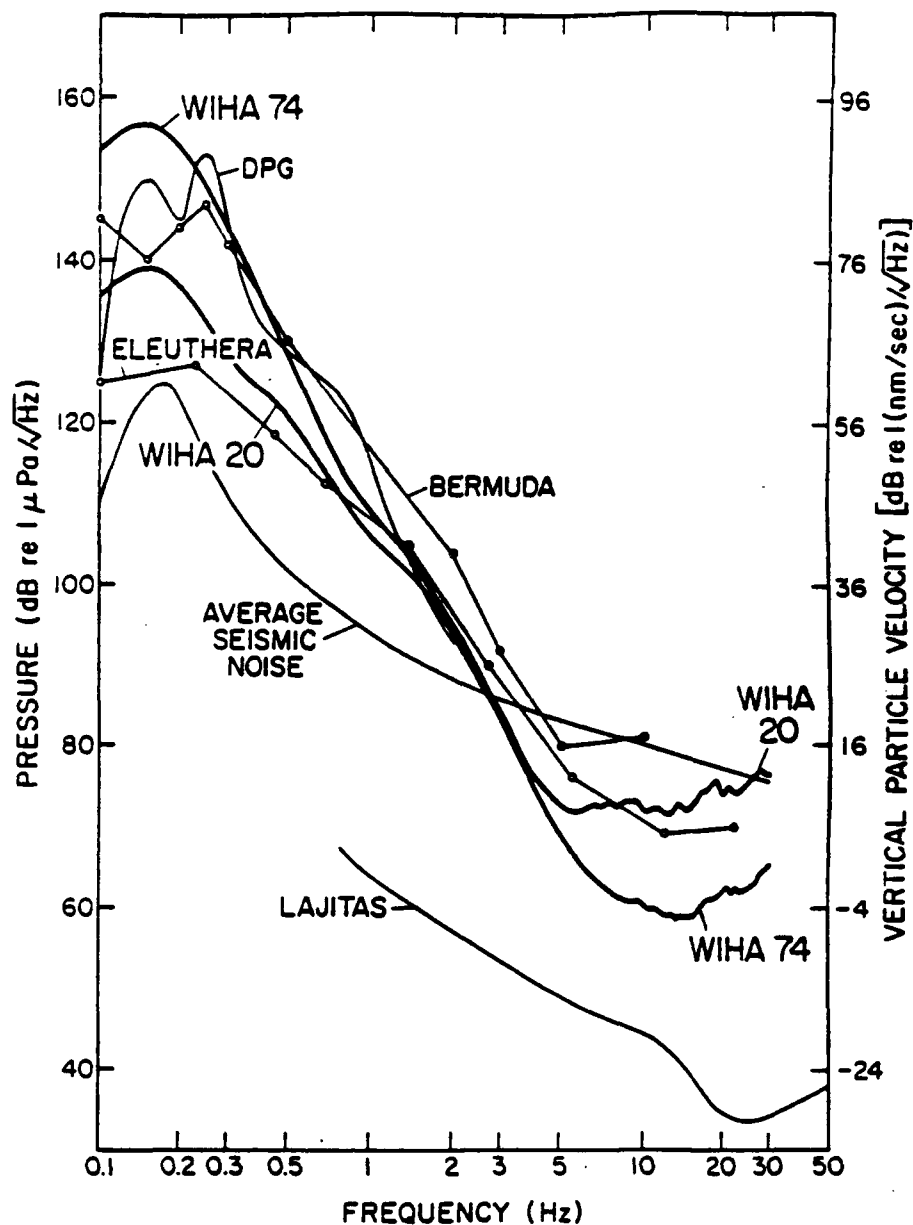


Fig. 13. One-year mean noise spectra of WIHA hydrophones 74 and 20 compared to ambient noise measurements made elsewhere. The Eleuthera Island measurement is a six-week average made by Nichols (1981) using a hydrophone at 1300 m depth. The Bermuda Island measurement is an average of four 10-minute samples taken during 6.4-m/s average winds using a hydrophone at 4300 m depth (Talpey-Worley data from Nichols, 1981). The differential pressure gauge data (DPG) reported by Cox et al. (1984) was collected at 1600 m depth off the California coast. The "average seismic noise" reported by Brune and Oliver (1959) is from vertical seismometer measurements made on continents. And, the Lajitas, Texas curve from Herrin (1982) represents very low continental noise.

power doesn't unduly influence the result. Similarly, note that in the 0-2 Hz band this type of averaging will de-emphasize the microseism peak data since it is represented only in the two lowest-frequency original time series.

A comparison of the 15 new time series for hydrophone 74 for the entire year shows that many of the features are present over numerous frequency bands (Fig. 14). Significant differences among the 15 time series are also seen. For example, the 2-4 Hz time series appears truncated across the top, and exhibits noise lows that are as much as 15 dB below the apparent noise ceiling. Similar features in the ambient noise data from a long-term deployment of HIG's Ocean Sub-bottom Seismometer down a deep-sea drill hole near the Kuril Islands were previously reported by Duennebier et al.(1986). The time series for frequencies above 6 Hz, on the other hand, appear somewhat truncated at the bottom and exhibit noise peaks with amplitudes 20 dB or more above the apparent noise floor. The 4-6 Hz time series seems to be a transition between the 2-4 and 6-8 Hz bands, and is flat-middled with some lows and some peaks. Only the 0-2 Hz curve appears to be unrestricted throughout its amplitude range. Some of the large amplitude signals prominent on the 16-18 Hz curve and also visible on adjacent curves are caused by whales.

One hundred days of ambient noise in six of the fifteen 2-Hz bands for all four hydrophones are shown in Fig. 15. Curves for the two bottom hydrophones, 74 and 76, appear similar in all bands as might be expected given that these two hydrophones are at the same depth and are only 40 km apart. Comparisons between curves for the bottom and the SOFAR hydrophones show far fewer similarities. They appear the most coherent in the 0-2 Hz range where absolute noise levels are also the most similar. Above 2 Hz, the SOFAR hydrophones appear decreasingly coherent with respect to the bottom hydrophones and also with respect to each other.

The relationship between the noise and the wind is demonstrated nicely in Fig. 16 which compares six of the 1-yr-long, 2-Hz-wide time series from hydrophone 76 with a

HYDROPHONE 74 NOISE LEVEL

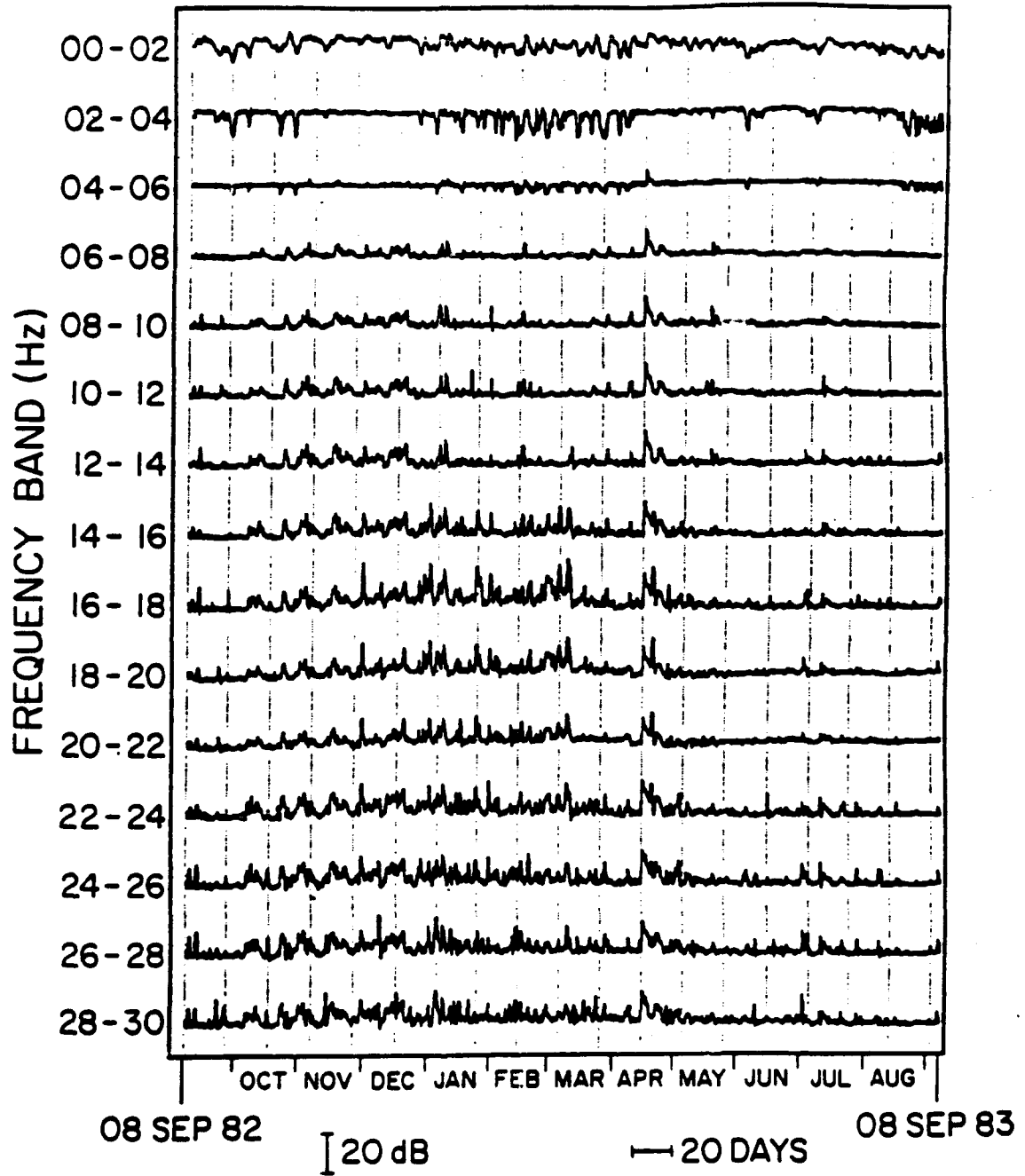


Fig. 14. Temporal variations in the ambient noise over a one-year period for all fifteen 2-Hz bands from WIHA bottom hydrophone 74.

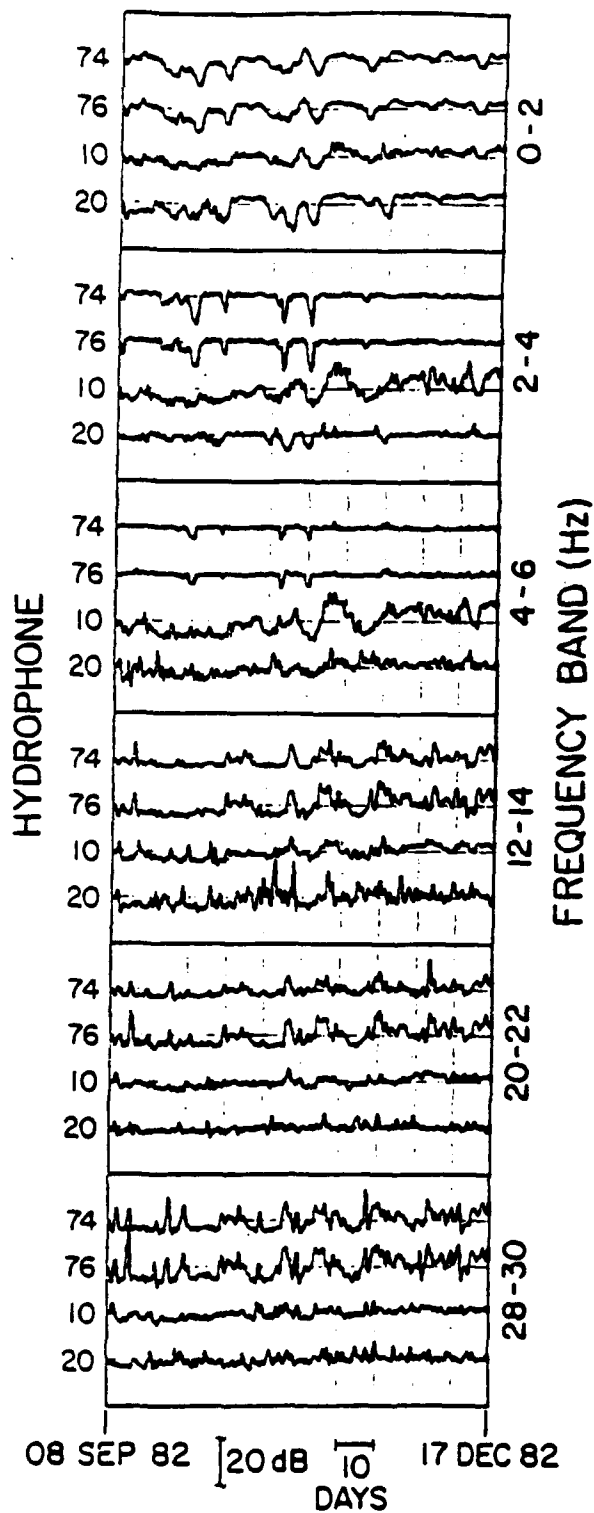


Fig. 15. Temporal noise level fluctuations over a 100-day period in six frequency bands for WIHA hydrophones 74, 76, 10, and 20.

HYDROPHONE 74
NOISE LEVELS AND SURFACE WIND

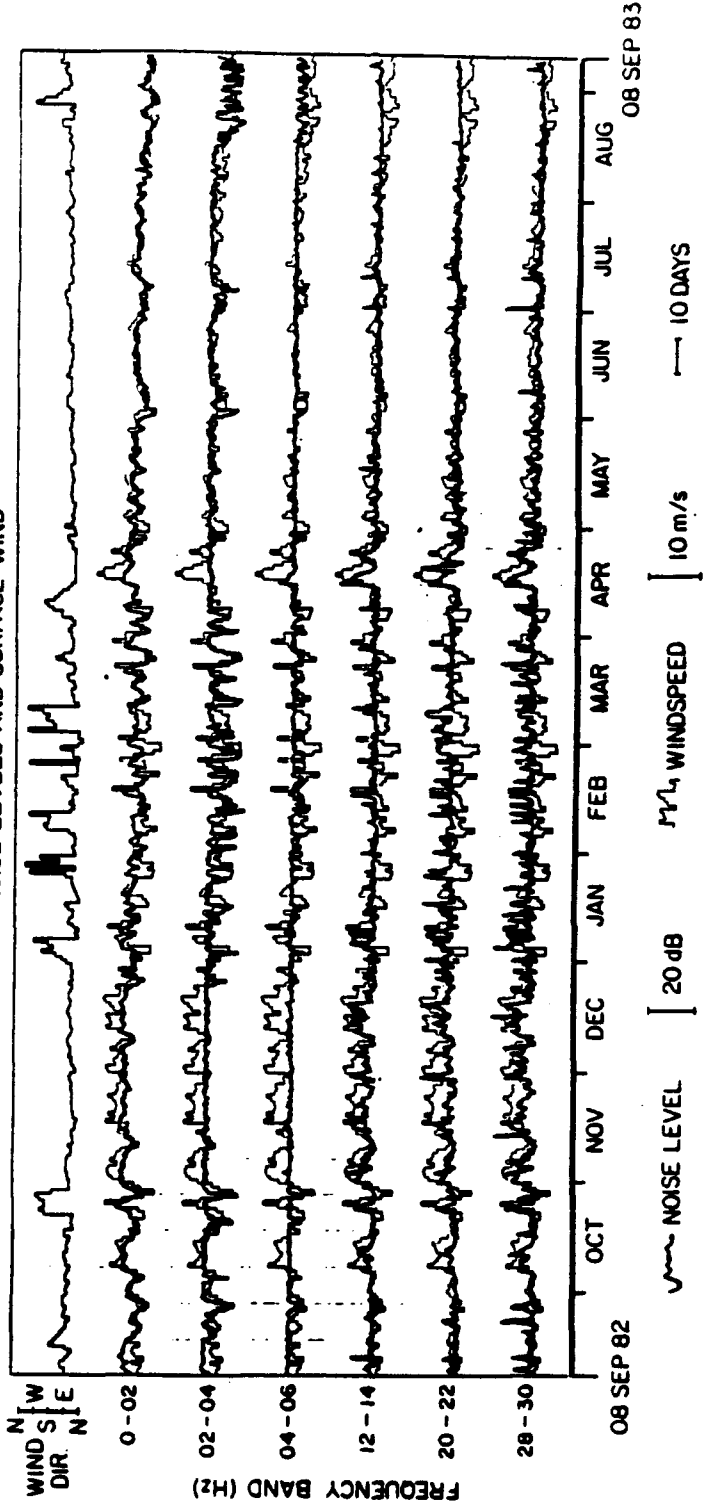


Fig. 16. Hydrophone 74 temporal noise level fluctuations in six frequency bands compared to the wind speed and wind direction measured at Wake Island.

time series of the Wake Island daily mean wind speed from the NWS Monthly Summaries. At 0-2 Hz, the two data sets are remarkably similar, with nearly all major features represented in both curves. At 2-4 Hz and 4-6 Hz, noise lows nearly always correspond with low wind, and above 6 Hz the noise peaks nearly always correspond with high wind.

To quantify these similarities, correlation coefficients and lag times were computed between the wind speed curve and each noise curve, and values are given in Table 1. The 0-2 Hz data have a fairly high correlation coefficient, 0.77, and a lag time of +6 h, indicating that the noise is delayed relative to the wind by an amount equal to one sampling interval. This time shift could be an indication of the lag between the onset of winds and the full development of waves. The correlation coefficient for the 2-4 Hz data is 0.54, again with a lag of +6 h. That correlation can be improved to 0.71, with the same lag, by truncating the wind speed curve for values above 6.26 m/s (the mean wind speed) to give it a more similar character to the truncated-appearing 2-4 Hz noise curve. The correlation coefficient for the 4-6 Hz data is 0.49 with a lag of 0 h. This lower correlation is probably attributable to the relative lack of features in the noise curve for this frequency band. The 12-14 Hz curve has a correlation coefficient of 0.67 with a lag of 0 h. Similar correlation and lag values are found for all other curves between 6 and 16 Hz not shown in Fig. 16. A much lower correlation, 0.34 with a lag of 0 h, was found for the 20-22 Hz data, and low values were also found for 16-18 and 18-20 Hz curves not shown. This low correlation is probably the result of the partial contamination of these data by the aforementioned 20-Hz artifact and whale noises. The correlation coefficient for the 28-30 Hz curve is 0.51 with a lag of 0 h. Like values were found for the other noise data between 22 and 28 Hz. The 0-h lag found for all curves above 4 Hz indicates that the noise at these frequencies responds quickly to changes in the wind speed. Correlations and lags for the data from hydrophone 76 are very similar to those of hydrophone 74, as might be expected, owing to their close proximity. The slightly higher correlation values for hydrophone 76 may be due to the fact

Table 1. Noise and Wind Speed: Correlations and Lags

Frequency Band (Hz)	Hydrophone 74	Hydrophone 76	Hydrophone 10	Hydrophone 20
00-02	.77/+06	.80/+06	.80/+06	.78/+12
02-04	.54/+06	.56/+06	.65/+12	.38/+12
04-06	.49/+00	.57/+00	.65/+18	.26/+36
06-08	.64/+00	.73/+00	.62/+18	.28/+30
08-10	.65/+00	.72/+00	.55/+18	.26/+30
10-12	.66/+00	.73/+00	.54/+18	.28/+12
12-14	.67/+00	.73/+00	.47/+24	.25/+06
14-16	.57/+00	.60/+00	.42/+18	.22/+06
16-18	.27/+00	.31/+00	.23/+18	.21/+12
18-20	.30/+00	.33/+00	.25/+30	.18/-06
20-22	.34/+00	.37/+00	.31/+30	.22/-06
22-24	.48/+00	.48/+00	.34/+18	.27/-06
24-26	.52/+00	.52/+00	.40/+12	.30/+00
26-28	.54/+00	.54/+00	.35/+18	.27/-06
28-30	.51/+00	.51/+00	.36/+18	.20/+00

Correlation coefficients and lag times for the wind speed time series compared to each ambient noise time series. Values shown are the maximum correlation coefficient followed its corresponding lag in hours. A positive lag indicates that the noise lagged behind the wind.

that this hydrophone is 40-km closer to Wake Island, the place where the wind speeds are measured.

Hydrophone 10, located just offshore of Wake Island, has a correlation of 0.80 and a lag of +6 h for its 0-2 Hz time series compared to wind speed. The 2-4 Hz time series has a correlation coefficient is 0.65 with a lag of +12 h. These values are similar to those found for the deep bottom hydrophones. Between 4 and 16 Hz the six correlation coefficients average 0.54, but there are five lags of +18 h and one lag of +24 h. These long lags indicate a that different kind of noise from that observed on the bottom hydrophones is dominant on hydrophone 10 at these frequencies. Between 16 and 22 Hz, correlations are again much lower, averaging 0.26. Above 22 Hz there is only a slight increase in the average correlation to 0.36. Lag times for these seven curves are also long, averaging more than 20 h. These long lags may indicate that this high frequency noise is due to surf pounding the Wake shoreline, and that surf is in turn due to the long-period ocean swell, which takes more time to build than the shorter-period wind waves.

The correlation coefficients for hydrophone 20 at 0-2 Hz and 2-4 Hz are 0.78 and 0.38, respectively, with lags of +12 h. This somewhat longer lag relative to the other hydrophones is probably due to a combination of hydrophone 20's location more than 150 km to the southeast of Wake and the northwesterly approach of most frontal systems passing Wake. Above 4 Hz, correlation coefficients are uniformly low, averaging 0.25, with lags that vary from -6 h to +30 h. These low correlations are also probably due to hydrophone 20's long distance from Wake, and they would seem to indicate that there is a more localized character to the high frequency noise in comparison to noise below 4 Hz.

Also shown in Fig. 16 is a time series of the daily mean wind direction at Wake. Kibblewhite and Ewans (1985) have noted significantly increased ambient noise levels between 0.1 and 5 Hz along the west coast of New Zealand at the time of large shifts in the offshore wind direction, even in a moderate wind field. They attribute this increased noise

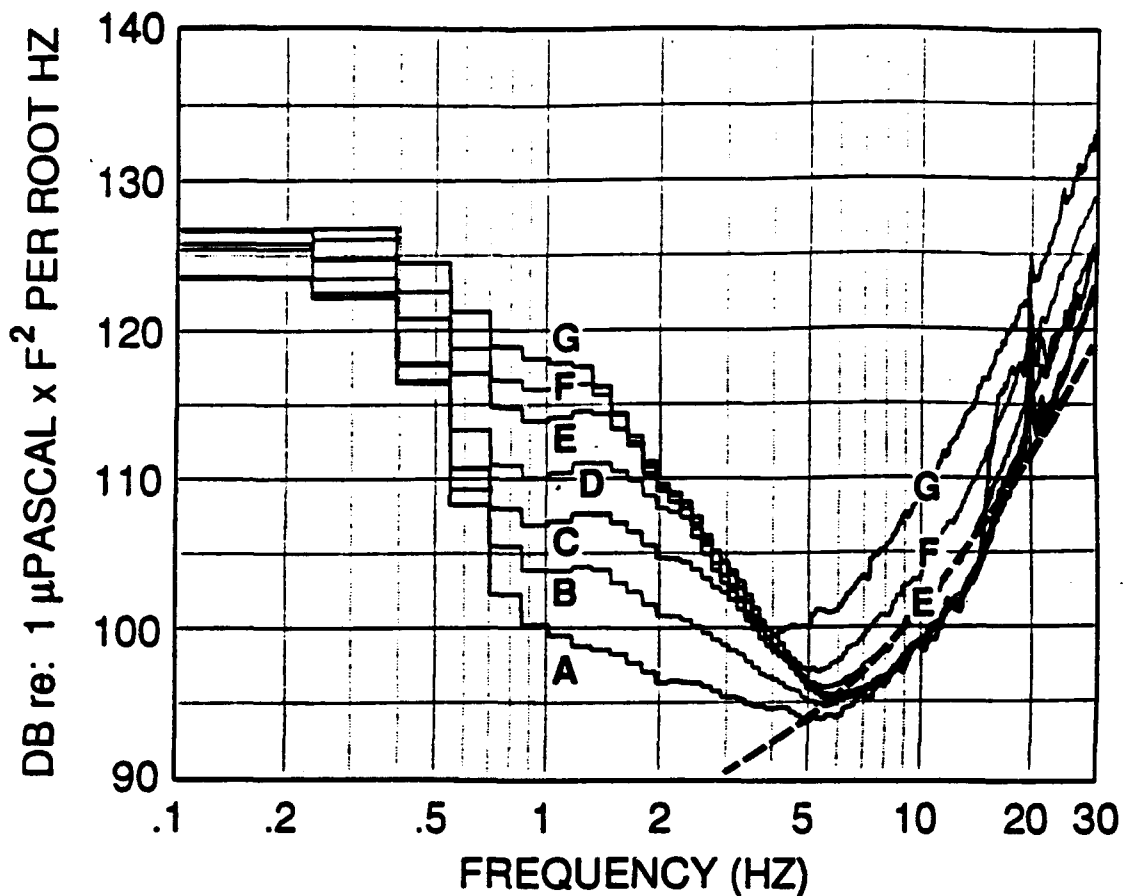
to increased pressure fluctuations on the ocean floor which are in turn caused by increased nonlinear wave-wave interactions on the ocean's surface due to the wind shift. The Wake data, however, do not seem to exhibit the effect observed by Kibblewhite and Ewans, since there are many large changes in wind direction unaccompanied by corresponding increases in the noise.

Spectral Variations

A comparison was made between the mean noise spectra for seven wind speed ranges from each of the four hydrophones (Fig. 17). Each individual spectrum was determined by averaging all noise spectra over the 1-yr period for a particular wind speed range and a particular hydrophone. The number of spectra averaged in each wind speed range is different and is indicated in the figure. The spectral level of each data point, in μ Pascals per root Hz, has been multiplied by its frequency squared before converting it to decibels (dB). This procedure has the effect of rotating each spectrum counterclockwise about its value at 1 Hz by 12 dB per octave. This rotation helps to visually clarify differences between individual spectra. Without this rotation, the seven spectra on each plot would be indistinguishable from each other because of their steep spectral slope. To convert a data point on this plot back to the more conventional units of "dB relative to μ Pascal per root Hz" simply add the term $-40 \times \log_{10}$ (frequency of the data point). Previous figures 11 and 13 show similar data in these more conventional units.

The spectra in Fig. 17 from the two bottom hydrophones are nearly identical. Between about 0.4 and 5 Hz, noise levels increase regularly with wind speed at rates of up to 2 dB per m/s until a saturation level is reached. This saturation level is clearly apparent between about 1.5 and 6 Hz and has a slope of about -23 dB per octave (-11 dB per octave on the rotated plot). This saturation level is not due to the instrumentation, since transient signals commonly exceed this level by tens of dB. Between about 0.3 and 0.8 Hz, the noise is

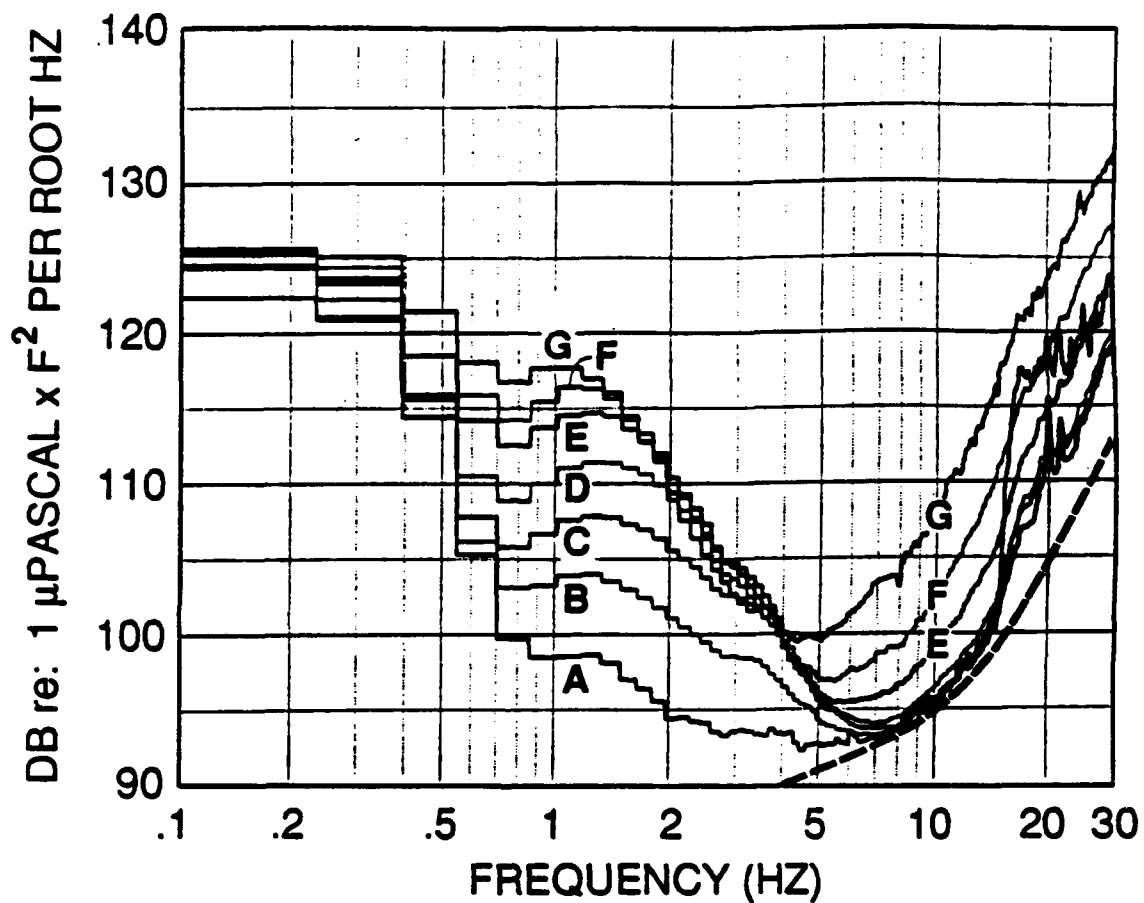
HYDROPHONE 74 (5.5-KM DEPTH)



- | | |
|---------------------------|-----------------------------|
| A: 0-2 m/s (n=20) | E: 8-10 m/s (n=204) |
| B: 2-4 m/s (n=219) | F: 10-12 m/s (n=104) |
| C: 4-6 m/s (n=473) | G: 12-14 m/s (n=12) |
| D: 6-8 m/s (n=428) | |

Fig. 17. Noise spectra from WIHA hydrophones 74, 76, 10, and 20 for seven wind speed ranges. The number of spectra averaged together in each wind speed range, n, is indicated in the legend. Estimated instrumental noise levels are indicated by dashed lines on each plot. The frequency resolution is 0.156 Hz. This figure continues on the following three pages, with the particular hydrophone from which the data are taken noted at the top of each page.

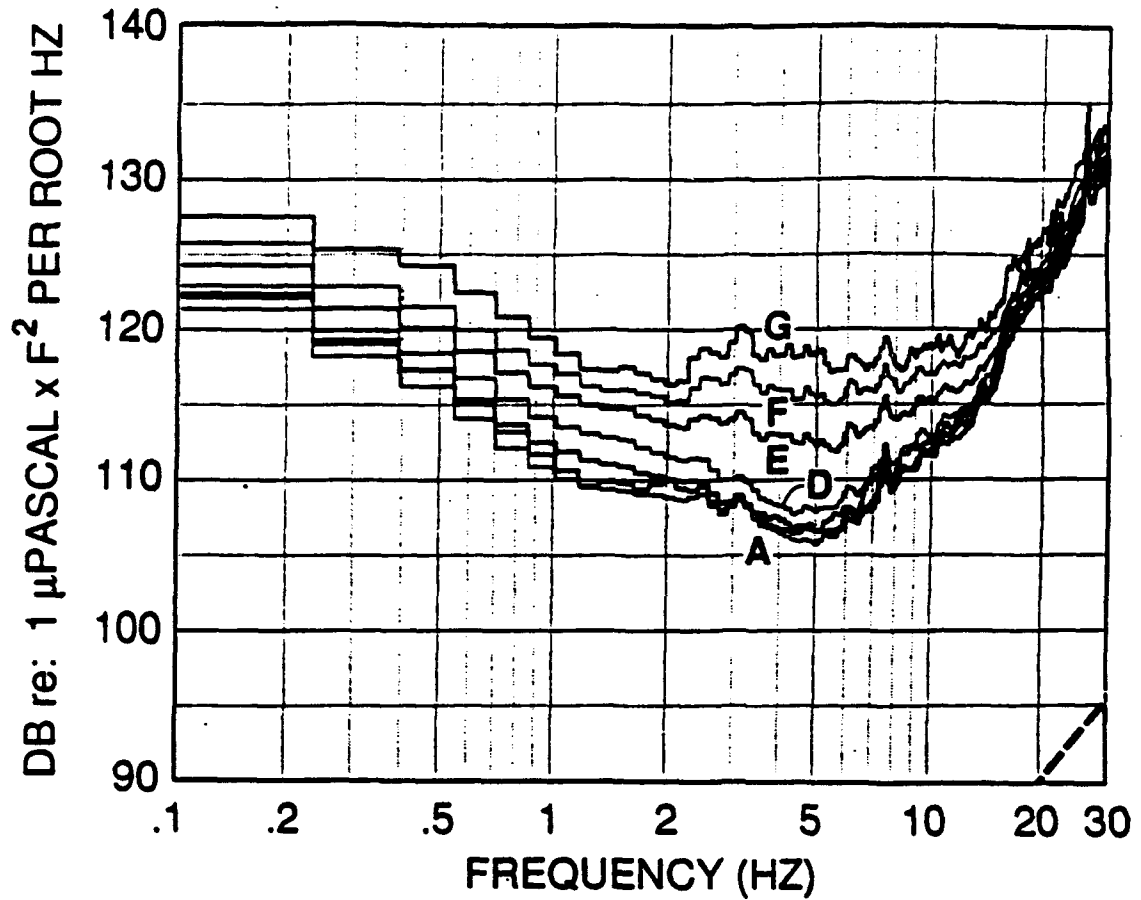
HYDROPHONE 76 (5.5-KM DEPTH)



- | | |
|---------------------------|-----------------------------|
| A: 0-2 m/s (n=20) | E: 8-10 m/s (n=204) |
| B: 2-4 m/s (n=219) | F: 10-12 m/s (n=104) |
| C: 4-6 m/s (n=473) | G: 12-14 m/s (n=12) |
| D: 6-8 m/s (n=428) | |

Fig. 17 (continued).

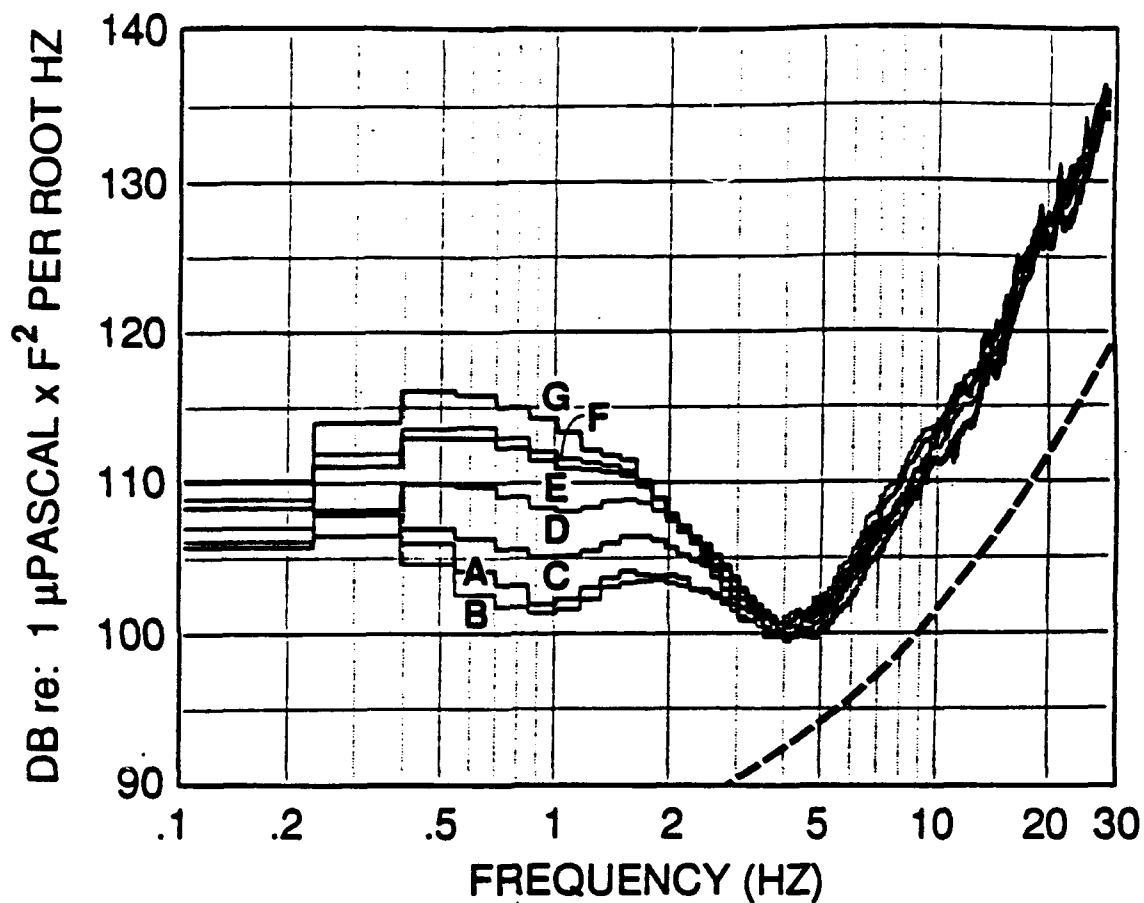
HYDROPHONE 10 (0.8-KM DEPTH)



- | | |
|---------------------------|-----------------------------|
| A: 0-2 m/s (n=20) | E: 8-10 m/s (n=204) |
| B: 2-4 m/s (n=219) | F: 10-12 m/s (n=104) |
| C: 4-6 m/s (n=473) | G: 12-14 m/s (n=12) |
| D: 6-8 m/s (n=428) | |

Fig. 17 (continued).

HYDROPHONE 20 (0.8-KM DEPTH)



- | | |
|---------------------------|-----------------------------|
| A: 0-2 m/s (n=20) | E: 8-10 m/s (n=204) |
| B: 2-4 m/s (n=219) | F: 10-12 m/s (n=104) |
| C: 4-6 m/s (n=473) | G: 12-14 m/s (n=12) |
| D: 6-8 m/s (n=428) | |

Fig. 17 (continued).

bounded from below by minimum levels having a slope of about -30 dB per octave (-18 dB per octave on the plot). Between about 6 and 30 Hz, minimum levels are close to the estimated recording system noise (dashed line). When the wind speed exceeds about 7 m/s, noise levels rise above this minimum at rates of up to 2 dB per m/s and exhibit spectral slopes that increase with frequency to about +4 dB per octave (+16 dB per octave on the plot) for frequencies above 10 Hz. Between 4 and 6 Hz increasing levels of this type of noise rise above the saturation level observed in the lower frequency noise.

The spectral view of these data complements the time series view discussed earlier. The flat top of the 2-4 Hz time series is the spectral saturation level; the flat middle of 4-6 Hz time series is also the saturation level, sometimes overridden at high wind speeds by the higher frequency noise; the flat bottoms of the time series above 6 Hz are the spectral noise minimum in this frequency band.

From these data it is clear that at least two distinct wind-related mechanisms are responsible for much of the noise observed on the deep ocean bottom between 0.4 and 30 Hz. The first type of wind-related noise is observed between about 0.4 and 6 Hz, and is characterized by levels that increase with wind speed to a sharply defined saturation level. This saturation has a spectral slope of about -23 dB/octave relative to pressure or particle velocity. The generating mechanism for this noise is probably not wind, but wind waves on the ocean's surface, with a correspondence between the saturation of the noise and the well known saturation of the wind waves (e.g., Phillips, 1977). Cato (1991b) has recently modelled the noise due to the saturation of the wind waves and found levels close to those observed here. This noise saturation has also been observed by Duennebier et al. (1987) in the data from a seismometer located down a deep sea drillhole. It is probably a feature of the noise in all the world's oceans and is called the "holu spectrum" from the Hawaiian word for deep ocean (Duennebier and McCreery, 1988). The second type of wind-related noise, observed at frequencies above 4 Hz, is also characterized by levels that increase with

wind speed (at least for wind speeds above 7 m/s) but it has a spectral slope markedly flatter than that of the first noise type. In addition, it is capable of overriding the saturation level of the first noise type between 4 and 6 Hz. Duennebier et al. (1986) have proposed that this higher frequency noise is the acoustic signal from whitecaps - waves breaking on the ocean's surface.

The noise spectra of SOFAR hydrophone 20 are very similar to those of the bottom hydrophones. Noise levels regularly increase with wind speed between 0.4 and 4 Hz at rates of up to 2 dB per m/s. A noise saturation level is also clearly visible between about 1.5 and 4 Hz with a slope of about -20 dB per octave (-8 dB per octave on the plot). Above 4 Hz there is again a sharp difference in spectral slope; however, the magnitude of increases in noise level with wind speed is less than 0.4 dB per m/s. The reduced level of these increases and the higher absolute amplitudes relative to those observed on the deep bottom may indicate that this hydrophone is receiving SOFAR-trapped noise generated over a much larger area of sea surface. Instrumental noise is not a factor in these spectra.

The spectra of hydrophone 10 are also clearly wind related, although they have a much different character than those of the other three hydrophones. At virtually all frequencies shown, from 0.1 to 30 Hz, noise levels increase with increasing wind speed at rates of up to 2 dB per m/s. There is no saturation level apparent in these spectra, nor is there an abrupt change in spectral slope at around 4 Hz, but only a more gradual change in slope between about 1 and 10 Hz. In addition, as noted previously, absolute noise levels are generally higher than those observed on the other three hydrophones. These differences are probably the result of hydrophone 10's close proximity to Wake Island, where additional noise is generated by surf breaking on the shore of the island.

Distribution of the Data

The distribution of the 1460 individual noise level measurements from hydrophone 74,

as a function of wind speed were examined at three discrete frequencies out of the possible 192 (Fig. 18). The largest range of noise levels is at 1.41 Hz, although the saturation level is clearly visible. Scatter at this frequency varies from about 20 dB at the lower wind speeds to less than 5 dB at the higher wind speeds where the noise is saturated. At 2.34 Hz the saturation level is dominant over a wider interval of wind-speeds, as can also be seen in the spectra of Fig. 17. Interestingly, the saturation level appears to be lower at the highest wind speeds, and this phenomenon will be discussed further in Chapter 6. Scatter at 2.34 Hz is similar to that observed at 1.41 Hz. At 9.84 Hz, the noise level is fairly constant at the lower wind speeds (the noise floor), and scatter is generally less than 10 dB throughout the plot.

At least three factors may contribute to scatter in the data. The first is simply the error in the measurement due to the randomness of the stochastic processes producing the noise. The chi-squared statistics underlying this spectral measurement lead to a range of scatter of about 3 dB for 90% of the data. This may be all that is needed to explain the scatter in the saturated noise. The second factor is that wind speed is measured at Wake Island and not directly over the hydrophones. Hydrophone 74, for example, is more than 100 km away from Wake. Thus, there may be a lead time or a lag time or even no correspondence at all between wind speeds at Wake Island and wind speeds directly over the hydrophones. The third factor is that wind-wave heights are a function of the duration of the wind and the fetch over which it blows, as well as the wind speed. For example, in the case of a fresh wind blowing over a calm sea, it is well known that the long-period wind waves take more time to reach their saturation level than the short-period wind waves. There is supportive evidence for this phenomenon in the correlation lags between the noise and wind speed time series previously discussed. A delay between the onset of wind and corresponding onset of noise has also been observed and described by Duennebier et al. (1987) using deep-ocean borehole seismometer data. Thus, if the noise is caused by the wind waves

HYDROPHONE 74 (5.5 KM)
SPECTRAL ESTIMATE #10: 1.41 HZ

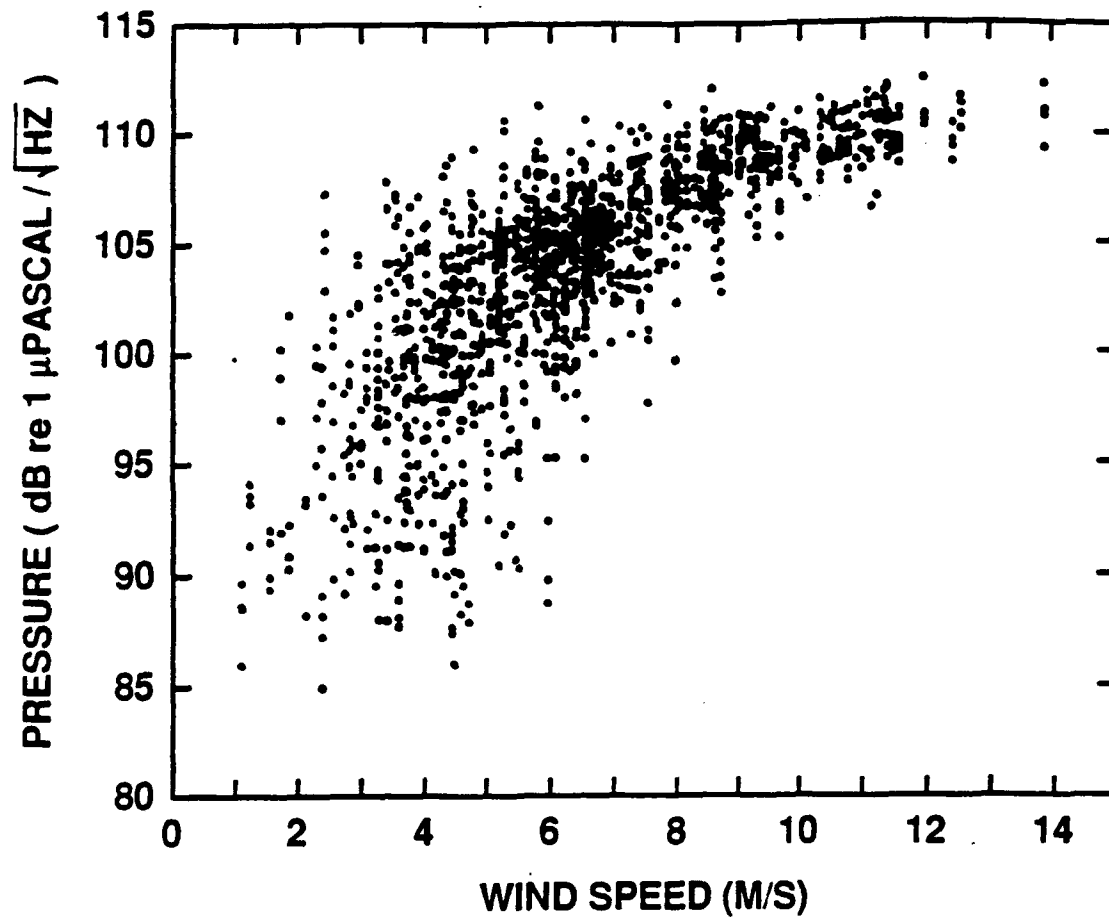


Fig. 18. Scatter in the noise level measurements as a function of wind speed. Each of 1460 noise level measurements from hydrophone 74 made over a one-year period at three discrete frequencies are shown. This figure continues on the following two pages. The spectral estimate number and its corresponding frequency are noted at the top of each plot.

HYDROPHONE 74 (5.5 KM)
SPECTRAL ESTIMATE #16: 2.34 HZ

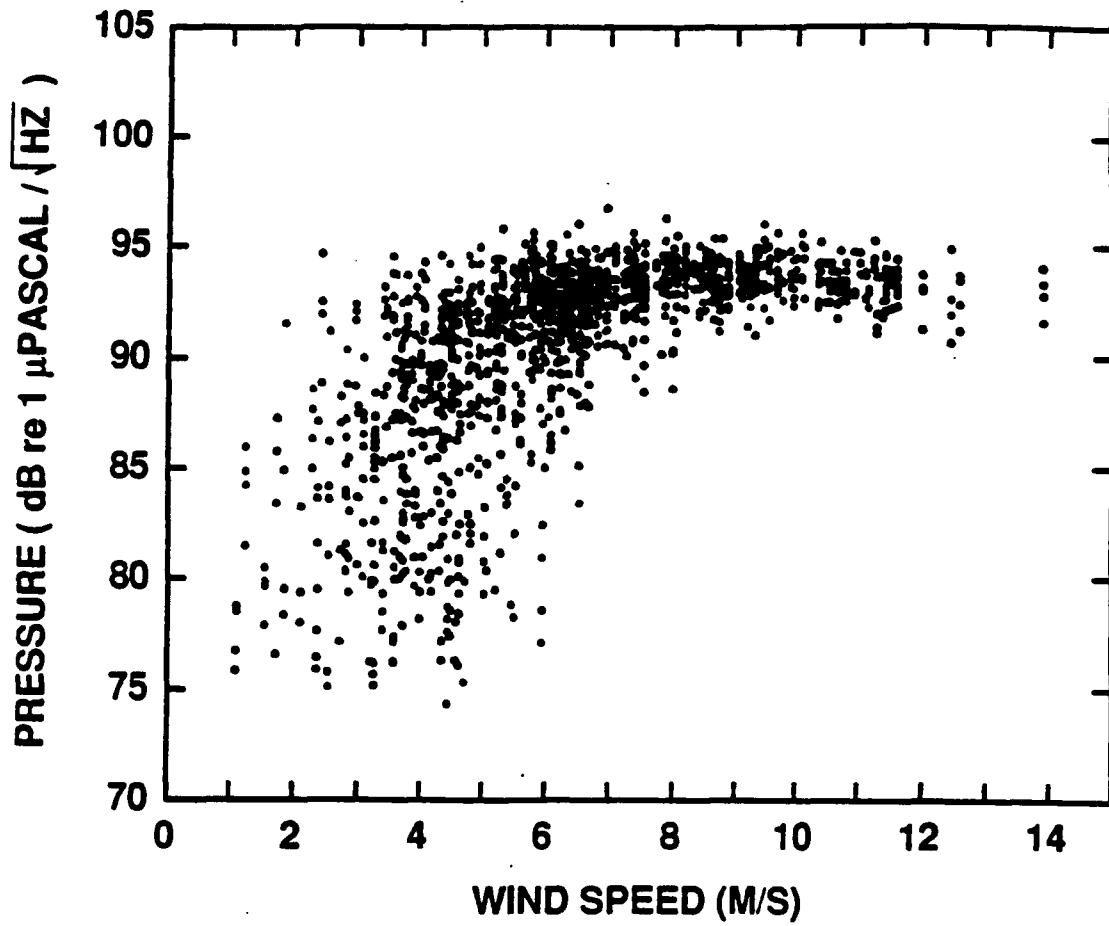


Fig. 18 (continued).

HYDROPHONE 74 (5.5 KM)
SPECTRAL ESTIMATE #64: 9.84 HZ

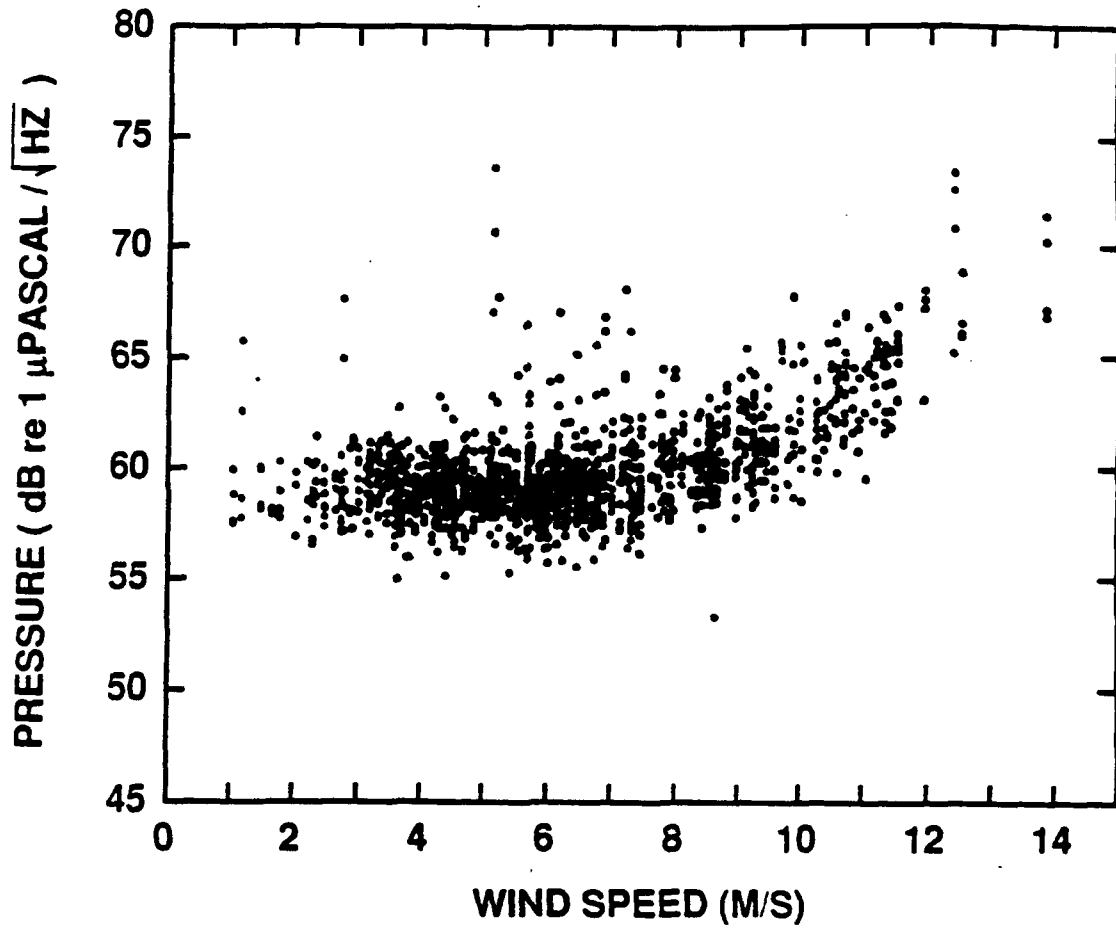


Fig. 18 (continued).

rather than by the wind, then scatter is introduced into these plots by the nature of the mechanism that converts wind energy into wave energy.

Note from these plots that the distribution of the 1460 noise levels at each frequency is not Gaussian. Referring back to Fig. 11, standard deviations shown on that plot should be viewed appropriately.

Also note that from the Fig. 18 plots for 1.41 and 2.34 Hz, it might be misconstrued that the saturation level is merely an artifact of plotting noise levels using a logarithmic scale (dB). If noise levels in non-logarithmic units (μ Pascals per root Hz) are linearly related to wind speed, and the scatter is uniform at all wind speeds, then plots of the data in dB might look similar to the plots in the figure. The data would bend to the right, and the scatter would appear reduced at higher noise levels. However, the WIHA data were tested for this possibility by making such non-logarithmic plots, and the saturation level remained a clear feature of the data.

CHAPTER 5. 0.1-5 HZ NOISE AND OCEAN WAVES

This study examines nearly four years of noise data from one of the deep WIHA hydrophones and compares these data to the estimated ocean waves. Some important characteristics of the long-term deep ocean noise are quantified, and the relationship between the noise and the waves is examined.

Data Set

The noise data analyzed for this portion of the study are the hourly three-minute-long noise samples for the time period: September 8, 1982 - July 20, 1986. The data in this time period are nearly continuous, with only 12 gaps longer than a day, the largest being 13 days in April 1985. In its entirety, the size of this data set is about 8 Gbytes, so some reduction of the data was needed to make it more manageable. As a first step, only the data from hydrophone 74 were extracted from the archive tapes, reducing the data volume to 1 Gbyte. The compromise of examining only one hydrophone was accepted, since a fine-scale comparison of the low-frequency noise on all hydrophones was anticipated in a later phase of the study. Each of the more than 32000 three-minute-long samples, 14400 data points in length, was then transformed using a single 16384-point FFT into 8193 power spectral estimates, representing frequencies from 0 to 40 Hz with a spectral resolution of about 0.0056 Hz. This resolution is much finer than that of the previous study, and it permits the examination of features in the spectrum near the microseism peak. The data were then further reduced by a factor of 8 by discarding the spectral estimates for frequencies above 5 Hz, which were not likely to be related to the much lower frequency ocean waves to which they were to be compared. Lastly, the hourly spectral estimates were averaged together for each 6-hour interval, the same time interval as the ocean wave data. This final data set is only 23 Mbytes in length, a much more manageable size.

Compared to these data are the SOWM directional wave height estimates. SOWM data

are only available through June 30, 1985, after which the wave model was upgraded to GSOWM. However, no comparison between the GSOWM data of July 1, 1985 to July 20, 1986 and the corresponding WIHA data has yet been made. The location closest to hydrophone 74 for which SOWM predictions were made is about 150 km away and is shown in Fig. 4. SOWM data are given at six hour intervals as the estimated power of the waves (the variance of the wave heights) at 15 frequencies for each of 12 directions. The wave power in most of the bins is usually zero. This does not mean there are no waves at those particular frequencies and directions, but that the variance of the wave height is either below the minimum resolution, 0.01 ft^2 , or that the data point was eliminated in the original data set because it was considered too low-energy, meaning it had a variance of less than 0.25 ft^2 . Elimination of low-energy data points was apparently only done sporadically, though, and probably affects less than 1% of the data based upon information given by the NCDC.

From the directional SOWM data, two reduced data sets were produced. The first was simply a sum of the power (i.e., the variances) over the twelve directions at each frequency for each point in time. The second was a sum of the product of the wave heights over the six opposing directions for each frequency. This second reduced data set was generated to provide a test of the nonlinear wave interaction theory of noise generation, since it requires opposing wave fields.

Long-Term Noise Characteristics

Spectrograms were generated for the 46 months of WIHA noise data. A logarithmic frequency scale was used to give adequate visual resolution at frequencies near the microseism peak and still display all frequencies up to the 5 Hz limit. Noise levels at each frequency were computed relative to the 46-month mean value at that frequency in order to emphasize changes in level rather than absolute levels. The resulting plots, 12 m in total

length, were divided into calendar years and attached to a large wall for simultaneous viewing. Because of their length, it is not possible to present the entire complement of these spectrograms in this dissertation. However, two 40-day sections (Figs. 19 and 20), one in the summer and one in the winter, are fairly representative of the whole, and from these shorter plots the most salient characteristics of the noise are easily discerned.

Firstly, the noise can be divided into three frequency bands. The first band is frequencies below 0.1 Hz. Within this band noise levels are generally uniform and this uniformity is attributable to the fact that this noise is mostly instrumental. Although it cannot be seen in the two figures, this instrumental noise actually grew slowly over the four-year period by about 10 dB, probably indicative of aging in the amplifier. The second frequency band spans from 0.1 to 0.4 Hz. Within this band are episodic lumps of relatively high amplitude noise. In general, these lumps last for a few days and are separated in time by one to two weeks. The third frequency band is from about 0.4 to 5 Hz. Within this band noise levels rise and fall more or less uniformly.

Secondly, there is a very distinct summer-winter pattern to the noise, with summer being defined from the data as the six-month period from April through September, and winter as October through March. The aforementioned 0.1-0.4 Hz noise lumps are higher in amplitude, have a longer duration, occur more often, and are lower in frequency during the winter months. The 0.4-5 Hz noise is also generally higher in amplitude in the winter, with more frequent and rapid variations between lows and highs. These seasonal noise patterns are suggestive of the annual weather patterns in the northern Pacific. In the winter there are frequent, large, swell-producing storms associated with low pressure systems that migrate across the Pacific. In the summer, the weather pattern is dominated by persistent trade winds and far fewer storms.

To further characterize the relationship between the noise at different frequencies, cross-correlations were computed between the 46-month-long time series of dB noise

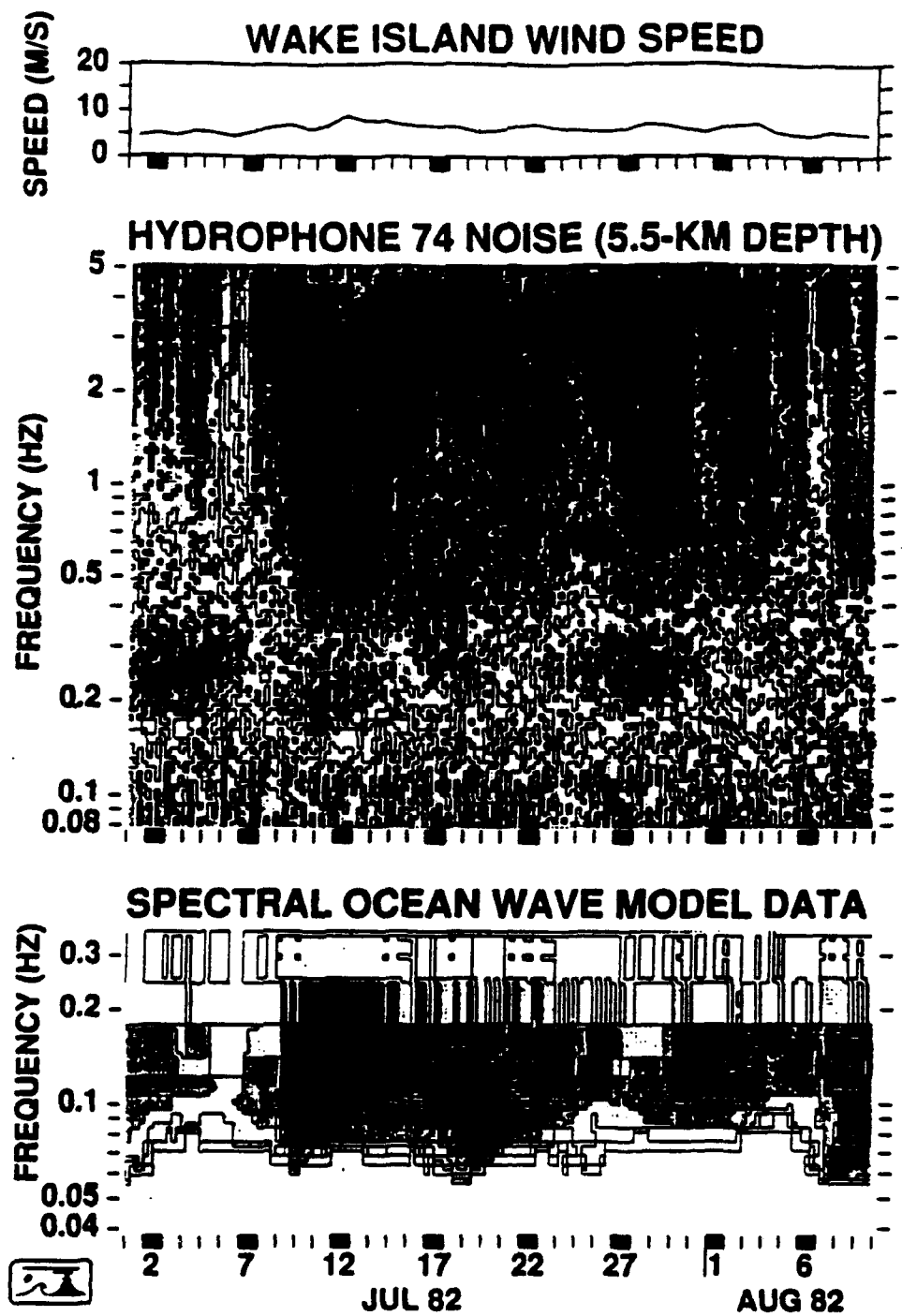


Fig. 19. A forty-day comparison of ocean noise, estimated ocean waves, and daily mean wind speeds typical of summertime. The ocean noise and waves are shown in spectrogram form, with 3 dB separating each gray shade. The total range of levels is approximately 24 dB from light to dark. White on the wave spectrogram indicates no data.

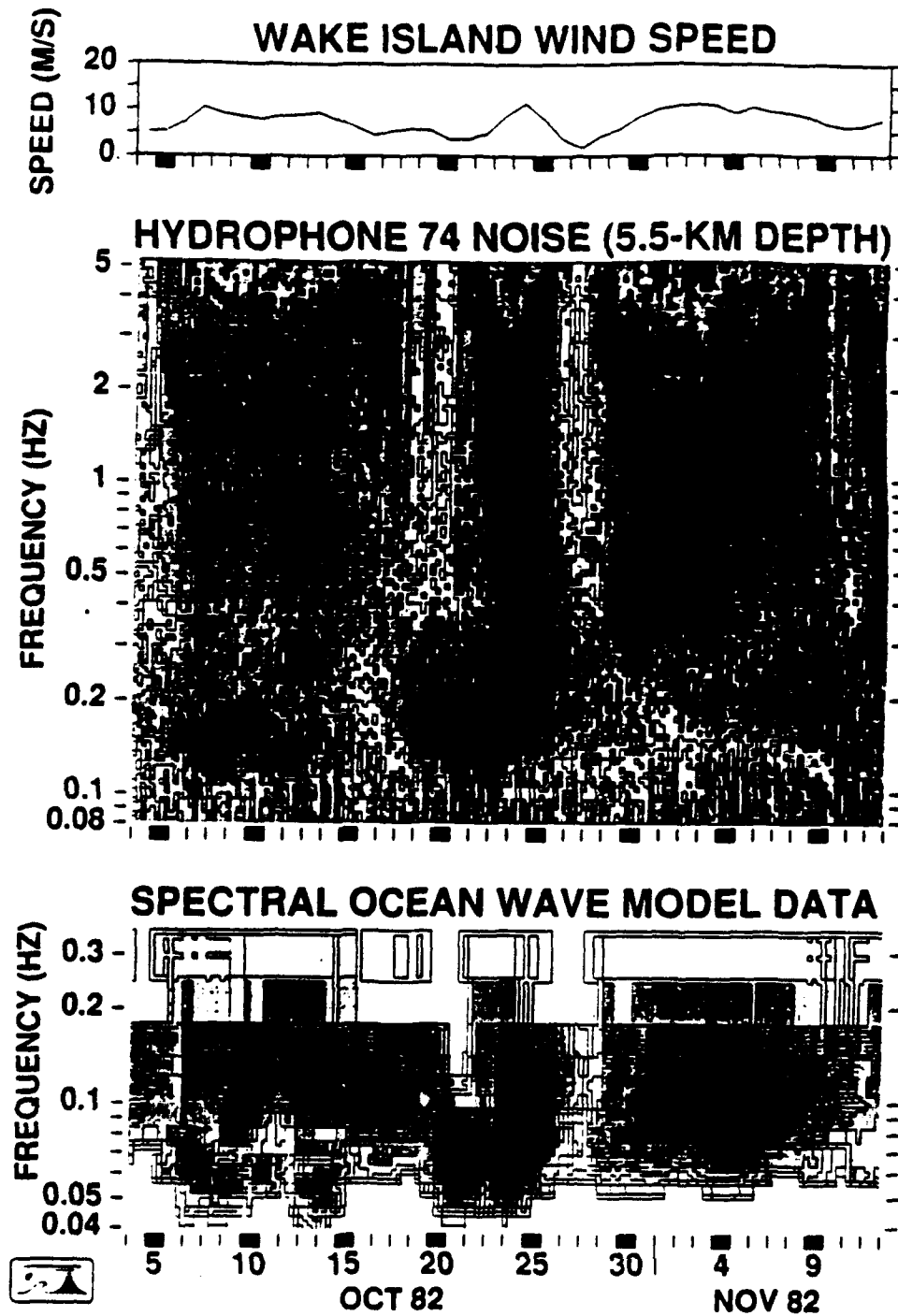


Fig. 20. A forty-day comparison of ocean noise, estimated ocean waves, and daily mean wind speeds typical of wintertime. (See Fig. 19 for further explanation.)

levels at each of 120 geometrically-spaced frequencies between 0.1 and 5 Hz (Fig. 21). The time series at each frequency was made by averaging together the appropriate time series of noise levels in dB from the original 256 time series arithmetically-spaced in frequency from 0 to 5 Hz. Each time series was further processed by removing the monthly mean from each data point. This monthly mean was computed using a Gaussian window of total length 4σ , with 1σ equal to 15 days. Removal of the monthly mean was made to ensure that cross correlations would be based on the more short-term temporal variations rather than the annual summer-winter pattern. The cross correlations clearly show a division of the data into two frequency bands. From 0.1 to 0.4 Hz, cross correlations are high over only a relative narrow range of frequencies. Thus, the noise at any frequency in this band is not related to noise at any other frequency unless that other frequency is very near (within about $\pm 25\%$ of the original value). The noise at frequencies between 0.4 and 5 Hz, on the other hand, are much more closely related. Cross-correlation values are high over this entire band, implying that noise levels in this band generally go up and down in unison.

To view the total range of absolute noise levels over the entire 46-month period, spectra were made that divide the range of noise levels at each frequency by the percent of time they occurred (Figs. 22, 23, and 24). Only spectral estimates from six-hour time intervals which had four or more three-minute-long noise samples were used in the distribution, and each spectral estimate, in dB, was averaged together with the four adjacent spectral estimates at both higher and lower frequencies before being included in the distribution. These steps were taken in order to increase the degrees of freedom of each estimate, and thus reduce its range of scatter. Otherwise, instead of being a distribution of ocean noise levels, these plots would be more of a distribution of the scatter in the spectral estimates. The average number of degrees of freedom was about 50, so the standard deviation of each spectral estimate is a little less than 1 dB. There is a 20-30 dB range of levels at all

NOISE VS NOISE CROSS CORRELATIONS
8 SEP 82 - 20 JUL 86
HYDROPHONE 74 (5.5-KM DEPTH)
TIME SERIES LENGTH = 5251

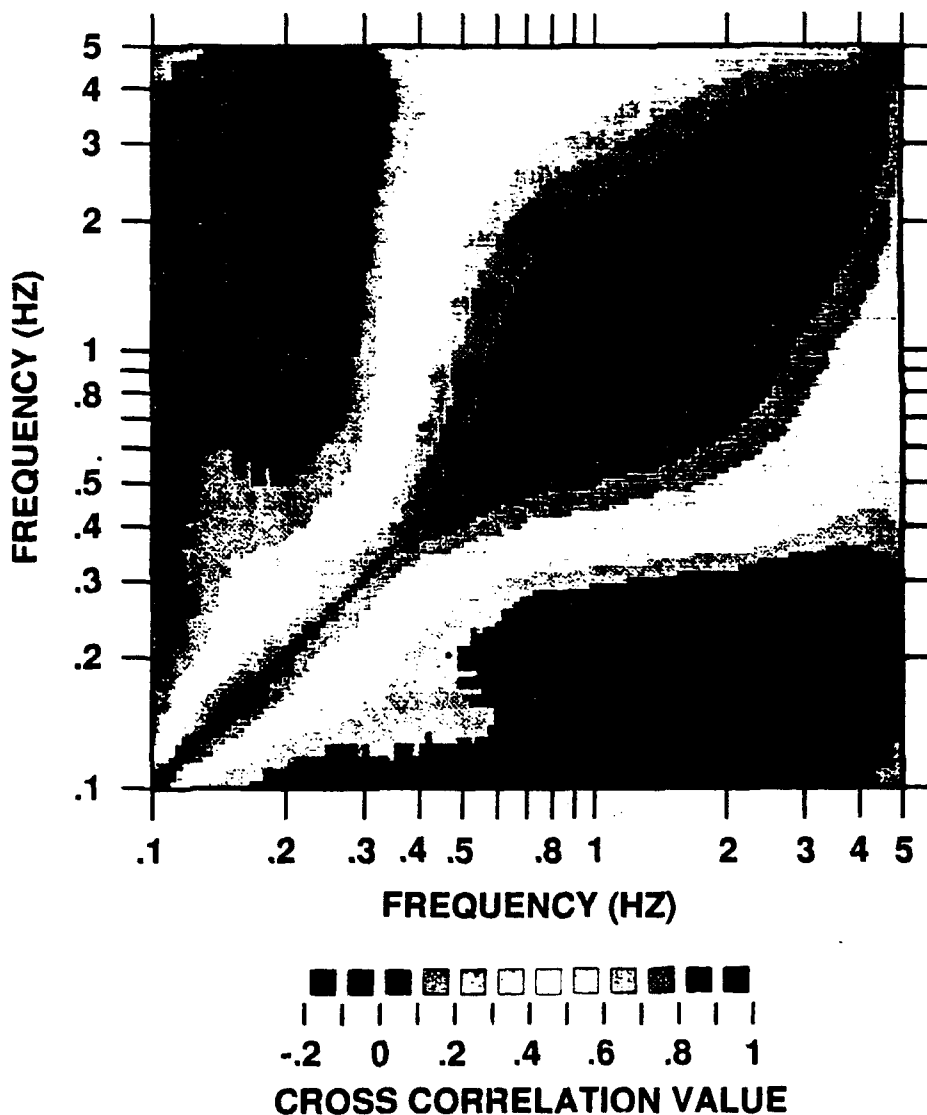


Fig. 21. Cross correlations between the hydrophone 74 noise level fluctuations at different frequencies. Cross correlation values for each color are indicated at the bottom of the plot. The data are naturally symmetrical about the diagonal where the cross correlation value is exactly 1. The total number of data points in each time series of noise level fluctuations is 5251, representing 46 months of data.

DISTRIBUTION OF NOISE LEVELS
8 SEP 82 - 20 JUL 86
HYDROPHONE 74 (5.5-KM DEPTH)

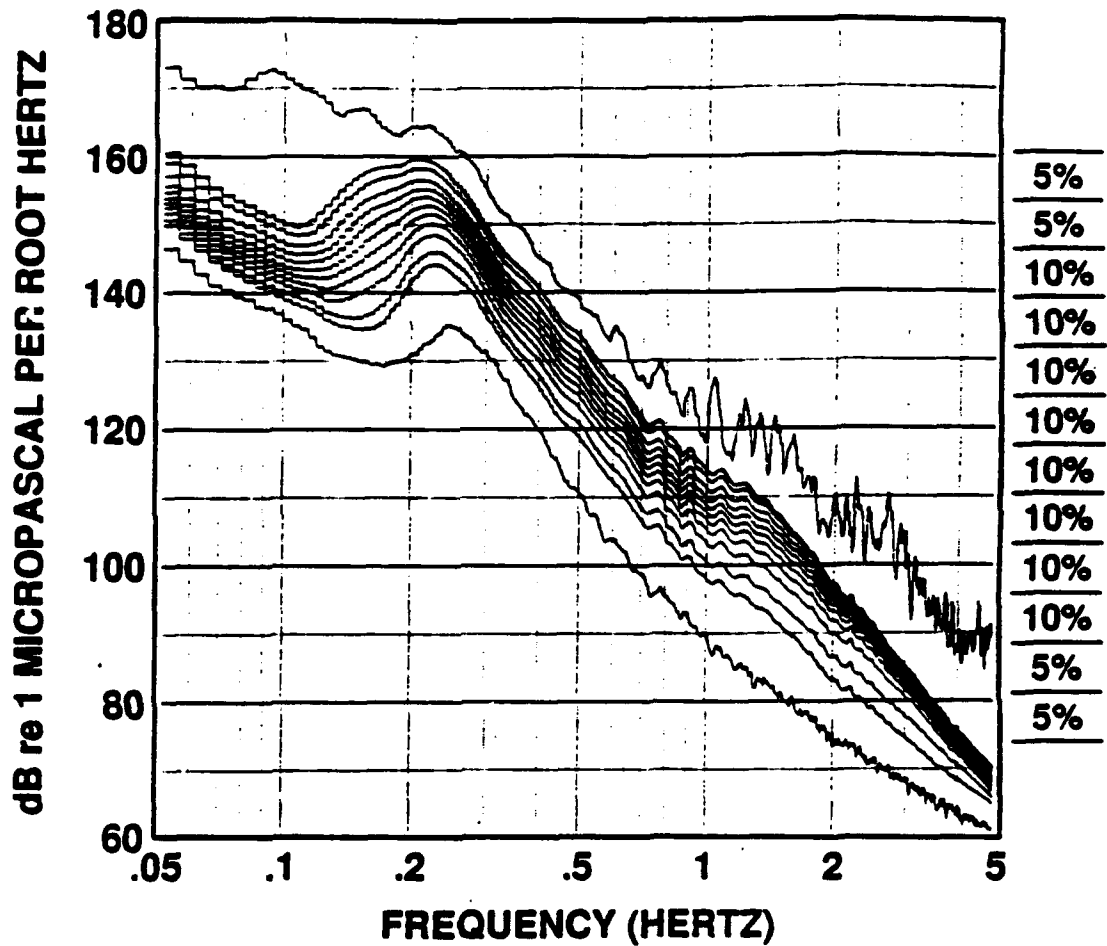


Fig. 22. Distribution of noise levels from hydrophone 74 over a 46-month period. The thirteen curves shown in the figure divide the data by percentages as indicated on the right of the plot.

**DISTRIBUTION OF NOISE LEVELS
8 SEP 82 - 20 JUL 86: SUMMER MONTHS ONLY
HYDROPHONE 74 (5.5-KM DEPTH)**

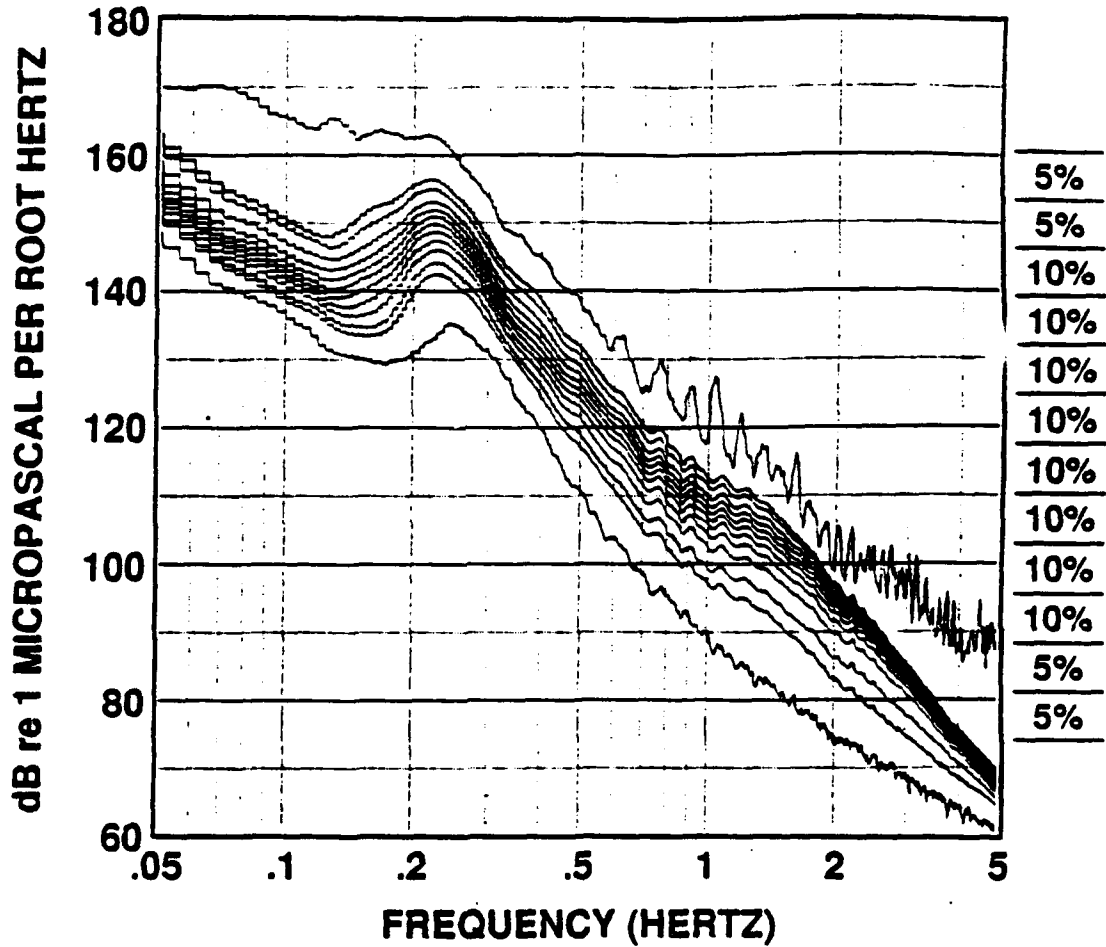


Fig. 23. Distribution of noise levels from hydrophone 74 over a 46-month period, with only the summer months of April through September represented. The thirteen curves shown in the figure divide the data by percentages as indicated on the right of the plot.

DISTRIBUTION OF NOISE LEVELS
8 SEP 82 - 20 JUL 86: WINTER MONTHS ONLY
HYDROPHONE 74 (5.5-KM DEPTH)

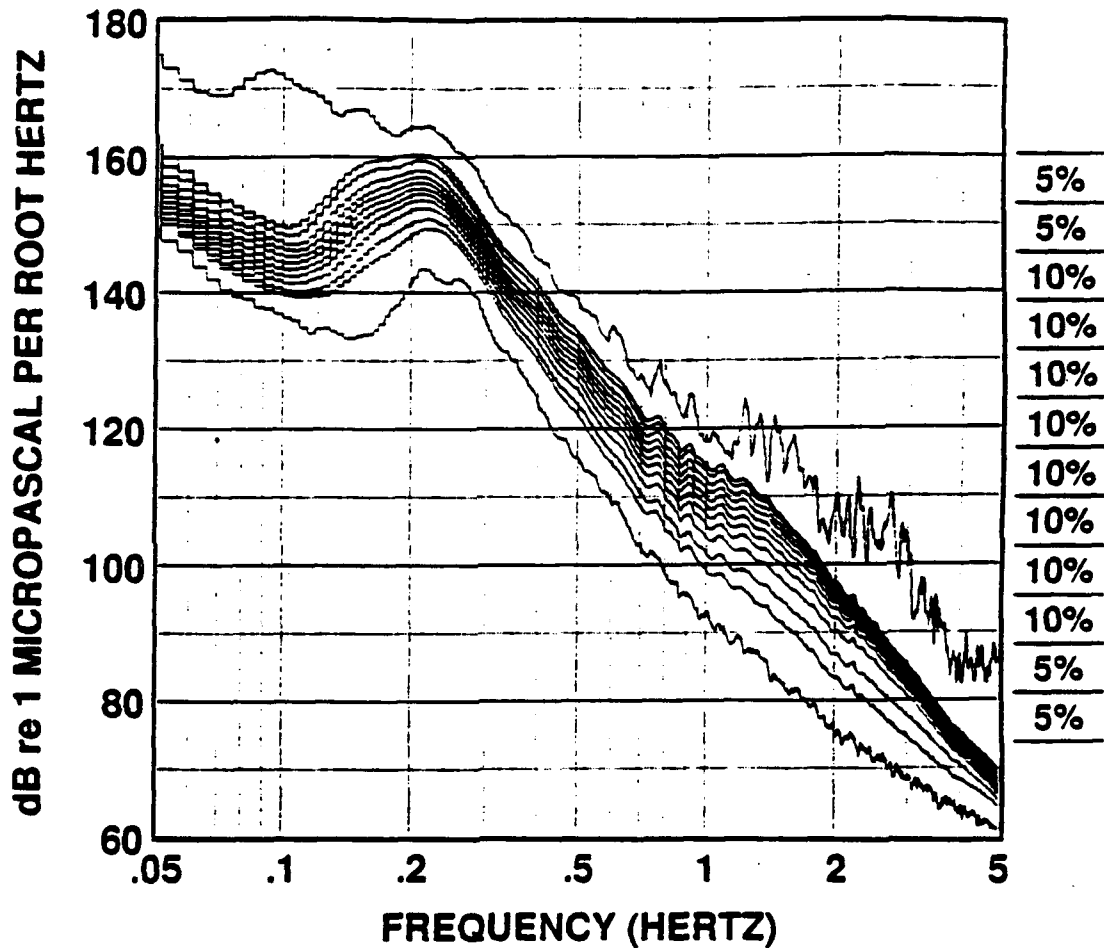


Fig. 24. Distribution of noise levels from hydrophone 74 over a 46-month period, with only the winter months of October through March represented. The thirteen curves shown in the figure divide the data by percentages as indicated on the right of the plot.

frequencies for all the data, but only a 10-20 dB range for the innermost 90% of the data. Levels in the winter months are systematically higher than levels in the summer months from 0.1 to 2 Hz, with the greatest seasonal difference, about 6 dB, occurring between 0.1 and 0.2 Hz. The range of levels below 0.1 Hz primarily represents the aforementioned long term gradual increase in system noise, except that the highest levels of this noise are due to Rayleigh waves from large earthquakes. Above 2 Hz, the noise is saturated more than 75% of the time. This bunching of curves between 2 and 5 Hz is the invariant holu spectrum, with the 3-4 dB range of levels representing the statistical scatter in the spectral estimates. Systematic bumps in the spectra, especially apparent between 0.6 and 3 Hz, may be due to reverberations of the noise energy in the sediment layers. Sediment structure has been inferred from similar features in the noise spectra from an ocean borehole seismometer (Butler et al., 1988).

The distribution of the microseism peak also shows a distinct summer-winter pattern (Fig 25). During summer months, the peak is almost always at a frequency between 0.20 and 0.28 Hz, with levels mostly falling between 145 and 155 dB. In winter months, however, the peaks are at frequencies between 0.14 and 0.26 Hz, with levels between 150 and 160 dB. The lower frequencies and higher levels in winter reflect what was seen in Figs. 19 and 20, namely that the prominent lumps of energy on those spectrograms are at lower frequencies and have higher levels in the winter. There also seems to be a bimodal distribution to the microseism peaks, with most of the peaks occurring between 0.2 and 0.26 Hz, and a second group of peaks occurring between 0.14 and 0.2 Hz. The first group of peaks represents the predominant microseism peak that is present year round. The second lower-frequency group of peaks is associated with the short-term episodic lumps of energy that occur primarily in winter, are due to the arrival of a large ocean swell, and are sometimes higher in level than the primary peak.

It should be noted with some interest that the microseism peak observed in these data

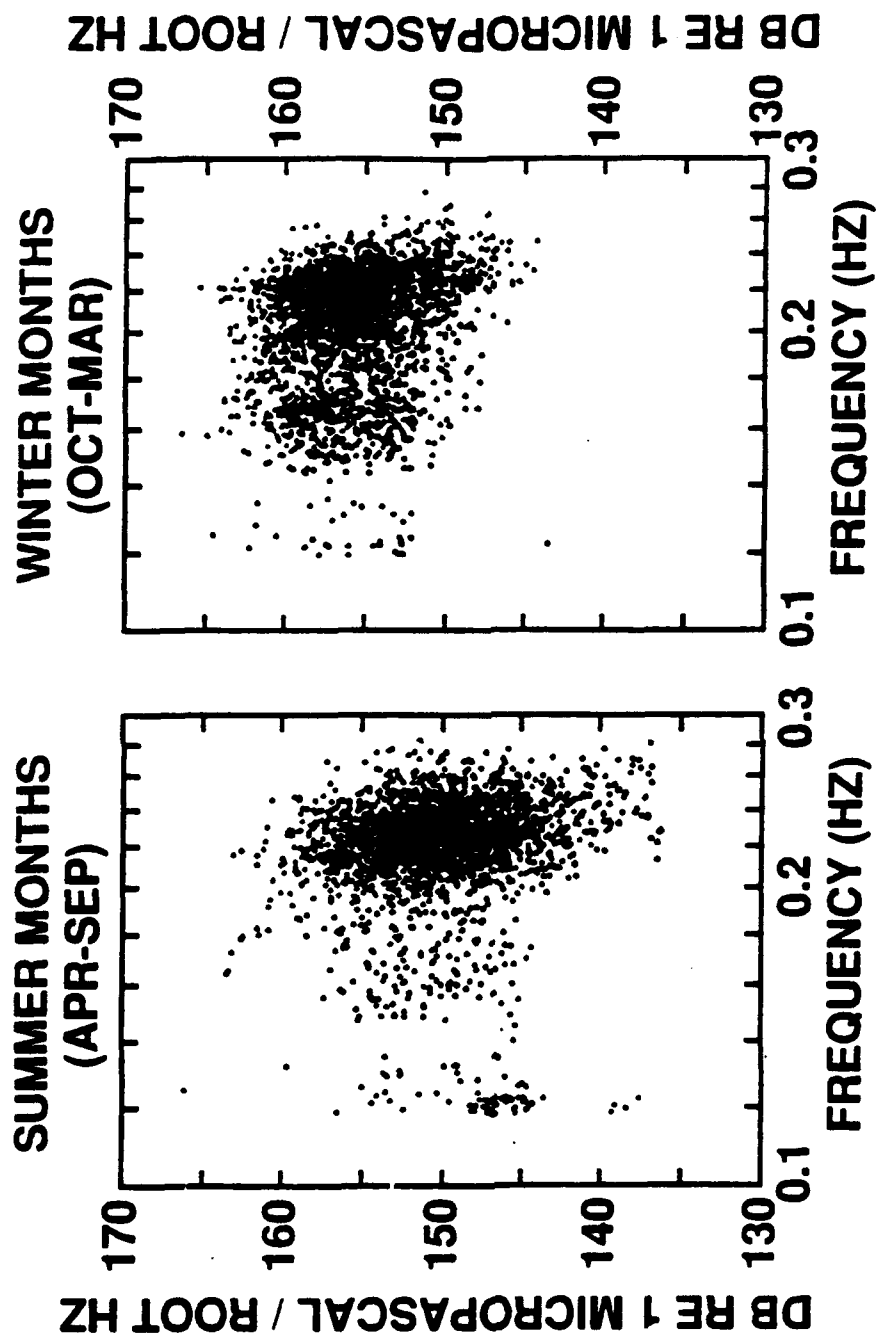


Fig. 25. Amplitudes and frequencies of the microseism peak on hydrophone 74 from measurements made every 6 hours over a 46 month period. The data are divided into summer and winter months. The microseism peak was defined, somewhat arbitrarily, as the largest amplitude in the spectrum between 0.12 and 0.28 Hz. The data points between 0.12 and 0.14 Hz are probably instrumental noise or earthquakes and should be ignored.

is generally higher in frequency than the microseism peak observed on land. That peak, as reported by Brune and Oliver (1959), has a frequency between about 0.12 and 0.20 Hz. This is roughly the location of the secondary peak in the Wake data associated with the arrival of ocean swell.

Noise and Waves

Spectrograms were also generated for the two forms of SOWM ocean wave data, the first form being the total wave energy at each frequency and the second form being the energy from opposing wave fields only. These wave spectrograms were scaled identical to the noise spectrograms in both the time and frequency directions, and they were displayed on the same large wall as the noise spectrograms, positioned one above the other for equivalent time intervals. It was immediately apparent that the opposing wave energy data is only marginally related to the ocean noise, if at all. Firstly, it is very sparse owing to the fact that most of the time there are no opposing wave fields in the SOWM directional data. Secondly, the opposing wave energy that was present on the spectrograms only corresponded occasionally to increased ocean noise. The total wave energy data, however, is much more clearly related to the ocean noise, with many similar features including a summer-winter pattern and corresponding episodic lumps of high energy. Representative portions of the total wave energy spectrogram are shown with cotemporal portions of the noise spectrograms in Figs. 19 and 20. While it can't be said that the two types of data in these figures are identical, their similarities are very clear. Also shown in the figures are the daily mean wind speeds measured at Wake Island. As demonstrated in the previous study, the higher frequency noise follows the wind speed. The higher frequency waves also follow the wind speed which is the forcing function of the SOWM model.

The fact that the noise data corresponds more clearly with the total wave energy data than it does with the opposing wave energy data, does not necessarily mean that the

generation of this noise is not by nonlinear interactions between opposing waves. The zeros in the SOWM data bins do not imply that there is absolutely no energy at those particular frequencies and directions, but merely that the energy is below the level of the minimum resolution of the model, 0.01 ft^2 . Thus, it can be assumed that there is probably some gravity wave energy opposing all of the wave energy that is reported by the SOWM model, albeit low level. This assumption is made throughout the rest of this discussion when referring to the noise from arriving swell, unless that noise is specifically attributed to the primary pressure fluctuations from the waves.

To better quantify similarities between the total wave energy and noise data, cross correlations between the two were computed. The SOWM data are given at 15 frequencies, and the dB levels at each of these frequencies make up 15 33-month-long time series (September, 1982 - June, 1985). Since the non-linear wave interaction theory of noise generation states that pressure variations occur at twice the frequency of the waves, the noise data in dB were averaged together into 15 corresponding frequency bands, double the frequency of the waves. Corresponding time series from the two data sets were cross correlated for a wide range of lags -- waves occurring 6 months before the noise to waves occurring six months after the noise (Fig. 26). At the lowest three frequencies, 0.078 to 0.1 Hz in the noise, cross correlations are near zero everywhere. This is not surprising since the noise is mostly instrumental in this range. At the lowest frequency there is a lot of scatter in the cross correlation values due to the small number of data points used. At the next five frequencies, 0.112 to 0.162 Hz in the noise, there is a peak in the correlation at zero lag with a value ranging from about 0.2 to 0.4. Towards the higher of these frequencies, this peak is increasingly superimposed on a broad seasonal high in the cross correlation. Oddly, the peak of the seasonal cross correlation is at a lag of around 200, indicating that the waves follow the noise by a couple of months. The reason behind this large lag is not yet understood. At the next five frequencies, 0.184 to 0.316 Hz in the noise,

CROSS CORRELATIONS HYDROPHONE 74 NOISE vs SOWM OCEAN WAVES

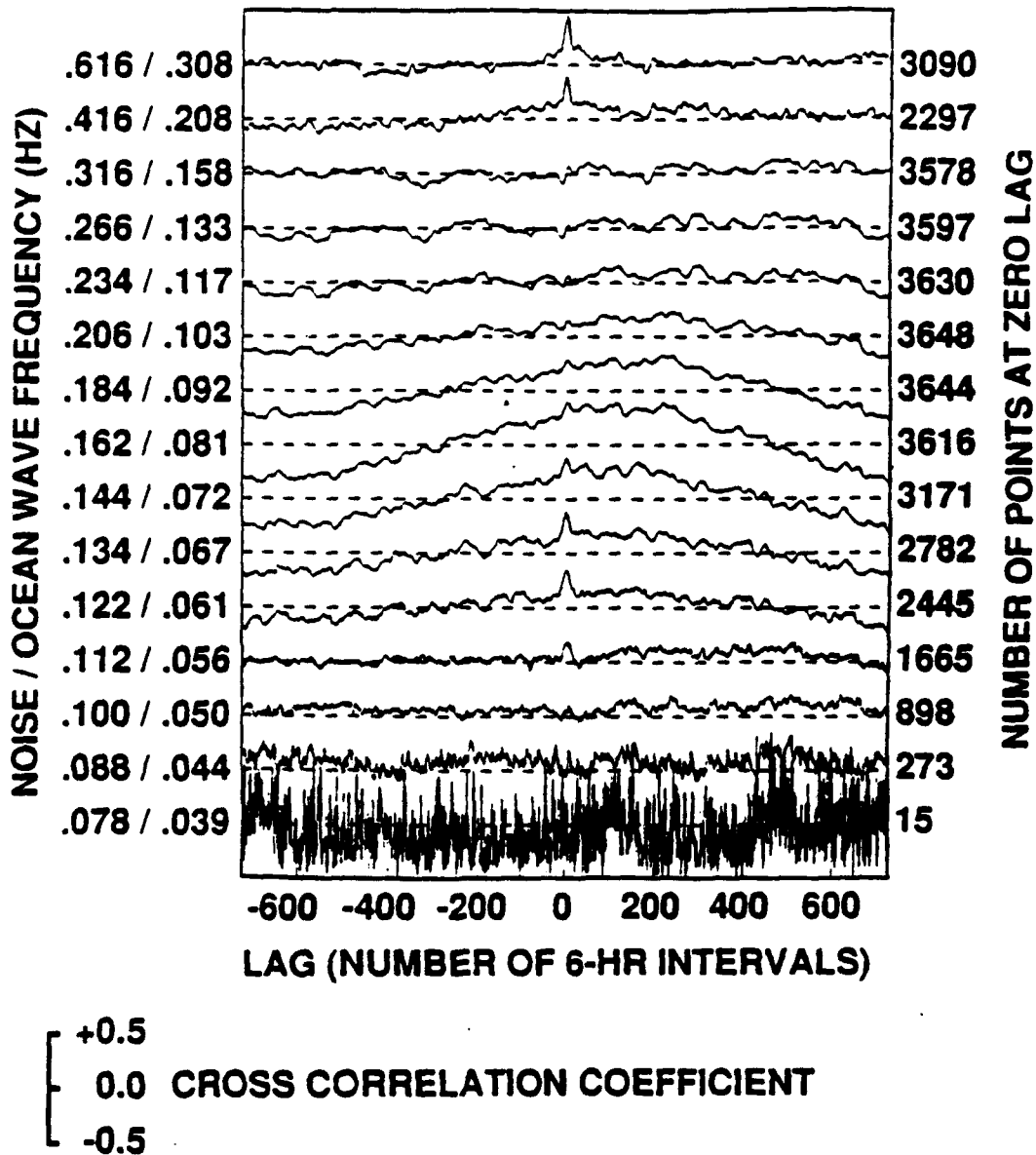


Fig. 26. Cross correlations between the noise and the waves for a ± 6 month range of lags. Fifteen frequency bands are represented, and the double frequency relationship between the noise and waves is assumed. Positive lags indicate that the waves follow the noise. The total number of points cross correlated at zero lag is indicated on the right.

there is no cross correlation peak at zero lag, and the seasonal peak wanes. This is a very interesting observation, since these are the microseism peak frequencies. At the highest two frequencies, 0.416 and 0.616 Hz in the noise, cross correlations are near zero for all lags except those lags close to zero. At zero lag the cross correlation values are near 0.5.

A reexamination of the spectrogram forms of the wave and noise data led to the conclusion that perhaps a 2:1 correspondence in frequency between the two was not appropriate. To investigate this possibility, cross correlations were computed between each of the 15 wave energy time series in dB, and each of 120 noise time series, geometrically spaced in frequency as they were for Fig. 21, at zero lag. The resulting pattern of cross correlations confirms that suspicion (Fig. 27). None of the peak cross correlation values occur with a 2:1 correspondence in frequency. In fact, there appear to be at least four different noise:wave frequency correspondences for four separate noise frequency bands. For noise between 0.1 and 0.2 Hz, peak cross correlation values of 0.40-0.45 occur with a frequency correspondence of about 2.5:1. For noise frequencies between 0.2 and 0.3 Hz (the primary microseism peak in the Wake data), peak cross correlation values of 0.25-0.35 occur with a frequency correspondence between 3:1 and 4:1. For noise frequencies between 0.3 and 2 Hz, peak cross correlation values range from 0.35 to 0.60 with a frequency correspondence ranging from 5:1 to more than 10:1. For noise frequencies above 2 Hz (the hulu spectrum), there are no isolated cross correlation maxima. This noise probably corresponds best with waves of higher frequency than those given by SOWM. There is also a drop in correlation values and in the noise:wave frequency correspondence for the next to highest wave frequency around 0.2 Hz. This seems to be a frequency of particular significance in the SOWM model, since there are considerably fewer data points given at this frequency than at the adjacent frequencies.

This surprising result implies one of three things. Either the SOWM wave data are in error, or the non-linear wave-interaction theory of noise generation is wrong, or some

**CROSS CORRELATIONS
HYDROPHONE 74 NOISE vs SOWM WAVES
8 SEP 82 - 23 JUN 85**

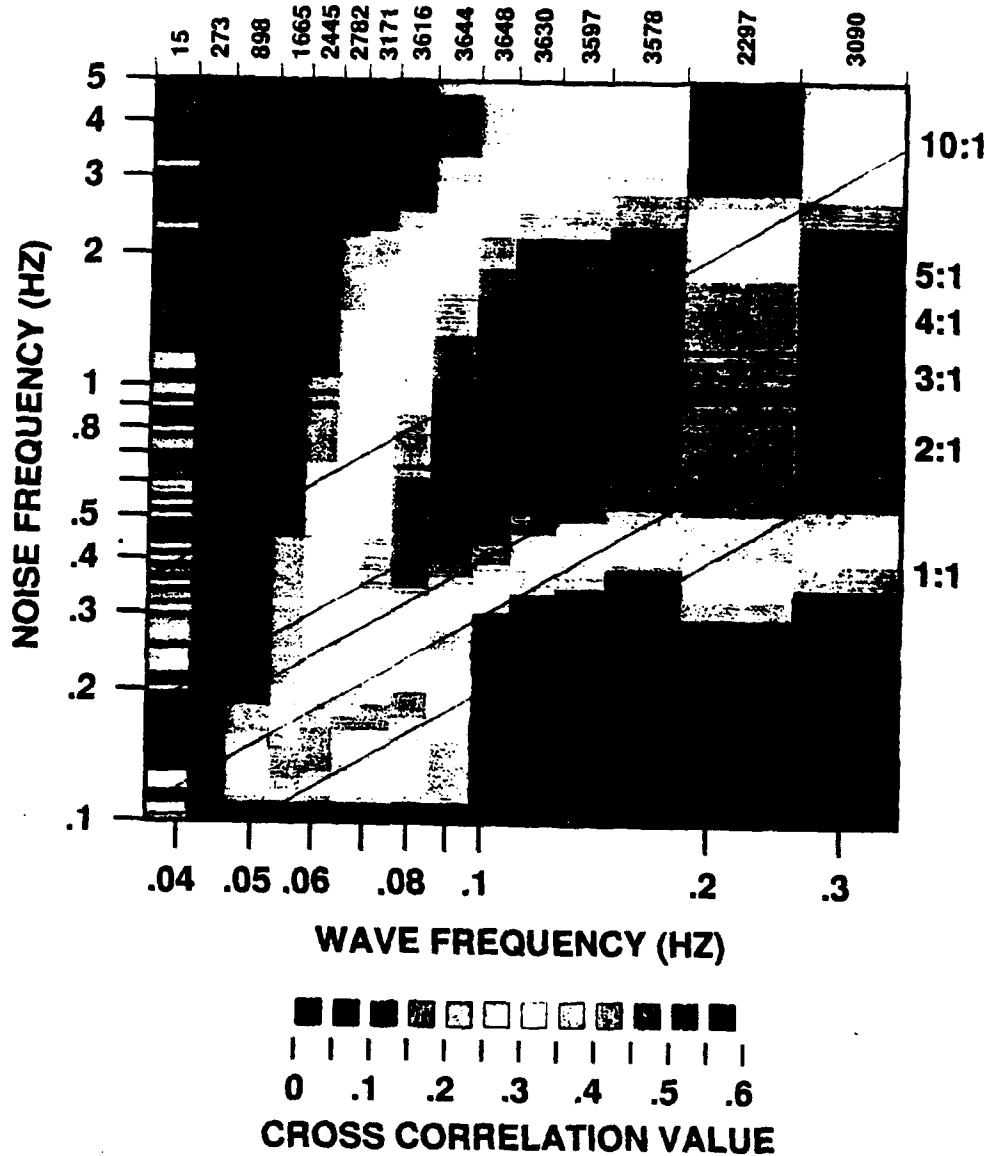


Fig. 27. Cross correlations at zero lag comparing each wave frequency with each noise frequency. Colors indicative of the cross correlation value are shown at the bottom. The number of data points cross correlated is indicated at the top. Narrow lines across the face of the figure indicate particular frequency correspondences between the noise and wave frequencies as noted on the right-hand edge of the plot.

combination of the two. There is plenty of reason to suspect the SOWM data. The theory on which this model is based is more than twenty years old, and wave modelling techniques have improved considerably since that time. And although the model was tested with some success by comparing buoy-measured significant wave heights with significant wave heights out of the model (Clancy et al., 1986), the individual frequency components have not been tested. The 2.5:1 frequency correspondence observed for noise between 0.1 and 0.2 Hz might really be 2:1 if there is only a small systematic error in the SOWM model. On the other hand, the frequency components of the SOWM model would have to be extremely far off to reconcile them with the noise between 0.3 and 2 Hz. For instance, the peak cross correlation coefficient for the 1 Hz noise is with waves having frequencies of about 0.12 Hz. Such ocean gravity waves have wavelengths of about 100 m, and phase speeds of about 45 km/hr. However, ocean waves with frequencies of 0.5 Hz, the ones that should be producing the 1 Hz noise by wave interactions, have wavelengths of only about 6 m and phase speeds of only about 10 km/hr. Furthermore, it seems a somewhat unlikely coincidence that the four noise frequency bands showing distinctly different noise:wave frequency correspondences happen to also be four distinctly different regions of the ocean noise spectrum: (1) below the microseism peak, (2) the microseism peak, (3) above the microseism peak but below the hulu saturation spectrum, and (4) the hulu saturation spectrum. This dilemma is unlikely to be resolved without directly comparing deep ocean noise with simultaneous ocean wave measurements.

CHAPTER 6. TYPHOONS

Typhoons and tropical storms are obvious phenomena to suspect as a source of ocean noise. They are present in the western north Pacific more than 100 days per year on average, and they have winds that can extend out hundreds of kilometers and generate large ocean waves. Near the center of the storms, there is an elevated level of wave interactions due to the inward radial component of waves generated by both the tangential and inward radial winds. These increased interactions should lead to increased pressure fluctuations in the water column, and possibly the excitation of Rayleigh waves. In addition, high winds near the center of the storms should produce increased levels of high frequency noise from whitecaps.

Typhoon Owen

Typhoon Owen began to develop 1000 km to the south of Wake on October 13th, 1982 (Fig. 28). It moved 2000 km to the west over the next few days, reached typhoon strength on October 18th, and then began to recurve back to the north and east. It reached its maximum intensity, with 54 m/s sustained winds, at a position about 1500 km to the northwest of Wake on October 20th. On October 24th, Owen passed only 500 km to the north of Wake, with a maximum sustained wind speed of 26 m/s. Some sample noise spectra from hydrophone 74 were made using the three-minute-long noise samples collected during this time period (Fig. 29). At frequencies between 0.1 and 0.2 Hz, noise levels were highest shortly after Owen reached its maximum intensity. Between 0.2 and 2 Hz, and also above 4 Hz, levels were highest when Owen made its closest approach to Wake. The mean wind speed at Wake that day was 11.5 m/s, a relatively high but not unusual value.

It was originally thought that the elevated level of noise below 0.2 Hz, occurring near the time that Owen was at its peak intensity, might be Rayleigh waves excited beneath the

TYPHOON OWEN: OCTOBER 13-28, 1982

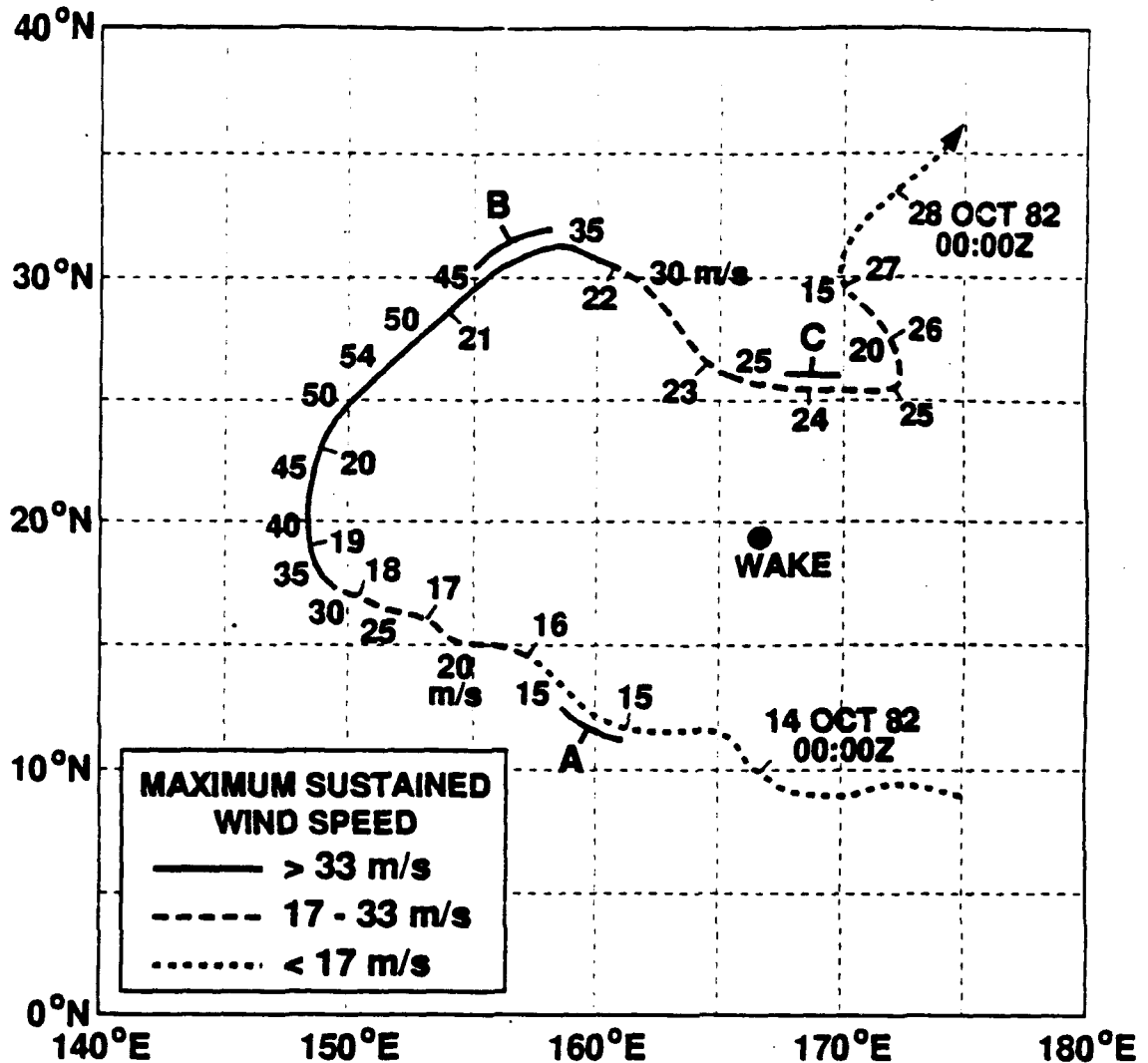


Fig. 28. The track of Typhoon Owen, October 13-28, 1982, taken from the *1982 Annual Tropical Cyclone Report*. Dates, at 00:00Z, are indicated along one side of the track, and maximum sustained wind speeds in m/s along the other side. The letters A, B, and C along the track indicate the position of the storm for the spectra shown in Fig. 29.

**TYPHOON OWEN, 15-27 OCTOBER 1982
HYDROPHONE 74 (5.5-KM DEPTH)**

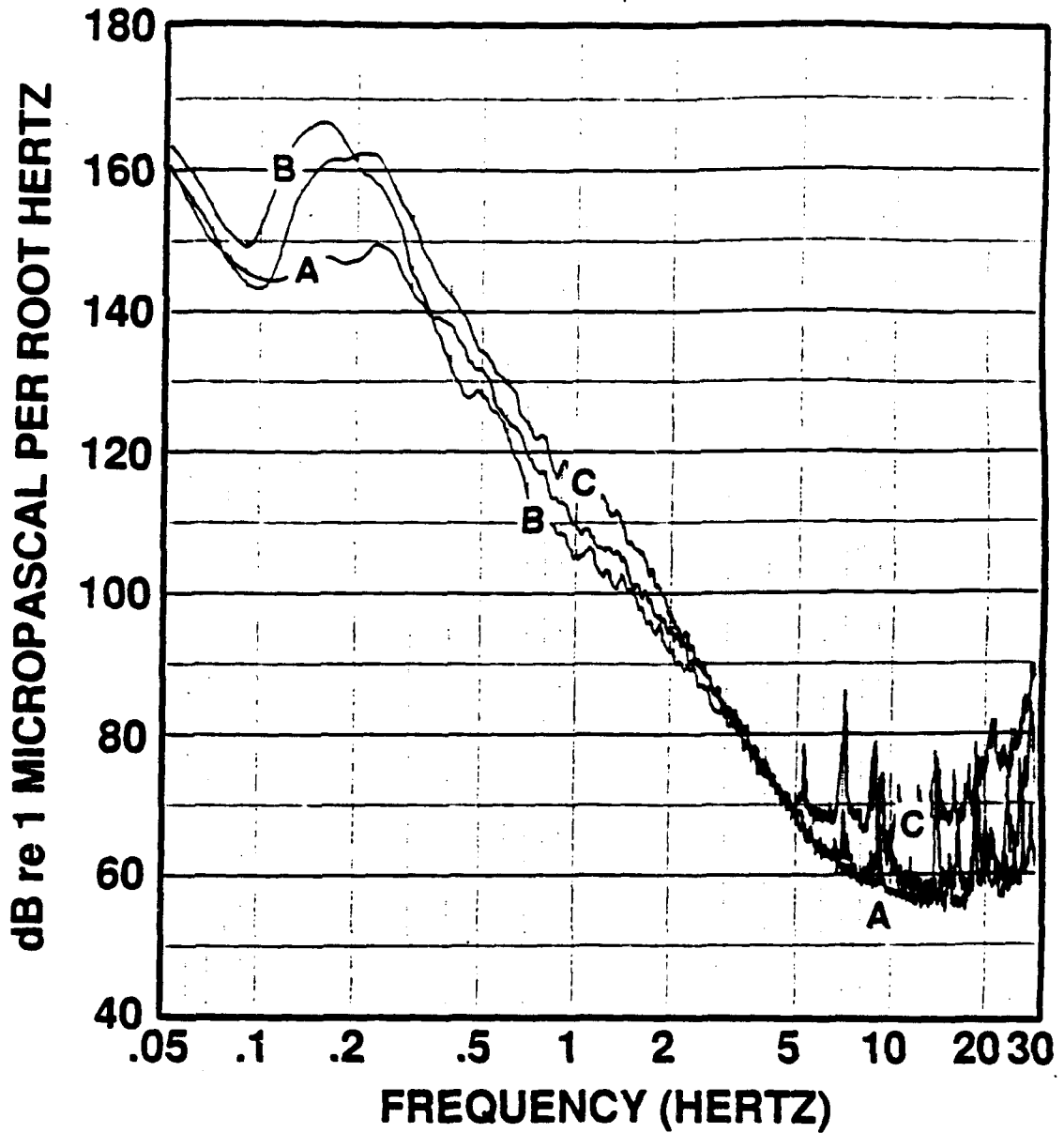


Fig. 29. Spectra from WIHA hydrophone 74 during the passage of Typhoon Owen. The letters A, B, and C identify spectra corresponding to the positions of Owen shown in the previous figure. The noise below about 0.1 Hz is system noise. The frequency resolution is 0.05 Hz.

storm. However, the SOWM ocean wave data for October 21st (Fig. 20) show that there was a large unrelated low-frequency swell arriving at Wake at the same time. Based on the study of the noise and ocean waves, this swell is the more likely the cause of that high noise. These waves, which continued for several days, may also be the cause of the elevated microseism peak on October 24th. The rest of the elevated noise on October 24th, from 0.3 to 2 Hz and above 4 Hz, is probably due to the locally generated wind waves and whitecaps, respectively.

Typhoon Doyle

On August 13, 1988 Typhoon Doyle began to develop about 500 km to the east of Wake (Fig. 30). On August 15th and 16th, Doyle passed to the north of Wake Island, and reached typhoon strength just as it was on top of the WIHA deep bottom hydrophones (Fig. 31). It reached its maximum strength, with 59 m/s sustained winds, only a few hours later as it moved off to the northwest. Over the next few days it recurved back to the northeast, slowly lost strength and dissipated. Continuous data for this time period are archived at HIG, and the data from hydrophone 76 for the period August 13-18th was extracted for analysis. The center of the storm passed directly over this hydrophone.

The first step in the analysis was the generation of a spectrogram so that all the data could be viewed together. Contiguous segments of the time series data, 400 seconds in length, were transformed to the frequency domain using a 32,768-point FFT. A logarithmic frequency scale was used, and levels were plotted relative to the mean level at each frequency. A portion of this spectrogram is shown in Fig. 32. The peak level of noise above 2 Hz was reached when Doyle was directly over the hydrophone, between 20:00Z and 21:00Z on August 15th. This is presumably when the wind was at its highest speed above the hydrophone and wave breaking was the most energetic. This high level noise caused some aliasing that is visible at the lowest frequency visible along the bottom edge

TYPHOON DOYLE: AUGUST 13-24, 1988

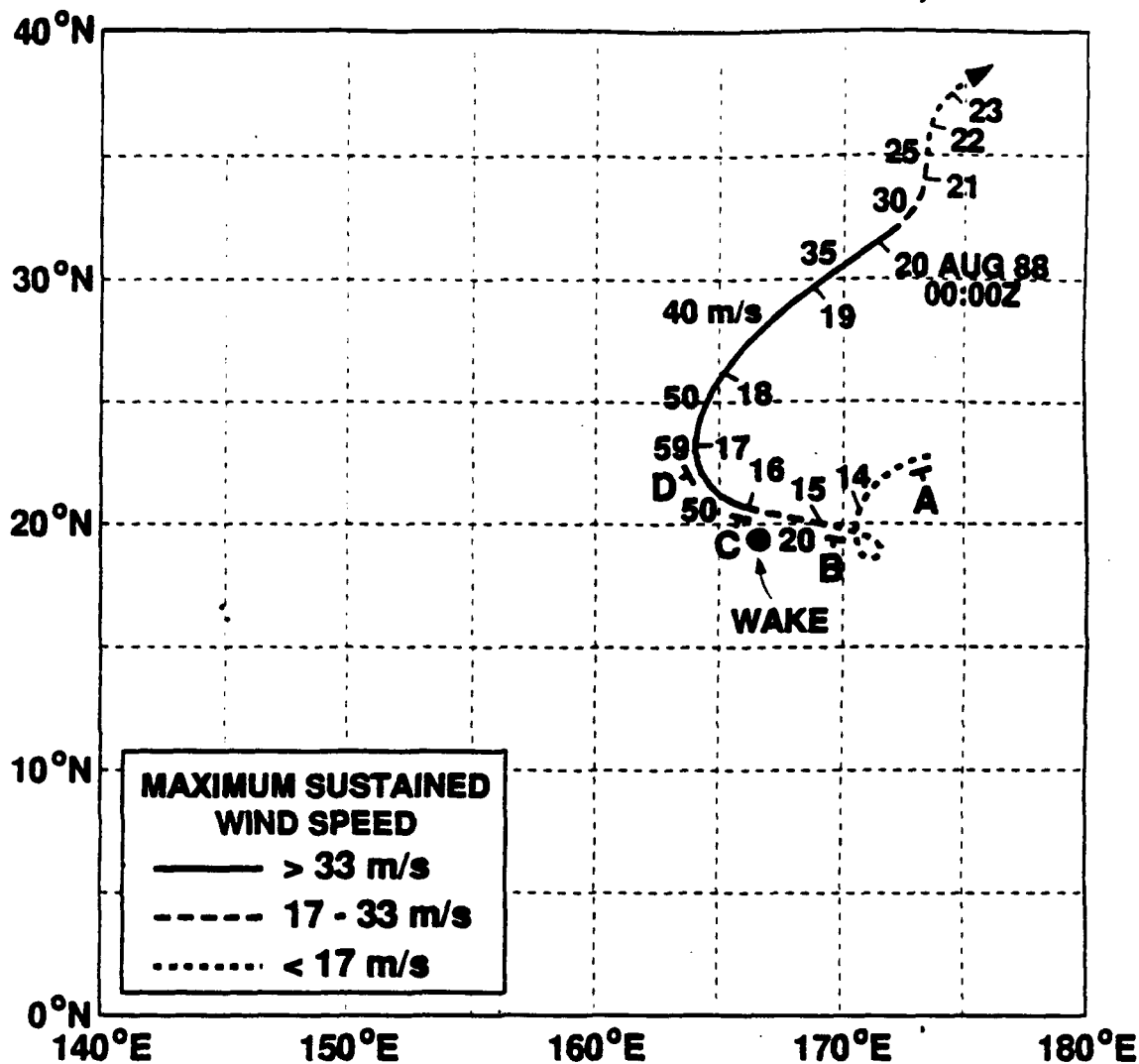


Fig. 30. The track of Typhoon Doyle, August 13-24, 1988, taken from the *1988 Annual Tropical Cyclone Report*. Dates, at 00:00Z, are indicated along one side of the track, and maximum sustained wind speeds in m/s are along the other side. The letters A, B, C, and D along the path indicate the position of the storm for the spectra shown in Fig. 34.

TYPHOON DOYLE: 13-24 AUG 1988

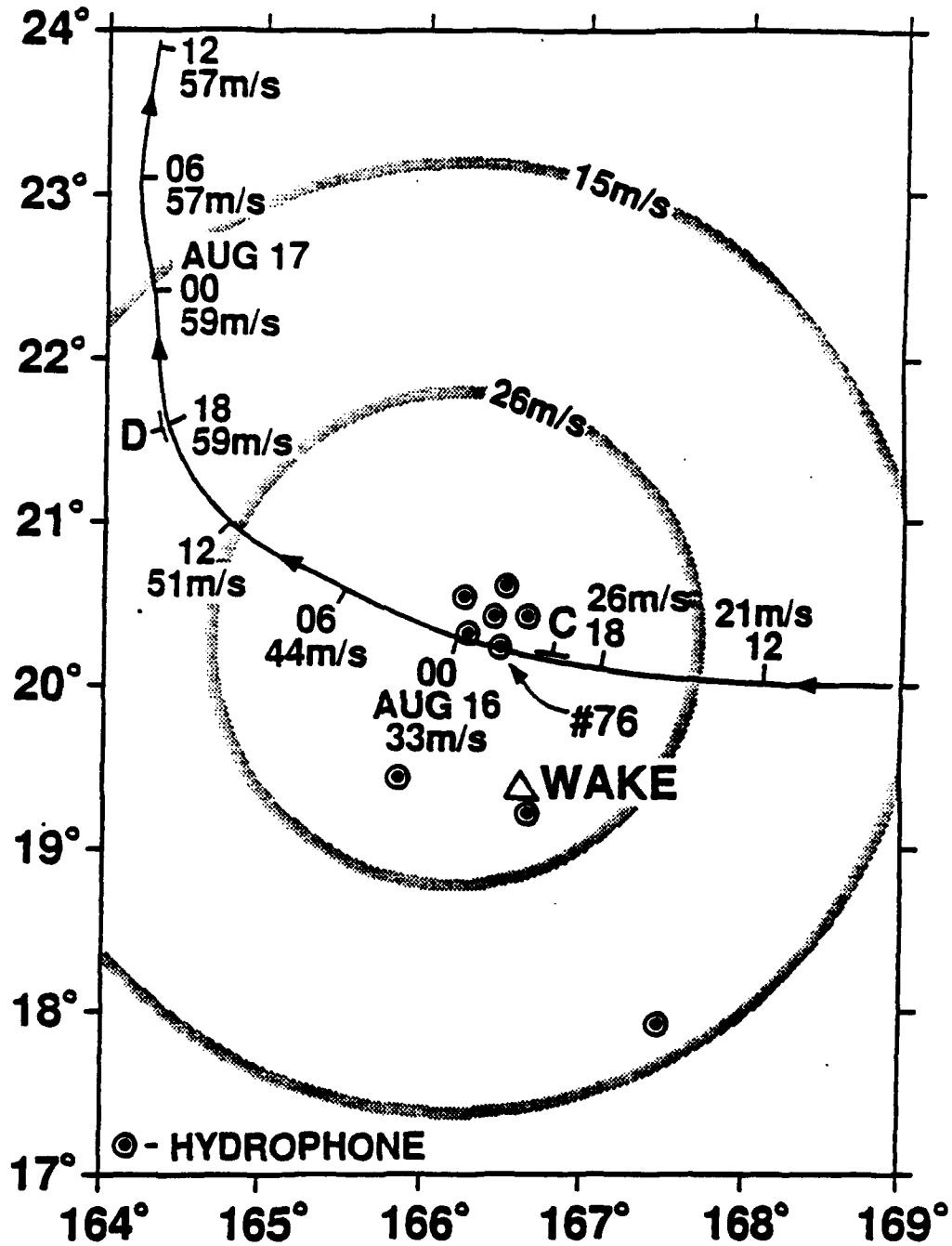


Fig. 31. The track of Typhoon Doyle across the WIHA hydrophones. The storm passed directly over hydrophone 76. Shaded circular bands show radii within which sustained winds were the indicated value or larger on August 16th at 00:00Z. Letters C and D indicate the position of Doyle for spectra shown in Fig. 34.

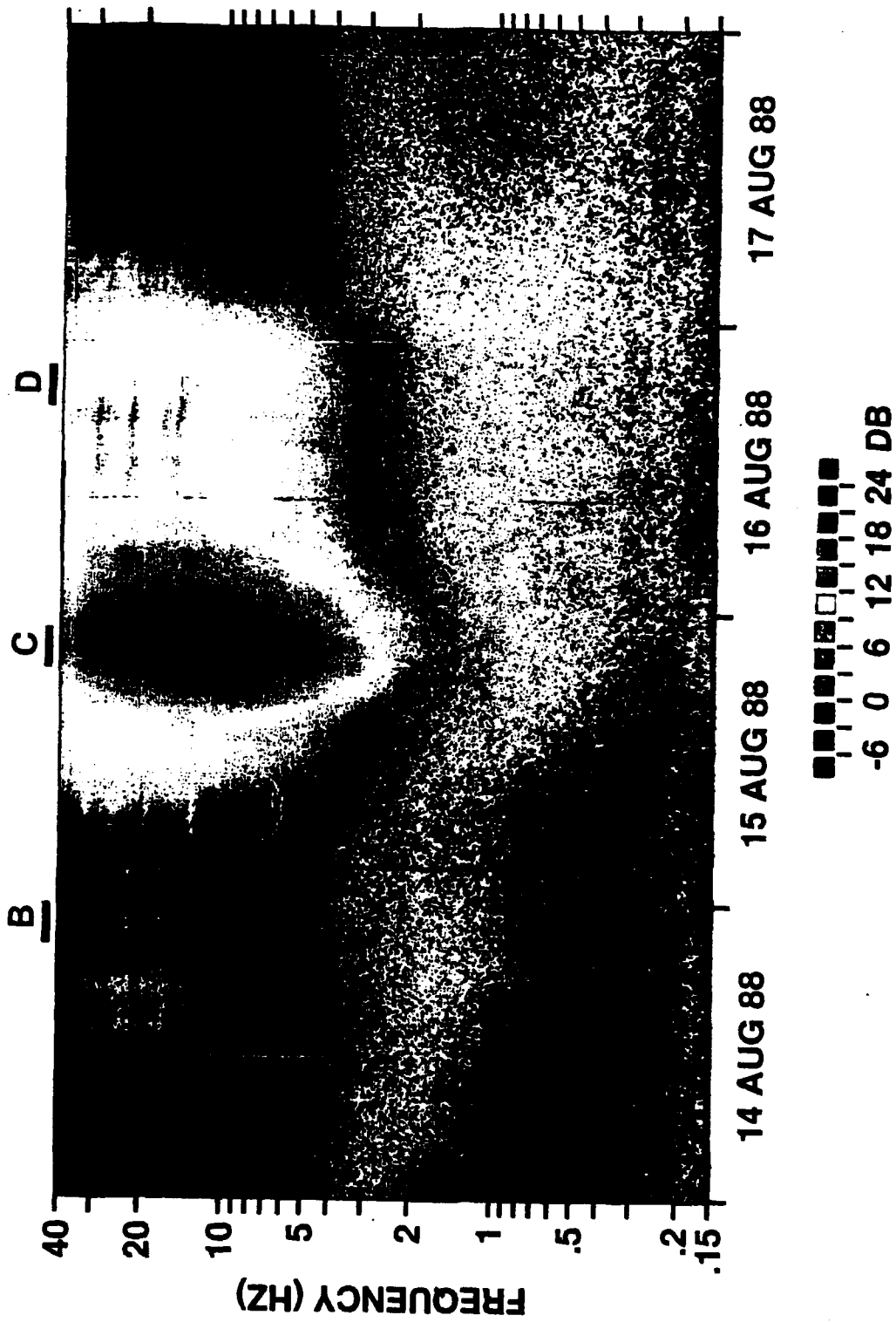


Fig. 32. Spectrogram showing the hydrophone 76 noise fluctuations due to Typhoon Doyle over a four day period. Letters B, C, and D indicate portions of the record used to compute corresponding spectra shown in Fig. 34.

of the plot. The slight reduction in noise at approximately 20:30Z (Fig. 33) is probably the eye of Doyle passing over hydrophone 76. Although sea conditions are known to remain energetic in the eye, the reduction in wind could be enough to produce a corresponding reduction in whitecaps leading to a lessening of the high frequency noise. JTWC reported the center of Doyle about 40 km away from the position of hydrophone 76 at this time, but this amount of error in the reported position, if that's what it represents, is not unusual considering that the eye was not yet even visible on satellite images. The holu spectrum, most commonly observed between 2 and 6 Hz, becomes saturated down to around 1 Hz during the passage of Doyle. An interesting characteristic of the holu spectrum, is that its level becomes depressed slightly on August 15th and 16th, when winds are particularly elevated. This is easily seen in Fig. 32 between 2 and 5 Hz as a dip to lower frequencies of the blue contour interval. The same characteristic is also suggested in previous data shown in Fig. 18. At 2.34 Hz in that figure, noise levels appear to go down slightly at the highest wind speeds. This is probably the result of these short wavelength ocean waves (0.2 to 6 m for wave frequencies of 3 to 0.5 Hz) having their tops sheared off by the wind and beaten down by the sea spray. At the lowest noise frequencies, 0.15 to 1 Hz, levels are highest in the interval from the time the storm is just overhead until about two days afterwards, and there is no large peak to this noise. The GSOWM wave data for this time period indicate that large waves were passing over the hydrophone during this time interval, produced by the storm as it intensified and moved to the north. Thus, this noise may be produced by these large waves interacting with the existing wave field, similar to what was seen in Chapter 5.

Absolute levels of the noise from typhoon Doyle, in the form of spectra, show a pattern similar to what is observed in the spectrogram (Fig. 34). Spectrum A, from before the start of the storm, has the lowest levels at all frequencies except those near the microseism peak. At this time the holu spectrum is only saturated above about 4 Hz. Spectrum B, taken near

NOISE FROM TYPHOON DOYLE HYDROPHONE 76

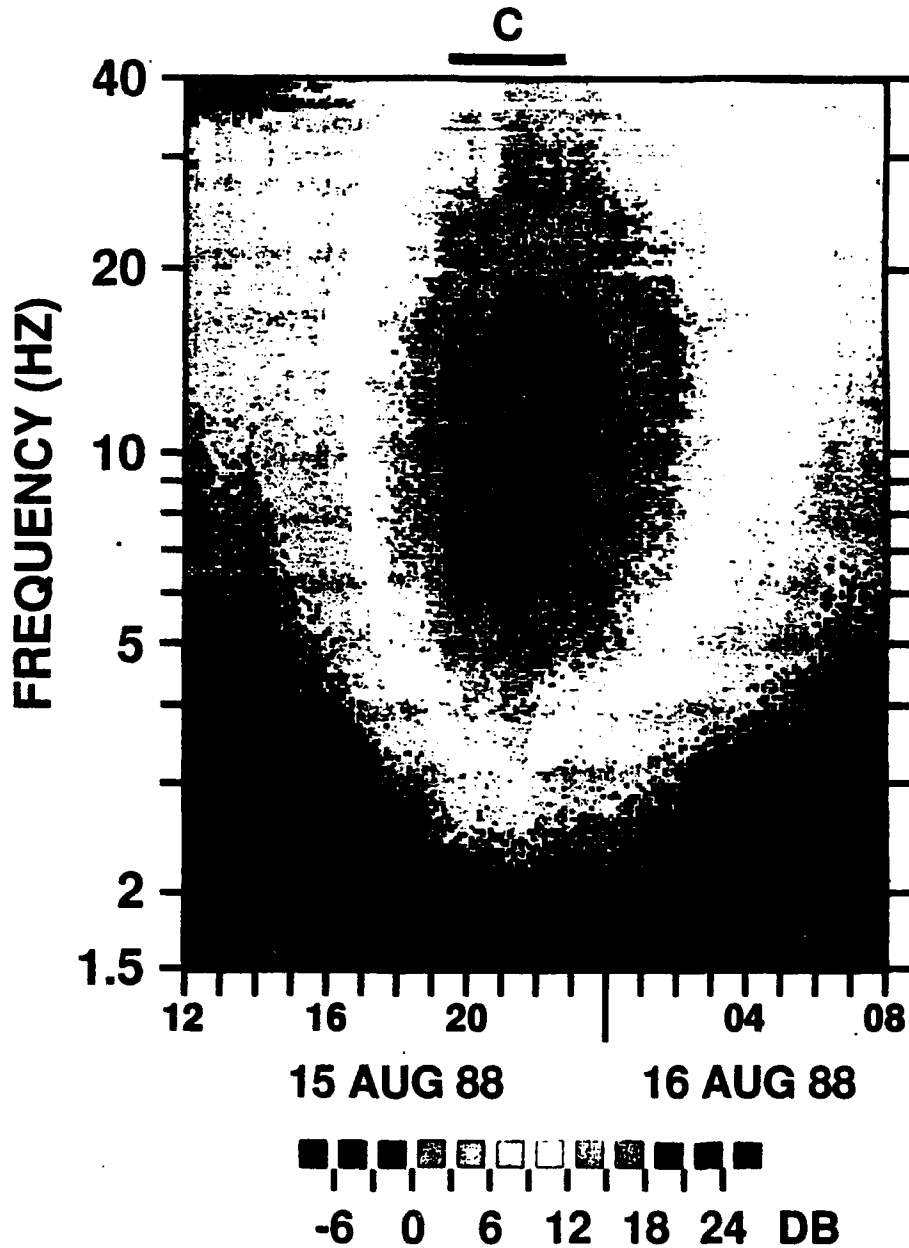


Fig. 33. Spectrogram showing the noise from Typhoon Doyle just as it passed directly over hydrophone 76. The slight reduction in noise level at 20:30UCT is the eye passing over the hydrophone. The letter C indicates the interval of data for the spectrum shown in the following figure.

**TYPHOON DOYLE, 13-24 AUGUST 1988
HYDROPHONE 76 (5.5-KM DEPTH)**

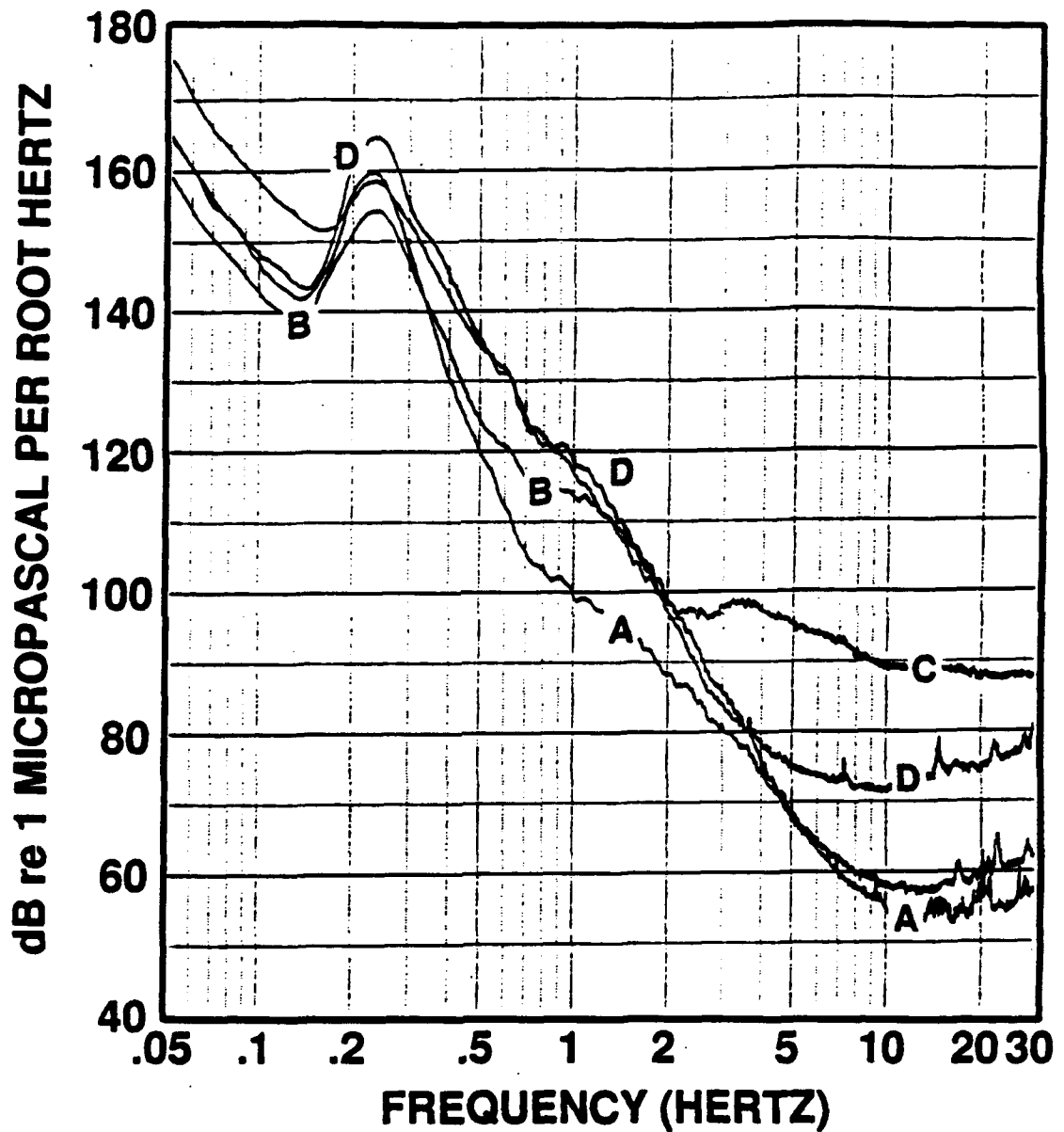


Fig. 34. Spectra from Typhoon Doyle. Letters identifying each spectrum correspond to letters on the previous four figures indicating the time and position of the storm. The noise below 0.15 Hz is instrumental. The frequency resolution is 0.05 Hz.

the end of August 14th when the winds had started to increase as Doyle approached, shows a saturation of the holu spectrum down to about 1 Hz, with a slight increase in the whitecap noise above 5 Hz. The microseism peak level, however, has dropped a few dB, indicating that the noise at these low frequencies is probably unrelated to Doyle up to this point in time. Spectrum C, from the time when Doyle was directly over the hydrophone, shows a dramatic increase in the whitecap noise above 2 Hz, the feature that is so prominent on the spectrogram. It also shows increased noise levels between 0.3 and 1 Hz that may be a further extension of the holu spectrum, but no increase in microseism levels. Spectrum D, about a day later and when Doyle has reached full strength, shows a reduction of whitecap noise indicative of local winds that are reduced but have not completely subsided. From 2 to about 0.5 Hz, the levels of spectrum D are essentially the same as those from spectrum C, but peak microseism levels are increased by about 5 dB. This increase in microseism levels is probably due to the arrival of large waves from the storm (as predicted in the GSOWM data), rather than to Rayleigh waves excited underneath the storm, since high-amplitude low-frequency pressure fluctuations were not observed when Doyle was directly over the hydrophone. Absolute microseism levels for all four of these spectra are high relative to levels shown in the long-term distribution of Figs. 22-24, but this does not seem to be due to the storm since the levels are high for spectrum A which is from before the storm began. The slight lowering of the holu spectrum in high winds can also be seen in this figure. Spectrum C is systematically lower than spectrum D by about 3 dB over the frequency range 1-2 Hz, although it represents higher winds. And spectrum C is systematically lower than spectrum B by about 3 dB over the frequency range 2-3.5 Hz, although it too represents the higher winds.

Other Typhoons

Using the 46-month-long spectrogram of noise from hydrophone 74 described in

Chapter 5, a search was made to determine if other typhoons in the western north Pacific might have generated high levels of noise at Wake. Some of these storms were much larger than Owen or Doyle, and had sustained winds in excess of 65 m/s. None of the storms passed as close to Wake as Doyle, and only a few came as close as Owen. Although the search was not exhaustive, no evidence was found to indicate that these typhoons generated any recognizable noise other than that which might be caused by a local increase in wind near Wake or by the production of swell that propagated over the hydrophones.

CHAPTER 7. 0.05-0.5 HZ FINE SCALE NOISE CHARACTERISTICS

The recording system installed at Wake in 1989 made it much easier to examine the longer-period noise in fine detail. The new amplifiers ensured that noise at frequencies below the microseism peak was being recorded with adequate digital resolution and minimal system noise; the lower 10 Hz sampling rate on the long-period amplifiers greatly reduced the amount of disk space needed to store long-term data sets; and the 8-mm video format meant it was very easy to access the raw data. A few days of continuous data were first extracted for hydrophones 74 and 76, the two hydrophones connected to the long-period amplifiers. Spectrograms of these data showed many interesting characteristics in the low-frequency noise. Subsequently, a 41-day-long section of continuous data, October 6th to November 15th, 1989, was extracted for each of the six deep bottom hydrophones and three of the SOFAR hydrophones, one from each site. These data were too lengthy to store on disk in their raw 100 Hz- sampled form (just one hydrophone is over 700 Mbytes), so they were digitally, anti-alias, low-pass filtered and then decimated down to a 2 Hz sampling rate. The two long-period channels were also resampled in this manner. Besides greatly reducing the size of the data set, this resampling permitted a much more efficient spectral analysis of the low frequencies. The fidelity of the resampled data was checked against the original raw data by comparing spectrograms of small portions of each data set.

Spectrograms were then produced for each of the hydrophones for the entire 41-day period, plotting levels relative to the mean level at each frequency to emphasize temporal variations. The character of the noise for each of the bottom hydrophones is essentially the same, except that hydrophones 72, 73, and 75 have some additional coherent, sporadic, broadband noise that must be associated with the small leaks to ground measured in their sea cables. Data from the three SOFAR hydrophones are more dissimilar. They have some of the characteristics observed on the bottom hydrophones, and some additional features as

well. The data from SOFAR hydrophone 10, located next to Wake Island, exhibit the least character with almost no variations observed below about 0.18 Hz. The data from SOFAR hydrophone 40 have more character, with features frequencies down to about 0.1 Hz. The data from SOFAR hydrophone 20 has the most character, with prominent features at frequencies well below 0.05 Hz. Hydrophones 20 and 40 are located in similar environments, both suspended in the SOFAR channel from the sides of seamounts, and the difference in their character is not understood.

Spectrograms from hydrophones 74 and 20 for the two-week time period October 21st to November 3rd are typical (Figs. 35 and 36). There is some contamination of the data by artifacts. The narrow, vertical, high-energy bands that are especially prominent in the data from hydrophone 20 are due to the occasional clipping of the original time series, primarily from large amplitude earthquake-generated signals propagating in the SOFAR channel. Also, the general lack of features above about 0.6 Hz in the data from hydrophone 74 is due to a combination of that hydrophone's long-period-amplifier anti-alias filter and the decimation anti-alias filter which have essentially deleted the information in that band.

Between 0.05 and 0.2 Hz are some high energy features due to Rayleigh waves from earthquakes. Some of the more prominent of these seen on hydrophone 74 are the one on October 26th, the two on October 27th, and the four on October 29th. A complete list of earthquakes producing Rayleigh waves that are visible on these spectrograms is given in Table 2. The high number of large magnitude earthquakes in this time span is somewhat unusual and is due primarily to an earthquake sequence in Honshu, Japan. However, considering that the WIHA data are limited by system noise at frequencies below about 0.1 Hz, and considering that the true ocean noise levels are probably 20-40 dB below the WIHA system noise levels, and also considering that the number of earthquakes occurring increases by about a factor of 10 for each unit reduction in magnitude corresponding to a reduction in signal amplitude by 20 dB, it is clear that Rayleigh wave signals from

NOISE LEVEL VARIATIONS: 21 OCT 88 - 3 NOV 88
 HYDROPHONE 74 (5.5-KM DEPTH)

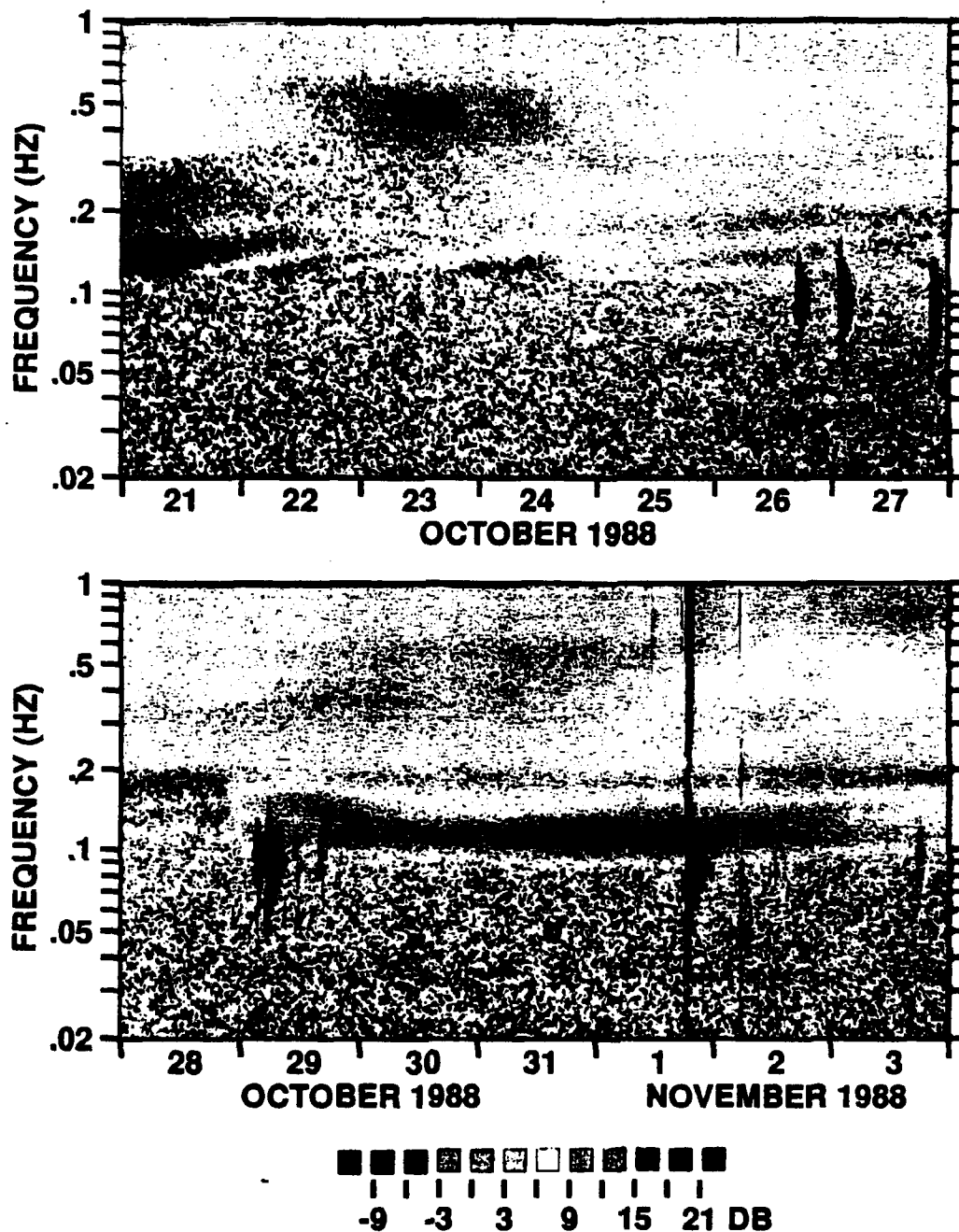


Fig. 35. Spectrograms of ocean noise over a two week period from deep hydrophone 74. Levels are plotted relative to the mean level at each frequency over the first five days.

NOISE LEVEL VARIATIONS: 21 OCT 88 - 3 NOV 88
 HYDROPHONE 20 (0.8-KM DEPTH)

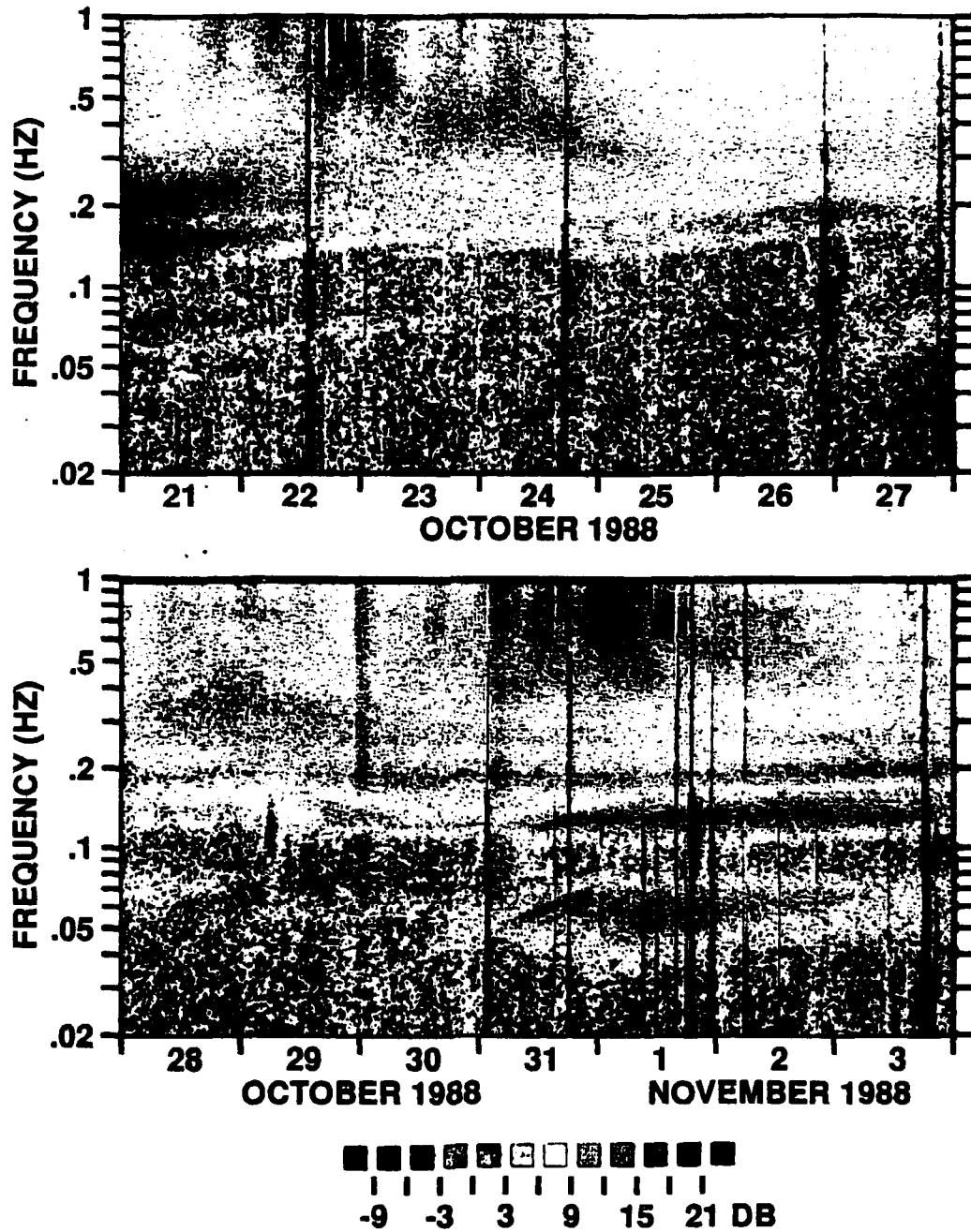


Fig. 36. Spectrograms of ocean noise over a two week period from SOFAR-depth hydrophone 20. Levels are plotted relative to the mean level at each frequency over the first five days.

Table 2.
 Earthquakes producing Rayleigh waves observed on the WIHA hydrophones:
 October 21 - November 3, 1989.[†]

<u>Date</u>	<u>Time (UCT)</u>	<u>M[‡]</u>	<u>Location</u>
10/26	17:06:41.6	5.8	Honshu, Japan
10/27	00:19:56.9	4.7	Honshu, Japan
10/27	01:45:55.0	6.2	Honshu, Japan
10/27	08:09:00.7	4.4	Honshu, Japan
10/27	21:04:51.8	7.0	Solomon Islands
10/29	03:09:10.7	5.9	Honshu, Japan
10/29	05:25:38.2	6.6	Honshu, Japan
10/29	10:51:25.3	5.3	Honshu, Japan
10/29	15:53:10.7	5.3	Honshu, Japan
11/01	11:46:59.7	5.5	Solomon, Islands
11/01	18:25:34.9	7.4	Honshu, Japan
11/02	11:59:48.8	5.5	Honshu, Japan
11/02	13:42:14.4	5.2	Honshu, Japan
11/03	17:39:10.8	5.7	Admiralty Islands

[†] Earthquake data from the National Earthquake Information Service's Monthly Listings
[‡] M is the standard earthquake surface wave magnitude

earthquakes are a significant source of noise in this band.

Between 0.1 and 0.2 Hz, during the week of October 21-27, there are some rather narrow band noise features that slowly rise in frequency over a two or three day period. These features are suggestive of the arrival of ocean swell from a distant storm. Ocean gravity waves also exhibit a dispersive character in deep water according to the relationship: $u=g/(4\pi f)$, where u is the group velocity of the ocean waves, g is the acceleration of gravity, and f is the wave frequency. Between October 21st and 23rd on hydrophone 20, another narrow band of dispersed energy can be seen between 0.05 and 0.08 Hz, that mirrors a narrow band at twice its frequency. This is almost certainly the direct pressure signal from the ocean waves, since their wavelength, 250 to 650 m, is close to the depth of the hydrophone, 850 m. From the dispersion relationship given above, and the slope of the noise feature (but plotted on a linear frequency scale), it is possible to compute the distance of the storm or winds producing these waves, and the time they were produced. This calculation must assume that the source is an unmoving point which is sometimes an unrealistic assumption. A search of the GSOWM data for this time period does not show this feature in the estimated waves, although that is not surprising since it is fairly low energy. A more positive identification of these features utilizing satellite, Pacific-wide, meteorological data is in progress.

The broad feature between 0.1 and 0.2 Hz occurring between October 29th and November 3rd is very high energy. It seems to be at least partially associated with the high energy feature on hydrophone 20 between 0.04 and 0.08 Hz. It also corresponds to an arrival of energy between 0.05 and 0.08 Hz in the GSOWM data over the period 10/31 to 11/2. It is not a narrowband feature like the ones seen between October 21st and 27th, and it may be more typical of noise from waves produced by the more large scale ocean weather systems common in the north Pacific during winter. There was in fact a large, but not unusual, low pressure cell to the northeast of Wake at this time which was producing

high winds over a fairly large fetch. There is a hint at the beginning of the lower frequency noise from hydrophone 20 between 0.05 and 0.08 Hz on October 30th and 31st of a series of narrow dispersed noise bands arranged en echelon. This feature is more suggestive of a large distributed source for the ocean waves which could correspond to that low pressure cell.

At the frequencies of the WIHA primary microseism peak, 0.2 to 0.3 Hz, there seem to be no sharp features in the data like those seen between 0.1 and 0.2 Hz, but only a more gentle rising and falling of levels. This is true for the entire 41-day interval studied. This observation suggests, along with the other data examined in Chapter 5, that deep ocean noise at the microseism peak is generally not due to the local ocean wave field. Instead, like its counterpart on continents, it may be Rayleigh waves from more distant sources. Work on these data is continuing.

CHAPTER 8. CONCLUSIONS

The ocean noise examined in this study is divided into six frequency bands based upon its observed properties. Probable mechanisms of noise generation and propagation in each of these bands is discussed below.

0.05-0.1 Hz

This frequency band represents the 20-second-period noise hole and the steep spectral slope that rises from that hole towards the microseism peak. Although the WIHA data in this band are limited by system noise, two types of natural noise are identified. The first type is Rayleigh waves from earthquakes. These signals are easily observed on the WIHA hydrophones from earthquakes with surface wave magnitudes above about 5.0 that occur anywhere along the seismically active rim of the western Pacific. Rayleigh wave signals from the larger of these earthquakes can persist for many hours. Measurements of other investigators have shown that the level of ambient noise in this frequency band may be 20-40 dB below what the WIHA system is capable of detecting. A much larger number of earthquake Rayleigh wave signals than recorded by WIHA is therefore present in the true ocean noise in this band. Absolute ambient levels of ocean noise at these frequencies are probably comparable to levels observed at quiet continental seismic stations. The vertical long-period seismic records from those stations typically contain Rayleigh wave signals from a few worldwide earthquakes each day. These signals are more prominent on the deep ocean bottom hydrophones than on the SOFAR hydrophones, since Rayleigh wave pressure variations are smaller at shallower depths in the water column by the relation: $P = \rho h \ddot{z}$, where P is the pressure, ρ is the seawater density, h is the depth from the surface in the water column, and \ddot{z} is the vertical particle acceleration at the ocean bottom.

In contrast, the second type of natural ocean noise observed in this band increases in amplitude at shallower depths. It is the primary pressure signal from the ocean gravity

waves. Such signals are often seen on hydrophone 20, at 850 m depth, but not on the bottom hydrophones at 5500m depth. This type of pressure signal decreases rapidly with depth in the water column by the relationship: $P=P_0[\cosh(2\pi h/\lambda)]^{-1}=\rho g\Delta h[\cosh(2\pi h/\lambda)]^{-1}$, where P is the pressure at depth, P_0 is the pressure at the surface ($=\rho g\Delta h$), h is the depth from the surface in the water column, λ is the wavelength of the ocean wave, ρ is the density of seawater, g is the acceleration of gravity, and Δh is the depth perturbation caused by the ocean wave (the height of the wave). An ocean wave with a frequency of 0.05 Hz has a wavelength of about 650 m. Thus, the signal produced by a 0.05 Hz ocean wave (with a wavelength of 650 m) will be almost 400 dB smaller at 5500 m versus 850 m.

0.1-0.2 Hz

This frequency band is located just below the band containing the primary microseism peak, as defined by the WIHA data. It is the band of the microseism peak observed on continents. It sometimes contains the peak in the noise spectrum, especially in winter months when there is large long-period ocean swell present, generated by storms in the north Pacific. This noise appears to be dominated by the double-frequency pressure fluctuations produced by long-period ocean swell. A precise double frequency relationship is clearly observed in some of the fine-scale noise studied in Chapter 7, utilizing the primary ocean wave pressure fluctuations observed on SOFAR hydrophone 20. And the dispersion observed in this noise is similar to dispersion that might be found in long-period ocean gravity waves that have propagated from distant storms. In Chapter 5, the noise in this band and the SOWM estimated ocean waves were found to correlate significantly and consistently at a level above 0.4 and to have a frequency relationship of about 2.5:1. This small discrepancy in the frequency ratio may be due to systematic errors in the SOWM wave estimates. Some of the 0.1-0.2 Hz noise features described in Chapter 7, however, did not appear to be accompanied by the arrival of corresponding ocean waves,

as detected by their primary pressure fluctuations. And other features which had corresponding ocean waves did not appear to be duplicate images of the ocean wave energy, as they should be if an exact 2:1 relationship is maintained. The theory of nonlinear wave interactions requires opposing waves, and the assumption in these discussions has been that the opposing waves are provided by a low-level ambient wave field having some unknown distribution of frequency and directional components. It may be that the lack of a perfect correspondence is due to the variations in this ambient wave field. Or, it may be that this discrepancy is in some way related to the puzzling observation that only hydrophone 20 detected primary pressure fluctuations, while hydrophone 40 located at a similar depth did not. Or there may be another mechanism producing some of the noise in this frequency band that has not yet been identified.

0.2-0.3 Hz

This is the frequency band of the primary microseism peak of the WIHA data. The noise in this band appears to be only marginally related to the local ocean waves. Evidence for this comes from several aspects of the WIHA data: (1) the sharp and varied ocean-wave-related features observed in the fine-scale noise at lower frequencies are absent at these frequencies; (2) the noise in this frequency band appears to be the least related to noise in other frequency bands based on the self cross correlation data shown in Fig. 21; (3) there is a distinct minimum in the cross correlation values between this noise and the SOWM ocean waves as shown in Fig. 27; and (4) there is a striking shift in the frequency correspondence between the noise and the SOWM estimated ocean waves that also occurs precisely across this noise frequency band as seen in the same figure. In the interior of continents, it has recently been shown that the Rayleigh wave microseism peak noise seems to originate from certain fixed locations along the coastline of the continent, and also from beneath weather systems at sea (Cessaro, 1992), although this relationship is

observed at the lower frequencies of the continental microseism peak. Perhaps the microseism peak noise observed in the deep ocean is an integration of Rayleigh wave energy produced by waves beneath weather systems and waves interacting with coastlines throughout the northwestern Pacific. This might explain the more gradual fluctuations to the noise in this band as well as its general unrelatedness to the local waves. However, no significant Rayleigh wave type microseism noise has been seen in the WIHA data from typhoons in the western north Pacific, and that evidence must also be considered. The answer to this puzzle is no doubt contained in the Wake data, but it will probably require a different form of analysis than has yet been done to bring it to light.

0.3-1.5 Hz

This is the frequency band in the noise spectrum that is above the microseism peak but below the hulu spectrum. Several characteristics distinguish this noise from noise in adjacent frequency bands. Noise level fluctuations within this frequency band correlate very well with each other and also with fluctuations at higher frequencies, unlike noise at the microseism peak (Fig. 21). Also, cross correlations with the SOWM waves show a distinct, albeit enigmatic, correspondence between the noise and wave frequencies of more than 5:1 and perhaps as high as 10:1 (Fig. 27). Lastly, there is a distinct break in spectral slope between this band as it falls off rapidly from the microseism peak and the higher frequency hulu spectrum (Fig. 22). Noise in this band is clearly related to the local wind waves, as was shown by the data comparing noise and wind in Chapter 4. If the mechanism for this noise is the standard nonlinear wave interaction mechanism, then the SOWM wave data are in error by a very large amount for these frequencies. On the other hand, if the SOWM data are correct, there is some other wind wave related mechanism responsible for this noise.

1.5-6 Hz

This is the frequency band of the holu spectrum. Noise in this band is characterized by levels that increase with increasing wind speed until a clearly defined saturation level is reached (Fig. 17) Between 2 and 5 Hz levels are saturated more than 80% of the time (Fig. 22). This noise is almost certainly caused by local wind waves. These waves also grow with the wind until they reach a saturation level. Assuming that a 2:1 relationship exists between the noise and wave frequencies in this band, the ocean waves responsible for the saturated noise between 2 and 5 Hz have wavelengths of only 1.5 to 0.25 m. These very short-length ocean gravity waves should also be saturated most of the time in the trade winds common to Wake. The assumption of a 2:1 frequency relationship, derived from the nonlinear wave interaction theory of noise generation, is neither supported or refuted by the comparison of noise and waves made in Chapter 5, since the SOWM waves are not given at frequencies greater than about 0.3 Hz. However, in his most recent efforts to model noise by nonlinear wave interactions, Cato (1991b) has predicted noise levels for the saturated ocean wave conditions described by Phillips (1977) that are very close to levels observed on the WIHA hydrophones. A subtle, but interesting feature of the holu spectrum is that it decreases in level by as much as 3 dB during high winds. This characteristic may be the result of the high winds blowing the tops off of these waves and beating them down with spray. The holu spectrum is probably a constant in all of the world's oceans, and its levels seem to vary little, if at all, with depth. It may provide a way to do in situ calibration of seismoacoustic instruments, as well as a way to measure the spectrum of the short period ocean gravity waves.

4-30 Hz

The noise in this band is thought to be due to acoustic signals from breaking open ocean waves or whitecaps. There is no direct evidence for this contention, but the indirect

evidence seems to be supportive. This noise is clearly related to the wind speed, although it must have a very different origin from the hulu spectrum noise since the two types of noise have markedly different spectral slopes (Fig. 17). It has a fairly constant level until wind speeds reach a certain threshold, about 8 m/s, after which the noise grows regularly with the wind. This is what might be expected for noise produced by whitecaps, since they too do not begin to form until wind speeds reach a certain threshold. The Beaufort scale puts the threshold for the first white caps at just over 4 m/s, with many whitecaps being present at 8 m/s. As wind speeds increase, this noise grows unchecked and it covers the hulu spectrum at lower and lower frequencies. During Typhoon Doyle, this noise was so great that it covered the hulu spectrum down to 2 Hz, and exhibited peak levels 30 dB or more above pre-storm levels.

REFERENCES

- 1982 Annual Tropical Cyclone Report*, U.S. Naval Oceanography Command Center, Joint Typhoon Warning Center, Guam, Mariana Islands, 236 pp.
- 1988 Annual Tropical Cyclone Report*, U.S. Naval Oceanography Command Center, Joint Typhoon Warning Center, Guam, Mariana Islands, 215 pp.
- Barstow, N., G.H. Sutton, and J.A. Carter (1989). "Particle motion and pressure relationships of ocean bottom noise at 3900 m depth: 0.003 to 5 Hz," *Geophys. Res. Lett.*, **16**, 1185-1188.
- Bertelli, T. (1872). "Osservazioni sui piccoli movimenti dei pendoli in relazione ad alcuni fenomeni meteorologiche," *Boll. Meteorol. Osserv. Coll. Roma*, **9**, 10 pp.
- Butler, Rhett (1988). "Shear wave properties of marine sediments derived from cepstral analysis of background noise," *Geophys. Res. Lett.*, **15**, 836-839.
- Brune, J. and J. Oliver (1959). "The seismic noise of the earth's surface," *Bull. Seism. Soc. Am.*, **49**, 349-353.
- Cato, D.H. (1991a). "Sound generation in the vicinity of the sea surface: source mechanisms and the coupling of the received sound field," *J. Acoust. Soc. Am.*, **89**, 1076-1095.
- Cato, D.H. (1991b). "Theoretical and measured underwater noise from surface wave orbital motion," *J. Acoust. Soc. Am.*, **89**, 1096-1112.
- Cessaro, R.K. (1992). "Sources of primary and secondary microseisms," *Science*, (submitted).
- Clancy, R.M., J.E. Kaitala, and L.F. Zambresky (1986). "The Fleet Numerical Oceanography Center Global Spectral Ocean Wave Model," *Bull. Amer. Meteor. Soc.*, **67**, 498-512.

- Cox, C., T. Deaton, and S. Webb (1984). "A deep-sea differential pressure gauge," *J. Atmos. Ocean Technol.*, **1**, 237-246.
- Duennebier, F.K., R.K. Cessaro, and P. Anderson (1986). "Geo-acoustic noise levels in a deep ocean borehole," in *Ocean Seismo-Acoustics* edited by T. Akal and J.M. Berkson, Plenum Publishing Corp., 743-751.
- Duennebier, F.K. and R.H. Johnson (1967). "T-phase sources and earthquake epicenters in the pacific basin," *Hawaii Institute of Geophysics Report*, **HIG-67-24**, 17pp.
- Duennebier, F.K., C.S. McCreery, D. Harris, R.K. Cessaro, C. Fisher, and P. Anderson (1987). "OSS IV: noise levels, signal-to-noise ratios, and noise sources," *Init. Repts. DSDP*, **88**, 89-103.
- Duennebier, F.K., and C.S. McCreery (1988). "The holu spectrum: a worldwide deep ocean constant and indicator of the ocean wave spectrum," *Trans. Am. Geophys. Union*, **69**, 1245.
- Gherzi, E. (1924). "Étude sur les microséismes," *Notes Seismol. Obs. Zi-Ka-Wei*, **5**, 16pp.
- Gilmore, M.H. (1946). "Microseisms and storms," *Bull. Seism. Soc. Am.* **36**, 89-125.
- Hasselmann, K. (1963). "A statistical analysis of the generation of microseisms," *Rev. Geophys.*, **1**, 177-210.
- Haubrich, R.A., W.H. Munk, and F.E. Snodgrass (1963). "Comparative spectra of microseisms and swell," *Bull. Seism. Soc. Am.*, **53**, 27-37.
- Herrin, E. (1982). "The resolution of seismic instruments used in seismic verification research," *Bull. Seism. Soc. Am.*, **72**, S61-S67.
- Johnson, R.H. (1966). "Routine location of T-phase sources in the Pacific," *Bull. Seism. Soc. Am.*, **56**, 109-118.

- Kibblewhite, A.C. and K.C. Ewans (1985). "Wave-wave interactions, microseisms, and infrasonic ambient noise in the ocean, *J. Acoust. Soc. Am.*, **78**, 981-994.
- Latham, G., R. Anderson, and M. Ewing (1967). "Pressure variations produced at the ocean bottom by hurricanes," *J. Geophys. Res.*, **72**, 5693-5704.
- Latham, G. and A. Nowroozi (1968). "Waves, weather, and ocean bottom microseisms," *J. Geophys. Res.*, **73**, 3945-3956.
- Lindstrom, T.E. (1991). "Predictions and observations of seafloor infrasonic noise generated by sea surface orbital motion," Ph.D Dissertation, Massachusetts Institute of Technology, 106pp.
- Longuet-Higgins, M.S. (1950). "A theory of the origin of microseisms," *Philos. Trans. R. Soc. London A* **243**, 1-35.
- McCreery, C.S., D.A. Walker, and G.H. Sutton (1983). "Spectra of nuclear explosions, earthquakes, and noise from Wake Island bottom hydrophones," *Geophys. Res. Lett.*, **10**, 59-62.
- McCreery, C.S. and D.A. Walker (1987). "Calibration of the Wake Island Array", *Trans. Am. Geophys. Union*, **68**, 1374.
- Miche, M. (1944). "Mouvements ondulatoires de la mer en profondeur constante on décroissante," *Ann. Ponts Chaussees* **114**, 25-87.
- Nichols, R.H. (1981). "Infrasonic ambient ocean noise measurements: Eleuthera," *J. Acoust. Soc. Am.*, **69**, 974-981.
- Northrop, J., W.C. Cummings, and M.F. Morrison (1971). "Underwater 20 Hz signals recorded near Midway Island," *J. Acoust. Soc. Am.*, **49**, 1909-1910.
- Phillips, O.M. (1977). *The Dynamics of the Upper Ocean*, Cambridge University Press, New York., NY, 2nd Ed., 336pp.

- Press, W.H., B.P. Flannery, S.A. Teukolsky, and W.T. Vetterling (1990). *Numerical Recipes: The Art of Scientific Computing*, Cambridge University Press, New York, NY, 702pp.
- Ramirez, J.E. (1940a). "An experimental investigation of the nature and origin of microseisms at St. Louis, Missouri: Part One," *Bull Seism. Soc. Am.*, **30**, 35-84.
- Ramirez, J.E. (1940b). "An experimental investigation of the nature and origin of microseisms at St. Louis, Missouri: Part Two," *Bull Seism. Soc. Am.*, **30**, 139-178.
- Scholte, J.G. (1943). "Over het verband tussen Zeegloven en microseismen," *Verst. Ned. Akad.*, **52**, 669-683.
- Schreiner, A.E. and L.M. Dorman (1990), "Coherence lengths of seafloor noise: effect of ocean bottom structure," *J. Acoust. Soc. Am.* **88**, 1503-1514.
- Sutton, G.H. and N. Barstow (1990). "Ocean-bottom ultralow-frequency (ULF) seismo-acoustic ambient noise: 0.002 to 0.4 Hz," *J. Acoust. Soc. Am.*, **87**, 2005-2012
- Sutton, G.H., W. McDonald, D. Prentiss, and S.N. Thanos (1965). "Ocean-bottom seismic observatories," *Proc. IEEE*, **53**, 1909-1921.
- Sutton, G.H., D.A. Walker, and C.S. McCreery (1980). "Short period (0.5-7 Hz) teleseismic (30-90°) P from explosions and earthquakes on Wake Island hydrophones," *Trans. Am. Geophys. Union*, **61**, 308.
- Tams, E. (1933). "Einige Korrelationen zwischen seismischer Bodenunruhe in Hamburg und der Brandung in West - und Nordeuropa," *Z. Geophys.*, **9**, 23-3.
- Tarr, A.C. (1974). "World Seismicity Map," published by the U.S. Geological Survey, National Oceanographic and Atmospheric Administration, Denver, Colorado, 122x91 cm.

- Thanos, S.N. (1966). "OBS calibration manual," Columbia University, Lamont Geological Observatory Technical Report, 49pp.
- Urick, R.J. (1983). *Principles of Underwater Sound*, McGraw-Hill Book Company, New York, 423pp.
- Walker, D.A., C.S. McCreery, G.H. Sutton, and F.K. Duennebier (1978). "Spectral analyses of high-frequency Pn and Sn phases observed at great distances in the Western Pacific, *Science*, **199**, 1333-1335.
- Walker, D.A. and C.S. McCreery (1988). "Deep ocean seismology: seismicity of the Northwestern Pacific Basin interior," *Eos*, **69**, 742-743.
- Webb, S.C. and C.S. Cox (1986). "Observations and modeling of seafloor microseisms," *J. Geophys. Res.*, **91**, 7343-7358.
- Webb, S.C., X. Zhang, and W.C. Crawford (1991). "Infragravity waves in the deep ocean," *J. Geophys. Res.*, **96**, 2723-2736.
- Wenz, G.M. (1962). "Acoustic ambient noise in the ocean: spectra and sources," *J. Acoust. Soc. Am.*, **34**, 1936-1956.